# POLITECNICO DI TORINO

**Master's Degree Course**
**in Civil Engineering LM23**

Master's Thesis

# Shear Strength of Steel fiber-reinforced Concrete Beams without shear reinforcement


**Supervisors**
prof. Alessandro Pasquale Fantilli
prof. Bernardino Chiaia

**Company Supervisors**
PhD Eng. Nicholas Sergio Burello
Eng. Jorge Camilo Diaz Garcia
PhD Eng. Davide Zampini

**Candidate**
Samuele Cimini

*Candidate's signature*

.....


Accademic Year 2024-2025

# *Acknowledgements*

*This thesis represents the culmination of my Master's degree in Civil Engineering at Politecnico di Torino, Italy.*

*I am deeply grateful to Professor Alessandro Pasquale Fantilli and Professor Bernardino Chiaia for introducing me to the fascinating field of concrete research.*

*My sincere thanks go to Dipartimento di Ingegneria Strutturale Edile e Geotecnica (DISEG) in Italy and to the Structural laboratory Centro de Innovación y Desarrollo in Mexico for their invaluable support throughout the different phases of the experimental campaign.*

*I am deeply grateful to the entire research center Cemex Innovation Holding in Switzerland, and in particular to Davide Zampini and Jorge Camilo Diaz Garcia, for making me feel at home from day one, for guiding me and for sharing their knowledge as well as for the financial support that made this internship and this thesis possible.*

*A special acknowledgment goes to my supervisor, Nicholas Sergio Burello, for his guidance and mentorship, for training me, and for showing me how to navigate such a dynamic and stimulating work environment. Thank you for demonstrating in a tangible way me how it is possible to create a sincere and honest relationship even in the working environment, which respects roles when necessary, but also leaves room for real and sincere sharing to carry with me over the years.*

Brügg, December 2025

Samuele Cimini

# Contents

**Abstract** 6

**1 Introduction** 7

1.1 Shear behavior of Plain Concrete . . . . . 7

1.2 Evolution of shear reinforcement . . . . . 12

1.3 Fiber-Reinforced Concrete (FRC) . . . . . 14

1.3.1 Introduction to FRC . . . . . 14

1.3.2 Mechanical characterization - Testing methods . . . . . 19

Compressive Strength . . . . . 20

Elastic Modulus . . . . . 21

Direct Tensile Strength . . . . . 22

Flexural Strength . . . . . 23

Direct Shear Strength . . . . . 28

1.3.3 Up-To-Date datasets of SFRC beams under shear loading . . . . . 29

1.4 Shear strength prediction models . . . . . 38

1.4.1 *fib* Model Code 2020 . . . . . 39

1.4.2 Eurocode 2 - Annex L . . . . . 41

1.4.3 ACI 544.4R-18 . . . . . 43

1.4.4 ACI 318-25 . . . . . 44

1.5 Research significance . . . . . 45

**2 Experimental Campaign** 47

2.1 Experimental program . . . . . 47

2.2 Preliminary Investigation #1 - Small-Scale Beams . . . . . 48

2.2.1 Test configuration - Setup #1 . . . . . 48

2.2.2 Material properties . . . . . 50

2.2.3 Shear tests - Experimental results . . . . . 53

2.3 Preliminary Investigation #2 - Full-Scale beams . . . . . 60

2.3.1 Test configuration - Setup #2 . . . . . 60

2.3.2 Material properties . . . . . 63

2.3.3 Shear tests - Experimental results . . . . . 67

2.4 Comprehensive investigation - Size-effect of beams with variable heights . . 73

2.4.1 Test configuration - Setup #3 . . . . . 73

2.4.2 Material properties . . . . . 78

2.4.3 Shear tests - Experimental results . . . . . 81

**3 Discussion of test results** 93

3.1 Experimental results vs Up-To-Date datasets . . . . . 93

3.2 Experimental results vs prediction models . . . . . 98

3.3 Considerations about ACI 318-25 . . . . . 106

3.4 Considerations about ACI 544.4R-18 . . . . . 109

**Acronyms** 114

**Notations and Conversions** 116

Symbology . . . . . 116

Conversions from International System of Units (SI) . . . . . 116

**List of Figures** 121

**List of Tables** 127

**Bibliography** 130

**Annex A – Summary of Quality Control test results** 137

Phase 1 – Preliminary Investigation 1 . . . . . 137

Phase 2 – Preliminary Investigation 2 . . . . . 137

Phase 3 – Size-Effect Investigation . . . . . 137

# Abstract

Although the subject of shear failure in steel-Fiber-Reinforced Concrete (FRC) beams has been widely addressed in recent decades, current databases show a lack of mechanical characterization according to current standard testing methods namely EN 14651 and ASTM C1609. With the aim of further investigate the correlation between shear strength and the contribution of fibers through residual flexural strength, several experimental campaigns were carried out on FRC beams cast by means of an industrial-based production methods. The experimental tests demonstrated the ability of deflection-hardening FRCs to increase the shear strength by up to five times respect to Plain Concrete (PC), as well as to compensate for the well-known size effect of concrete. The experimental results were in good agreement with performance-based prediction models, while they showed poor representativeness compared to current prescriptive models such as ACI 318-25.

# Chapter 1

# Introduction

## 1.1 Shear behavior of Plain Concrete

The analysis of the shear behavior of concrete elements has long been a topic of fundamental importance within structural engineering. Despite decades of research, the shear failure mechanism is still representing a challenge experimentally and numerically, test results present high deviation and, as a consequence, numerical prediction models must guarantee a high degree of conservatism. In an heterogeneous material such as the concrete, the main challenges arise from the large amount of parameters that can play a key role, such as concrete tensile strength, steel reinforcement ratio and grade, maximum aggregate size, and so on.

As experimentally observed, unreinforced PC members, as one-way slabs and beams, are characterized by a sudden and catastrophic shear failure mechanism which is directly related to their inability to withstand diagonal tension when shear loading is applied [1,2].

Throughout the years, various test configurations have been developed to directly assess the shear strength of small-scale samples as those commonly used for quality control purpose. These setups often incorporate geometric modifications, such as the introduction of one or more notches [3], to concentrate shear stresses in a specific section of the specimen. This resulted in the development of various specimen shapes, as well as challenges in interpreting experimental outcomes, and heterogeneous data. Furthermore, the direct

shear strength so measured proved to be poorly correlated with the real behavior of full-scale elements. Consequently, the experimental approach evolved to directly test elements of a representative size[4,5].

The experimental approach therefore focused on carrying out numerous investigations aimed at analyzing the behavior of all types of structural elements (i.e., beams, columns, floors, etc.). The variability of the proposed test setups and the resulting findings required the systematic data management, with the information collected into datasets[6] for analysis and for the development of new design formulas[7].

Among the experimental research conducted on horizontal elements (i.e., beams and one-way slabs), the study of Gaspar N. J. Kani certainly played a important role. One of his most important studies dates back to 1967, where the influence of the sample dimensions was analyzed and the validity of the design shear strength formula proposed by American Concrete Institute (ACI) was questioned[5]. The matter was addressed by testing several sets of beams with varying heights in the range between 305 to 1220 mm (12 to 48 in.) reinforced with with only flexural reinforcement. The beams were made with the same concrete recipe (i.e., nominal compressive strength), while longitudinal steel reinforcement ratio and grade were maintained nearly constant. For each effective depth, $d$, several shear-span to effective depth ratio, $a/d$, were also analyzed. The setup was a symmetrical 4-Points Bending Test (4PBT) according to the scheme proposed in Figure 1.1.

As discussed in the paper[5], the parameter $r_u$ namely the ratio between bending moment at failure, $M_u$, and numerical prediction, $M_{fl}$, was expected to decrease monotonically as the shear span $a$ decreased. As shown in Figure 1.2, where the $r_u$ is plotted against the height and the shear span-to-depth ratio, $a/d$, local minima were observed in the vicinity of $a/d = 2.5 \div 3.0$. For this reason, the region of $a/d$ between 2.5 and 3.0 is also known as *Valley of the critical failure* and researchers commonly use this parameter when designing test configurations of members subjected to flexural/shear loading.

In the same study, the influence of the beam width $b$ has also been evaluated. More precisely, the shear force at failure of two beams with overall width $b_0$ and 4 $b_0$ were compared, as shown in Figure 1.3. The results returned a scatter lower then 10% between

the shear force at failure of the beam with $b = 4\ b_0$ and four times that of the beam with width $b = b_0$. This deduction demonstrated that shear resistance is directly proportional to the width of the element.

Conversely, a certain non-linearity between the shear capacity and the beam height was observed. In fact, as shown in Figure 1.4, a decreasing trend can be noticed when plotting the average shear stress, $\tau$, expressed as the ratio between the shear force at failure, $V_u$, and the cross sectional area, $b_w \cdot d$ versus the beam height. More precisely, it is plotted the effective beam depth $d$ that is defined as the overall height $h$ minus the concrete cover up to the centroid of the longitudinal reinforcement. As shown, this phenomenon has been repeatedly observed also in more recent studies[4,8]. It is worth noting that only PC beam with $a/d$ between 2.5 and 3.0 are depicted for the sake of the comparison.

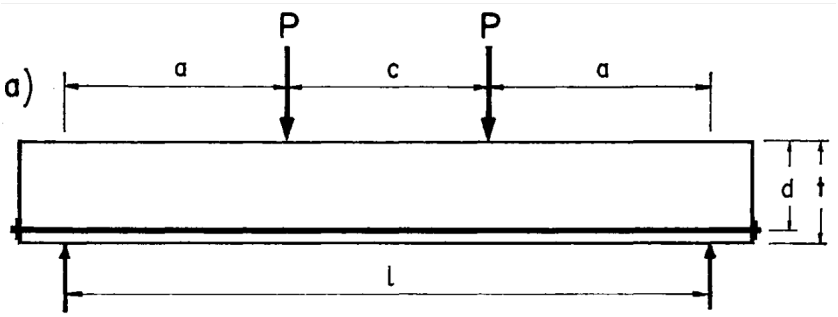



Figure 1.1. "Typical loading arrangement and cross sections of the four beam series" (Fig. 3a, Kani, 1967)[5]

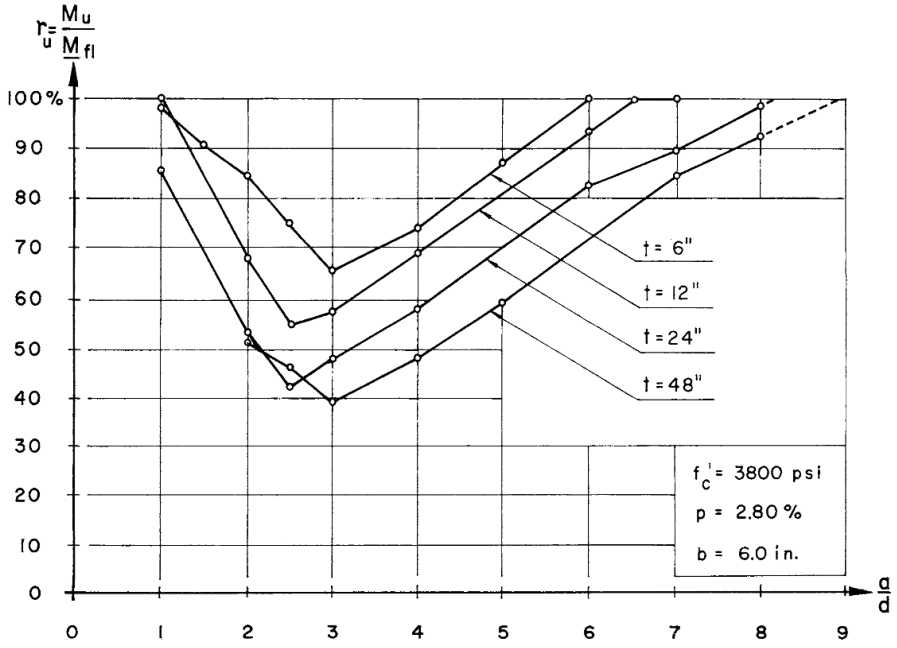



Figure 1.2. "Relative strength $r_u$ versus a/d reinforced concrete beams of various depths" (Fig. 5, Kani, 1967) [5]

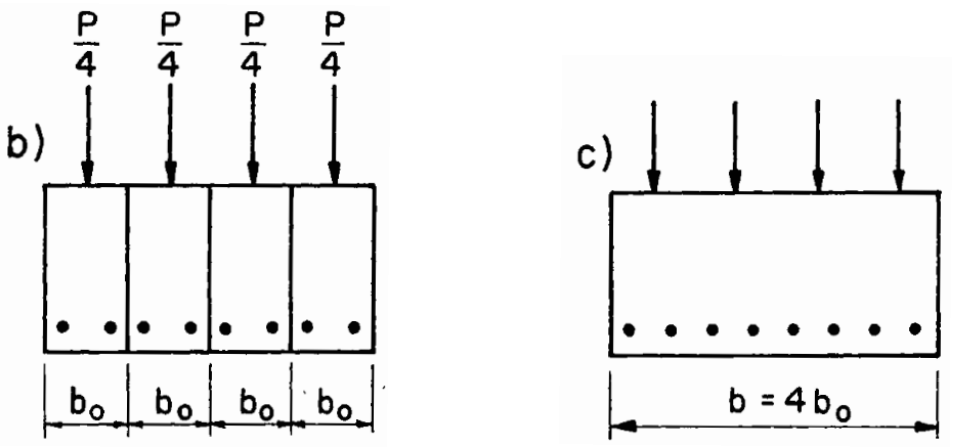



Figure 1.3. "Influence of beam width" (Details from Fig. 8, Kani, 1967) [5]

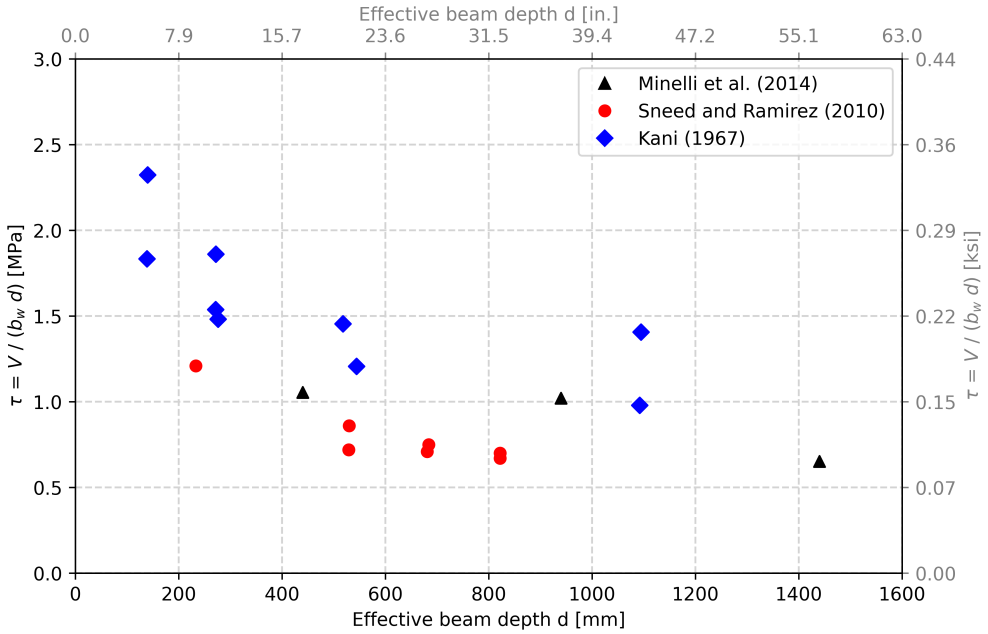



Figure 1.4. Average shear strength vs Effective beam depth with $2.5 \leq a/d \leq 3.0$ for PC from Kani (1967), Sneed et al.(2010), Minelli et al.(2014)[4,5,8]

The size-effect of PC remained a relevant topic of analysis over the years. More recently, Bažant et al.[6] studied this phenomenon by analyzing a database of 398 beams - named Evaluation Shear Database (ESDB) - characterized by beam depth in the range between 110 to 2000 mm (4.3 to 78.7 in.), without shear reinforcement and tested in either 3-Points Bending Test (3PBT) or 4PBT as depicted in Figure 1.5.

It resulted in the *energetic size-effect formula* (Equation 1.1) where $\nu_0 = V_c/b_w d$ represents the size-independent average concrete shear strength and $\nu_c$ the average shear strength affected by the size-effect.

The correlation between the two terms is expressed only respect to $d_0$, experimentally determined as a function of the maximum aggregate size, and the effective beam depth $d$ confirming the phenomenon.

$$\nu_c = \frac{\nu_0}{\sqrt{1 + d/d_0}} \tag{1.1}$$

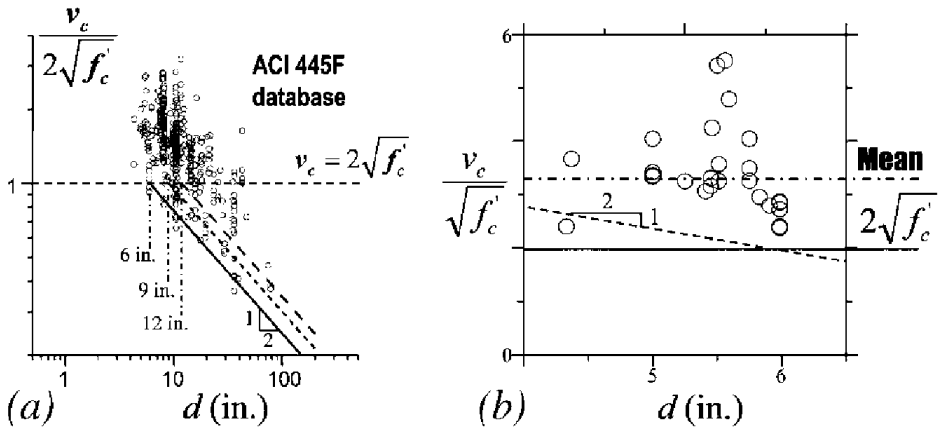



Figure 1.5. "Alternative simplified size effect formula compared with: (a) complete ESDB; and (b) small-size portion of that database in expanded scale." (Fig. 2, Bažant et al., 2007) [6]

In 2010, Sneed et al. discussed the *Influence of Effective Depth on Shear Strength of Concrete Beams* [4] respect to four basic mechanism of shear transfer:

- Shear stress in uncracked concrete (flexural compression zone)
- Interface shear transfer (aggregate interlock)
- Dowel shear action
- Arch action

## 1.2 Evolution of shear reinforcement

The longitudinal reinforcement is traditionally designed to absorb tensile stresses in the tension zone due to bending and, although it also contributes in part to the shear strength of the member, it is often unable to withstand all the shear stress.

For this reason, in order to prevent the formation of diagonal and arch cracks due to shear, dedicated shear reinforcement, commonly called stirrups, is introduced to ensure a more effective distribution of steel with respect to the inclination of the crack (Figure 1.6).

However, a large number of stirrups can cause excessive and very dense reinforcement in case of high shear actions making it difficult to pour concrete inside the element. For this reason, the use of a Steel Fiber-Reinforced Concrete (SFRC) can become an attractive

solution and has been the subject of numerous studies in recent decades.
The traditional shear reinforcement and confinement systems are beyond the scope of this thesis and thus will not be addressed.

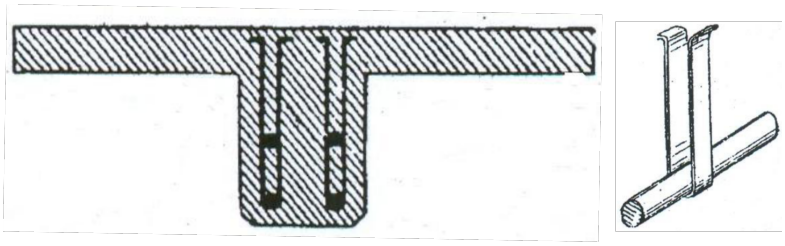


Figure 1.6. "Shape of stirrups at end of 19th century"
(Fig. 1.1, Ritter, *fib* Bulletin 57, 1899) [9,10]

The approach to the topic has evolved significantly, giving rise to a wide range of empirical and numerical models that aim to capture the complex mechanisms governing shear resistance. The earliest documented reference to shear reinforcement dates back to 1899, when Whilhem Ritter discussed the use of steel strips as stirrups in reinforced concrete structures [9,11] already highlighting the key role of bond and anchorage capacity.

Few years later, in 1908, Emil Mörsch introduces the concept of simple and multiple truss systems - nowadays called *strut-and-tie* model - characterized by a constant inclination of the compressive strut at 45 degrees as illustrated in Figure 1.7 and more then 50 years later, in 1962, Donald H. Kupfer proposed a variation of the strut angle to ensure the yielding of the longitudinal reinforcement based on the principle of the minimum deformation work. [12,13]

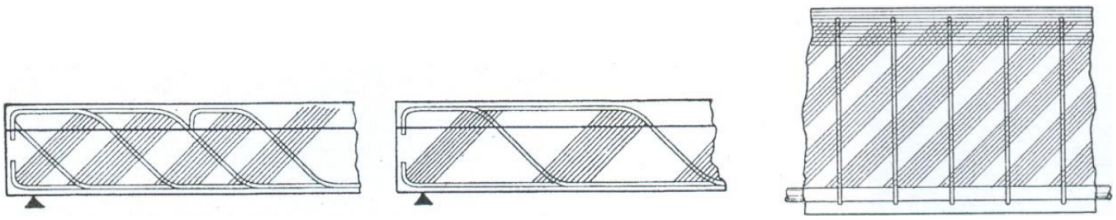


Figure 1.7. "Simple or multiple truss systems with bent-up bars and with stirrups
(Mörsch, 1908)" (Fig. 1.4, *fib* Bulletin 57, 2010) [10,12]

Frank J. Vecchio and Michael P. Collins made a significant contribution in 1986 by introducing the Modified Compression-Field Theory (MCFT)[14]. This model formalizes the behavior of Reinforced Concrete (RC) under shear through three sets of equations - equilibrium, compatibility, and stress–strain relationships - introducing a variable cracking angle $\theta$ along the beam length and describing the shear resistance as the combination, basically the sum, of the ability of the cracks to transmit the shear stress ($V_c$) and the contribute of the shear reinforcement ($V_s$).
The model formalises how the the assumption of sections remaining plane is no longer valid in the proximity of point loads or and end-restraints and, according to the the Walraven's study[15], how the maximum aggregate size $a_g$ defines an upper bound for shear stress transmission across crack interfaces. The use of this, or similar models, still forms the basis of various predictive models (e.g., *fib* Model Code 2020 (MC2020)).

Recent research continues to refine these models, incorporating real test results and introducing new relevant parameters to obtain a description that is as consistent and robust as possible. The transition, over the years, from purely empirical formulations to hybrid empirical-theoretical approaches reflects the improvement needed for reliable design tools that can accommodate more performing and advanced materials other then more complex scenarios.

Understanding shear behavior remains critical not only for ensuring structural safety but also for optimizing design efficiency, particularly in applications where traditional reinforcement strategies may be limited or impractical. As such, the study of shear capacity represents a dynamic and evolving field, bridging historical insights with modern engineering challenges.

## 1.3 Fiber-Reinforced Concrete (FRC)

### 1.3.1 Introduction to FRC

*"Since ancient times, fibers have been used to reinforce brittle materials. Straw was used to reinforce sun-baked bricks, and horsehair was used to reinforce*

*masonry mortar and plaster. A pueblo house built around 1540, believed to be the oldest house in the U.S., is constructed of sun-baked adobe reinforced with straw..."*[16]

The FRC is a composite material characterized by the presence of discrete, generally randomly distributed fibers throughout the concrete matrix with the objective of improving critical PC issues such as brittleness, crack propagation, impact resistance (energy absorption) and durability by increasing flexural strength tensile strength, ductility and toughness.

Several types of fibers are commercially available worldwide depending on their intended use with specific mechanical properties and benefits (Table 1.1 and Figure 1.8).

Table 1.1. "Physical properties of some fibers" (Table 6, Löfgren, 2005)[17]

| Type of Fibre | Diameter [μm] | Specific gravity [g/cm$^3$] | Tensile strength [MPa] | Elastic modulus [GPa] | Ultimate elongation [%] |
|---|---|---|---|---|---|
| **Metallic** | | | | | |
| Steel | 5-1 000 | 7.85 | 200-2 600 | 195-210 | 0.5-5 |
| **Glass** | | | | | |
| E glass | 8-15 | 2.54 | 2 000-4 000 | 72 | 3.0-4.8 |
| AR glass | 8-20 | 2.70 | 1 500-3 700 | 80 | 2.5-3.6 |
| **Synthetic** | | | | | |
| Acrylic (PAN) | 5-17 | 1.18 | 200-1 000 | 14.6-19.6 | 7.5-50.0 |
| Aramid (e.g. Kevlar) | 10-12 | 1.4-1.5 | 2 000-3 500 | 62-130 | 2.0-4.6 |
| Carbon (low modulus) | 7-18 | 1.6-1.7 | 800-1 100 | 38-43 | 2.1-2-5 |
| Carbon (high modulus) | 7-18 | 1.7-1.9 | 1 500-4 000 | 200-800 | 1.3-1.8 |
| Nylon (polyamide) | 20-25 | 1.16 | 965 | 5.17 | 20.0 |
| Polyester (e.g. PET) | 10-8 | 1.34-1.39 | 280-1 200 | 10-18 | 10-50 |
| Polyethylene (PE) | 25-1 000 | 0.96 | 80-600 | 5.0 | 12-100 |
| Polyethylene (HPPE) | - | 0.97 | 4 100-3 000 | 80-150 | 2.9-4.1 |
| Polypropylene (PP) | 10-200 | 0.90-0.91 | 310-760 | 3.5-4.9 | 6-15.0 |
| Polyvinyl acetate (PVA) | 3-8 | 1.2-2.5 | 800-3 600 | 20-80 | 4-12 |
| **Natural - organic** | | | | | |
| Cellulose (wood) | 15-125 | 1.50 | 300-2 000 | 10-50 | 20 |
| Coconut | 100-400 | 1.12-1.15 | 120-200 | 19-25 | 10-25 |
| Bamboo | 50-400 | 1.50 | 350-50 | 33-40 | - |
| Jute | 100-200 | 1.02-1.04 | 250-350 | 25-32 | 1.5-1.9 |
| **Natural - inorganic** | | | | | |
| Asbestos | 0.02-25 | 2.55 | 200-1 800 | 164 | 2-3 |
| Wollastonite | 25-40 | 2.87-3.09 | 2 700-4 100 | 303-530 | - |

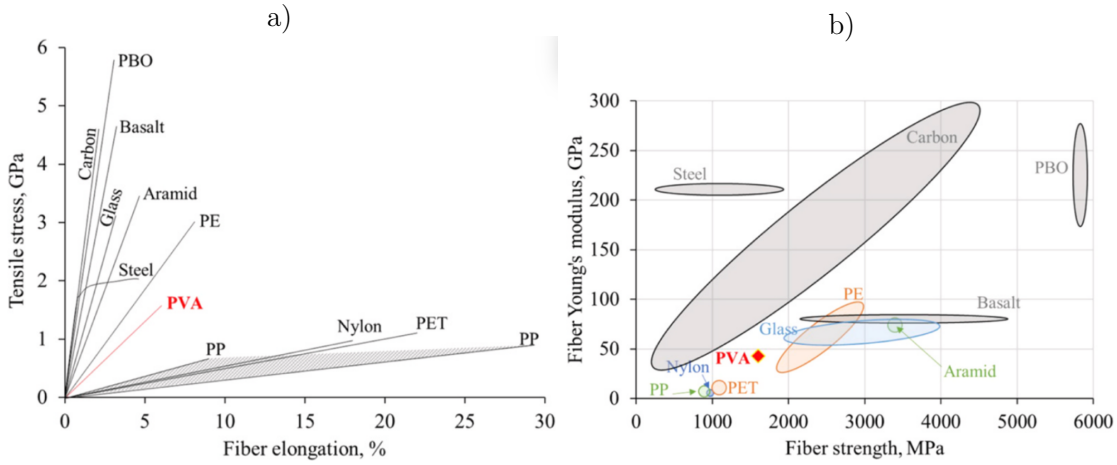



Figure 1.8. a)"Tensile stress vs elongation of various fibres" (Fig. 5, Pham, 2025); b)"Fibre tensile strength vs Young's modulus" (Fig. 6, Pham, 2025) [18,19]

The classification of fibers naturally varies according to different standards. Both European Committee for Standardization (CEN) and American Society for Testing and Materials (ASTM) define the production techniques as a primary criterion.

EN 14889-1 [20] identifies five groups:

- Group I - Cold-drawn wire
- Group II - Cut sheet
- Group III - Melt extracted
- Group IV - Shaved cold drawn wire
- Group V - Milled from blocks

and ASTM A820 [21] four types:

- Type I - Cold-drawn wire
- Type II - Cut sheet
- Type III - Melt-extracted
- Type IV - Other fibers

Nonetheless, several key parameters must be considered depending on the intended application, among which:

- length
- (equivalent) diameter

- aspect ratio (i.e. ratio of length to equivalent diameter)
- fiber shape (see Figure 1.9)
- density
- tensile strength
- elastic modulus
- ductility
- coating (if applicable)

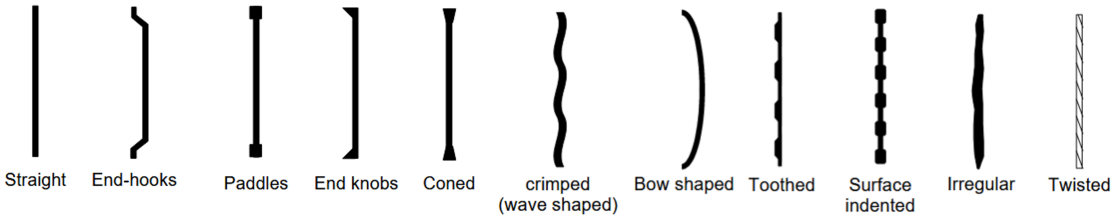



Figure 1.9. "Examples of some typical fibre geometries" (Figure 10, Löfgren, 2005) [17]

The significant changes in the material's properties are primarily attributed to the so-called *bridging effect* provided by the fibers in the presence of a crack. Unlike PC, where a crack leads to a complete separation, the two extremities remain connected, allowing continued stress transmission. This mechanism generally results in enhanced performance and increased energy absorption required for crack propagation. Several failure mechanisms may take place directly affecting the matrix (e.g. matrix cracking), the fibers (e.g. fiber yielding) and the interaction among them (e.g. fiber pull-out, sliding friction) as reported in Figure 1.10 which translates directly in several variables and contributions to take into account.

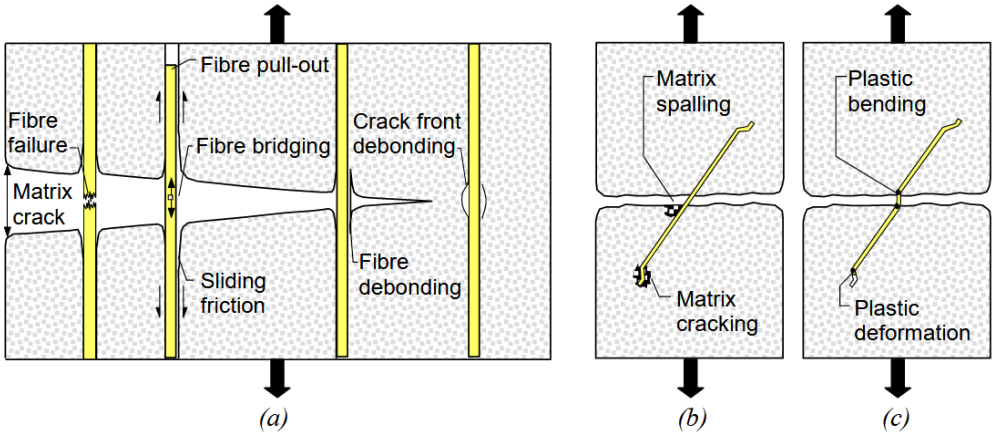



Figure 1.10. "(a) A schematic illustrating some of the toughening effects and crack front debonding, the Cook-Gordon effect (Cook and Gordon, 1964), and debonding and sliding in the crack wake. (b) Matrix spalling and matrix cracking. (c) Plastic bending (deformation) of inclined fibre during pullout – both at the crack and at the end-anchor" (Figure 19, Löfgren, 2005) [17,22]

The fiber bridging mechanism can be enhanced by several contributing factors. The high modulus of elasticity of steel fibers directly influences stress transfer, thereby improving peak flexural strength and post-peak behavior due to increased resistance to crack initiation [18,23,24]. The geometry of the fibers plays a crucial role in mechanical interlocking: straight fibers are more susceptible to pull-out compared to those with more complex shapes. Conversely, fibers with low tensile strength may rupture even when properly anchored to the matrix [18,25–29]. The evident increase in toughness compared to PC is clearly illustrated in Figure 1.11, which depicts the typical and expected behavior of this material.

Nevertheless, although the general rule suggests that an higher fiber dosage leads to reduced cracking and improved bridging performance, it is essential to consider the associated drawbacks, particularly those affecting the fresh-state properties of the composite material. These risks may include reduced workability, increased viscosity, increased porosity, and potential issues with fiber dispersion, all of which can compromise the overall quality and consistency of the mix [18,30,31].

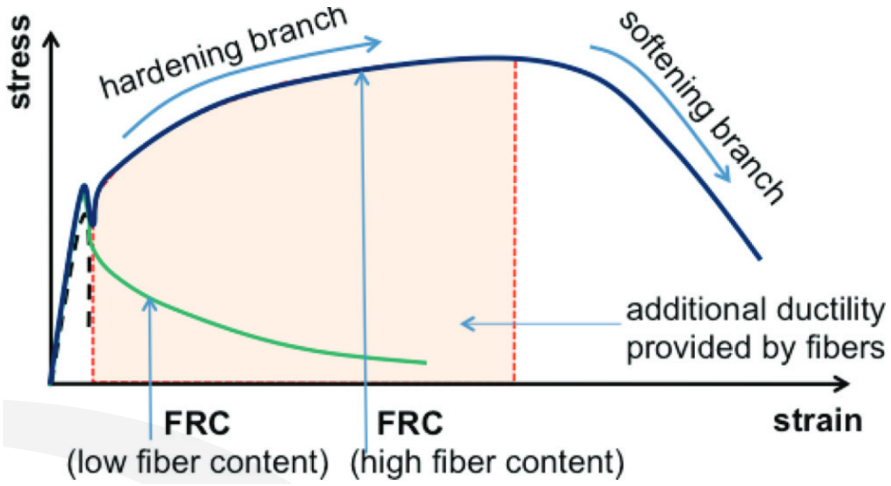



Figure 1.11. "Fiber contribution to tensile/flexural performance, obtained from flexural test, showing softening and hardening behaviors"
(Fig. 3.4b, ACI 544.4R, 2018) [16]

From a practical perspective, the use of fiber-reinforced composites presents a notable opportunity to reduce on-site labor requirements and to mitigate the reinforcement congestion. This is primarily due to the potential decrease in the need for conventional reinforcing bars, both longitudinal and shear one, provided that appropriate measures have to be taken to ensure uniform fiber integration, distribution and orientation. Such systems may also prove advantageous in specific structural scenarios, particularly where the reduction or elimination of shear reinforcement is desirable. In these cases, fibers can help mitigate reinforcement congestion, which often complicates placement and affects construction efficiency. Overall, the adoption of fiber-reinforced solutions can lead to meaningful reductions in labor time and associated costs, while improving constructability and performance in targeted applications.

### 1.3.2 Mechanical characterization - Testing methods

The mechanical characterization of the FRC is both based on standard tests specific for the PC and specifically developed testing methods to highlight the different response of these two materials.

### Compressive Strength

The compressive strength $f'_c$ is not significantly affected by a moderate addition of fibers in the pre-peak behavior while their contribution can be analyzed (Figure 1.12) [32,33]. According to EN 12390-3 [34] and ASTM C39 [35], this parameter is defined considering the maximum axial force applied at a constant speed rate up to failure on cubical or cylindrical samples with fixed geometry. The compressive strength $f'_c$ is established through:

$$f'_c = \frac{F}{A_c} \tag{1.2}$$

where

- $F$ is the maximum axial compressive force
- $A_c$ is the cross-sectional area of the specimen on which the compressive force acts

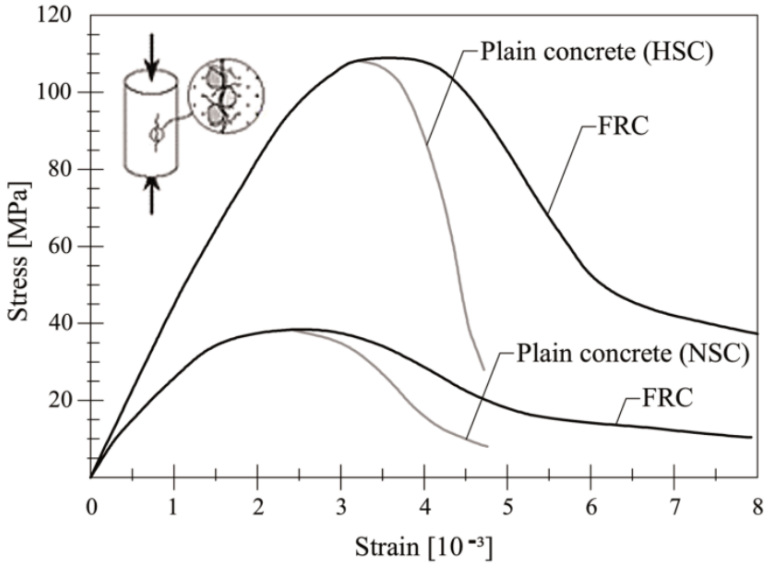



Figure 1.12. "Main differences between plain and fibre reinforced concrete having both normal and high strength under uniaxial compression"
(Figure 18.2-1, MC2020, 2012) [33]

### Elastic Modulus

The elastic modulus $E_C$ is related to the response of the material in the elastic domain evaluated in compression and therefore the influence of fibers is not significant in this case either.

EN 12390-13[36] provides two definitions for the elastic modulus obtained by testing a cylindrical sample with strain gauges positioned diametrically opposite each other. The initial one, $E_C$ (Figure 1.3), and the stabilized one, $E_{C,S}$ (Figure 1.4). The test consist in running a specific loading cycle whose upper stress levels are defined as a given percentages of the compressive strength $f'_c$ which guarantee remaining in the elastic domain of the material:

$$E_{C,0} = \frac{\Delta\sigma}{\Delta\varepsilon_0} = \frac{\sigma_a^m - \sigma_b^m}{\varepsilon_{a,1} - \varepsilon_{b,0}} \tag{1.3}$$

$$E_{C,S} = \frac{\Delta\sigma}{\Delta\varepsilon_S} = \frac{\sigma_a^{\mathrm{m}} - \sigma_b^{\mathrm{m}}}{\varepsilon_{a,3} - \varepsilon_{b,2}} \tag{1.4}$$

where

- $\sigma_a^{\mathrm{m}}$ is the measured stress corresponding to nominal upper stress
- $\sigma_a^{\mathrm{m}}$ is the measured stress corresponding to nominal lower stress
- $\varepsilon_{a,n}$ is the average strain at upper stress on loading cycle n
- $\varepsilon_{b,n}$ is the average strain at lower stress on loading cycle n

With a similar setup, ASTM C69[37] imposes to load the specimen twice. The first one guarantee the seating of the gauges while the second provides for a constant stress loading speed of up to 40% of $f'_c$ computed according to ASTM C39[35]. The Elastic modulus $E$ is computed as:

$$E = \frac{S_2 - S_1}{\epsilon_2 - \epsilon_1} \tag{1.5}$$

where

- $S_2$ is the stress corresponding to 40% of $f'_c$
- $S_1$ is the stress corresponding to $\epsilon_1$

- $\epsilon_2$ is the longitudinal strain produced by $S_2$
- $\epsilon_2$ is the longitudinal strain of 50 millionths

### Direct Tensile Strength

The tensile strength is unquestionably the main parameter needed to properly determine the mechanical contribution of FRC either pre- and post-cracking. Similarly to steel reinforcement, the Direct Tensile Test (DTT) is ideally the optimal testing method to assess it. However, the technical complexities involved in accurately performing this test have limited their use to academic purposes only, making it difficult to implement for quality control processes at industrial scale. In addition, due to the limited dimensions of the samples which smaller sides remain in the range between 13 and 50 mm (0.51 to 1.97 in.), DTT is mostly suitable for concretes with small coarse aggregates and maximum fiber length of 13÷15 mm (respectively, 0.04 to 0.12, 0.51 to 0.59 in.). Indeed, DTT are nowadays standardized and effectively used only for Ultra High-Performance Fiber-Reinforced Concrete (UHPFRC) (e.g., JSCE 2008[38], SIA 2052[39], and AASHTO T-397[40]).

By way of example, the DTT proposed by JSCE 2008 is herein described more in details. The test is performed on a dogbone-shape sample in order to intensify the stress in the central region inducing a controlled crack. Two Linear Variable Differential Transformers (LVDTs) are placed diametrically opposite as described in Figure 1.13 and the mean value of deformation is considered constant across all the section for which the tensile strength $f_{ti}$ can be expressed, analogously to the compressive strength, as:

$$f_{ti} = \frac{F_t}{A_0} \tag{1.6}$$

where

- $F_t$ is the maximum axial tensile force
- $A_0$ is the central cross-sectional area on which the tensile force acts

In reality, it is difficult to observe the same displacement at opposite ends of the crack

due to the eccentric application of the load. This imprecision induces a non-constant stress distribution across the section which could even result in a compressed region inducing a material response that is clearly different from the desired one. Thus, the main challenge of the test lies in eliminating any eccentricity to ensure a uniform tensile response. A further limitation is the possibility the crack may not occur in the central region, invalidating the outcome as it is outside the area controlled by the LVDTs.

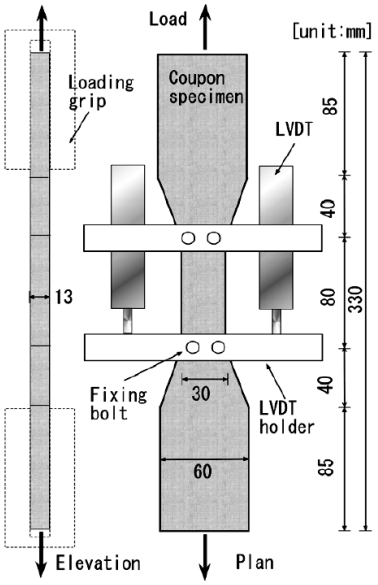



Figure 1.13. "Outline of uniaxial tension test" (Fig. T2.3.1, JSCE 2008, 2008) [38]

### Flexural Strength

Due to the relative simplicity of performing the flexural tests, these methods are commonly used for characterizing conventional FRC and HPFRC. Indeed, it is possible to determine the tensile strength through an inverse analysis starting from the flexural state, that is a combination of compression and tension.

These tests have made it easier (from a technical point of view) to characterize these types of materials, which are known to be made with aggregates as large as 16 mm (0.63

in.) and fiber length up to 60 mm (2.36 in.). As a matter of the fact, flexural tests are usually performed on prismatic samples with grater dimensions than DTT minimizing the influence of aggregate size and fiber length.

EN 14651 [41] and ASTM C1609 [42] propose similar approaches in the determination of the so-called residual flexural strength. EN 14651 is performed on notched beams under a 3PBT configuration (Figure 1.14). It measures the Crack Mouth Opening Displacement (CMOD) of the saw-cut notch realized at midspan and the applied load. The notch has the function of localizing the stresses in the midspan section, whereas the load $F$ is applied by means of a controlled crack-opening or midspan-deflection rate (namely displacement-controlled), as shown in Figure 1.15. The section is considered to remain plane with a linear stress distribution for which the flexural stress $\sigma_{fl}$ can be computed as:

$$\sigma_{fl} = \frac{3}{2} \cdot \frac{F_j \, l}{b \, h_{sp}^2} \tag{1.7}$$

where

- $F_j$ is the load corresponding with CMOD = CMOD$_j$
- $l$ is the span length
- $b$ is the width of the specimen
- $h_{sp}$ is the distance between the tip of the notch and the top of the specimen

The relevant parameters for design are defined as follows. The test measures the flexural stress at the Limit of Proportionality (LOP) identified as $f_L$:

$$f_L = max(\sigma_{fl})\Big|_{CMOD \leq 0.05mm} \tag{1.8}$$

In addition, the residual flexural strengths $f_{R,j}$ are the values of $\sigma_{fl}$ computed at specific values of CMOD$_j$, with $j$ from 1 to 4 correspondent, respectively, to CMOD equal to 0.5, 1.5, 2.5 and 3.5 mm.

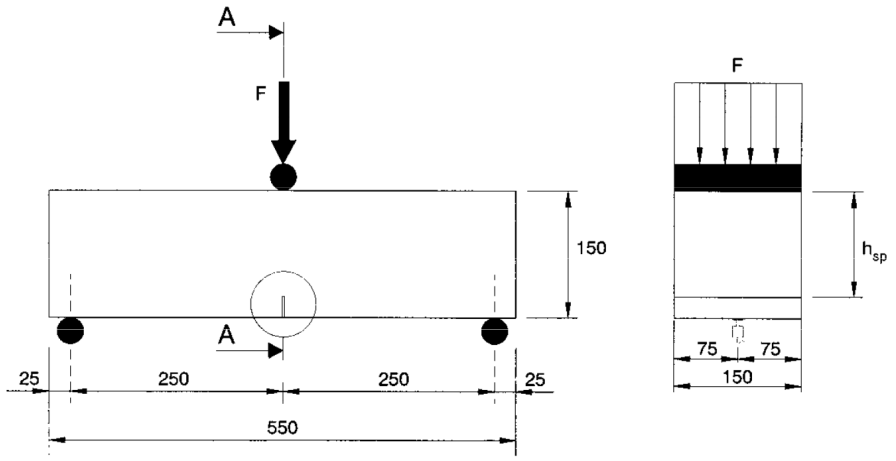



Figure 1.14. "Typical arrangement for measuring CMOD" (Figure 4, EN 14651, 2005) [41]

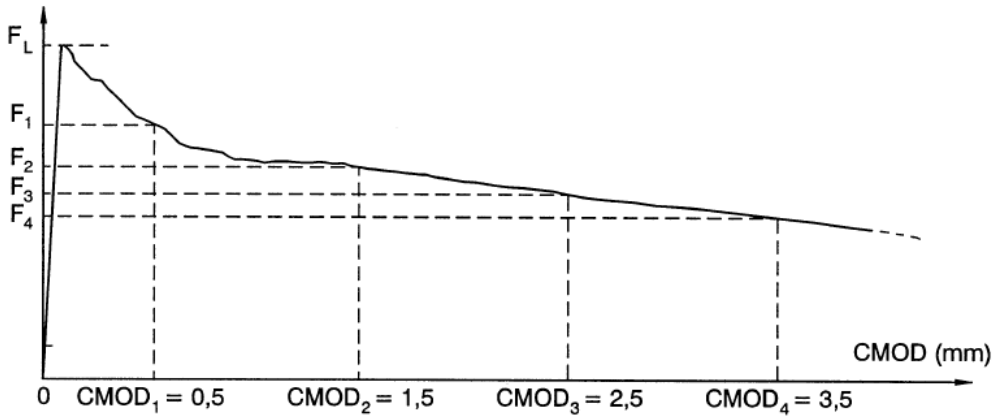



Figure 1.15. "Load-CMOD diagram and $F_j$" (Figure 7, EN 14651, 2005) [41]

Similarly, ASTM C1609 considers an un-notched beam in 4PBT (Figure 1.17) where the residual flexural strength is computed with the same assumption that is linear stress distribution in the section. Due to the change in the test configuration (i.e., 4PBT instead of 3PBT), the flexural strength is computed as:

$$\sigma_{fl} = \frac{P\,L}{b\,d^2} \tag{1.9}$$

where

- $P$ is the load

- $L$ is the span length
- $b$ the average width of the specimen at the fracture, as oriented for testing
- $d$ is the average depth of the specimen at the fracture, as oriented for testing

The absence of the notch induces a variability in the effective position of the main crack and sometimes greater variability in results. The test is considered valid only when the main crack is located in the middle third of the span.
Similarly to EN 14651, the main parameters for design are the first-cracking flexural strength $f_{1^{st}peak}$ and the residual flexural strength at $L/600$, $L/300$, and $L/150$ with the span length $L$ expressed in mm. Other parameters such as the toughness $T_j^D$, computed as the area under the load vs. net deflection curve, can be relevant for design purposes.

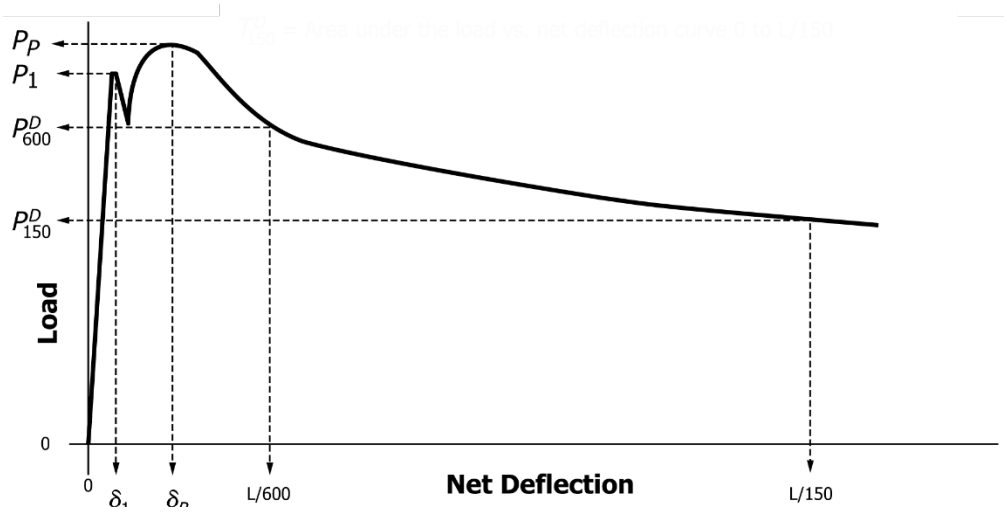



Figure 1.16. "Example of Parameter Calculations when Peak Load is Greater than First-Peak Load (Not to Scale)" (FIG. 5, ASTM C1609, 2024) [42]

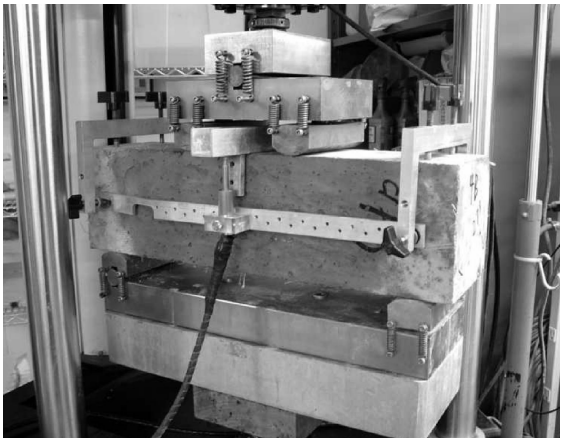


Figure 1.17. "Arrangement to Obtain Net Deflection by Using Two Transducers Mounted on Jig Secured to Specimen Directly Above Supports" (FIG. 2, ASTM C1609, 2024)[42]

The relation between the flexural strength and the DTT is discussed in MC2020[33]. After the elastic phase, the FRC can respond with a softening or an hardening behavior. *In the case of softening behaviour (a) the deformations localise in one crack. In the case of hardening behaviour (b) multiple cracking occurs before reaching the peak value. [...] A FRC with softening behaviour in tension can develop hardening behaviour in bending. A FRC with softening behaviour in bending can exhibit a monotonically increasing load in the structure*[33] as reported in Figure 1.18. Whereas, strain-hardening materials in DTT always shows deflection-hardening behavior in flexural testing. However, the strain-hardening response observed in flexural testing does not guarantee the reverse, as it may be associated with strain-softening one in DTT.

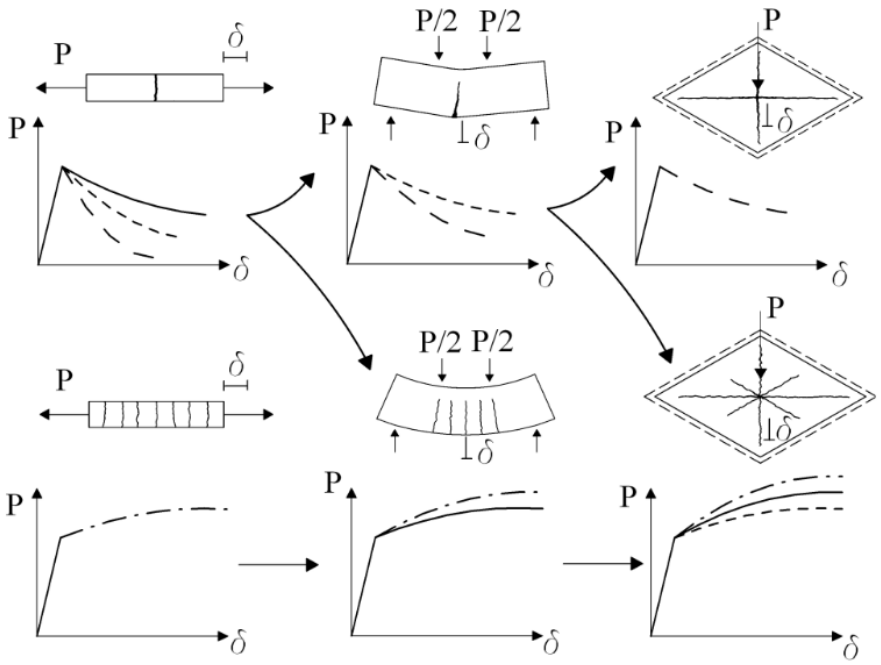



Figure 1.18. "Different response of structures made of FRC having a softening or hardening behaviour under uniaxial tension or bending loads" (Figure 18.2-11, MC2020, 2020) [33]

### Direct Shear Strength

Over the years, the evaluation of the shear capacity of SFRC has lacked a universally accepted definition. Several setup configurations have been proposed with the purpose of inducing a controlled cracking surface, which served as basis for corresponding analytical model. A comprehensive overview of these approaches is provided by Shoaib (2012) [43] and more recently by Sahlab et al. (2024) [44]. A review of the test configurations on non-standardized specimens is depicted in Figure 1.2 [1,44–53].

The prevailing approach involves introducing a notch in the sample to concentrate the stresses along a predefined surface, tereby converting compressive stresses into tangential ones. However, this approach remains complex for the shear evaluation due to the difficulty of unequivocally achieving a representative shear failure. Moreover, factors such as aggregate size, fiber cross-sectional area and section depth could directly influence the results, particularly when dealing with reduced dimensions.

Table 1.2. "State of the art of shear testing method found in literature" (Table 1, Sahlab et al., 2024) [44]

| Test type | Test method | Specimen | Reference | Shear strength | Advantages | Challenges |
|---|---|---|---|---|---|---|
| Reinforced Z(S)-type specimen | Direct shear |  | (Valle & Büyüöztürk, 1993) [3] (Trindade, et al., 2021) [5] | $\tau = \frac{P}{A_s}$ | Simple load application | Complex reinforcement required |
| JSCE SF6 | Direct shear |  | JSCE SF6 (Tonon, 2021)[18] (Mirsayah & Banthia, 2002) [17] | $\tau = \frac{P/2}{A_s}$ | Simple sample and load application | Shear failure is not always guaranteed |
| Uniaxial compression / Brazillian | Tensile and compressive |  | (Sivakugan, et al., 2014) [10] | $\tau = \frac{\sigma_t(2-\sin\phi)}{\cos\phi}$ | Standard samples and tests | Not suitable for FRC |
| Shear box | Combined shear and compression |  | (Meng, et al., 2018)[15] (Lelovic & Vasovic, 2020) [16] | $\tau = \frac{P\sin\gamma}{A_s}$ | Complete shear properties of concrete can be obtained | Relatively complex molds |
| Double notched cylinder | Direct shear |  | (Barr & Derradj, 1990) [11] (Barr & Hasso, 1986) [12] (De Souza, et al., 2019) [13] | $\tau = \frac{P}{A_s}$ | Quick, Standard samples and simple load application | Difficulty in introducing the notches |
| Double Edge notched beam | Direct shear |  | (Barr & Derradj, 1990) [11] (Barr & Hasso, 1986) [12] (De Souza, et al., 2019) [13] | $\tau = \frac{P}{A_s}$ | Quick, Standard samples and simple load application | Difficulty in introducing the notches, Mixed mode failure |

### 1.3.3 Up-To-Date datasets of SFRC beams under shear loading

In light of these constraints, the longitudinally-reinforced beam remains the most widely adopted test as it provides a representative response of full-scale element [7,54]. However, significant criticalities persist, including non-homogeneous arrangement of the longitudinal reinforcement, risk of local tensile failures in the proximity of the loading point and uneven distribution of the strains, as described by Zarrinpour and Chao [54].

In 2006, Gustavo J. Parra-Montesinos collected one of the first database containing 147 SFRC and 45 RC. He emphasized the importance of cracking distribution, crack width, and aggregate interlock highlighting how the beneficial effect of the fibers is much more evident up to $V_f$=0.75%. An higher percentage still induces an increment in strength but with a lower effectiveness [55].

An updated version of this database dated back to 2010 in Chapter 15 of *fib* Bulletin 57 [10]. Respect to the previous publication, the criteria adopted remained basically the same except for the exclusion of the crimped fibers, the removal of the limitation to fiber

tensile strength and the new range for the beam depth (from the previous between 180 mm to 570 mm). A total of 84 SFRC beams - 59 from literature and 25 from this last investigation - were filtered resulting in these distribution ranges:

- shear span-to-depth ratio ($a/d \geq 2.5$)
- beam depth $h$ between 230 mm and 685 mm
- longitudinal reinforcement ratio $\rho$ between 1.2% and 4.5%
- concrete cylinder strength $f_c$ between 20.7 MPa and 104 MPa
- hooked steel fibres in volume fractions ranging between 0.5% and 2%
- fibre tensile strength $\geq$ 1030 MPa
- fibre length-to-diameter ratio between 55 and 100

More recent shear strength prediction models were based on standard performance-based properties, as the residual flexural strength defined as outlined in Section 1.4. These design equations[16,33,56] are typically proportional to the residual flexural strength, whereas others[57] consider these parameters as part of compliance criteria at quality control stage only.

Fausto Minelli, Giovanni A. Plizzari et al. made a significant contribution to the final draft of *fib* Model Code 2010 (MC2010)[8,58–62]. In particular, they addressed the size-effect in a manner opposite to Kani[5] mantaining a constant ratio $\frac{a}{d}$ while varying span length, longitudinal reinforcement, beam depth, and fiber volume fraction. The tests indicated that the fibers mitigate - but do not eliminate - the size-effect.
In case of FRC *"it is quite difficult to properly define a stabilized crack stage: the development of new shear cracks continues up to the failure and a more distributed crack patter forms, with narrower and closely spaced cracks"*[8] and the residual flexural performances of the material have to be considered.

Several other studies focus on this phenomenon confirming such behavior. At shear failure, the SFRC is characterized by wider and longer cracks respect to the PC. This comparison suggests that the bridging mechanism provided by the fibers is more relevant respect to the interlock, which is function of the maximum aggregate size[54,63,64].

In 2018, Estefanía Cuenca et al.[65] presented a *material-performance-based* database collecting data in the period from 1985 to 2016 and the lack of fundamental mechanical parameters was already marked out in Figure 1.19. In addition to the 58 tests performed on FRC, a further 64 tests on PC were conducted with the explicit aim of enabling a comparative analysis between the two matrices, for a total of 122 samples.

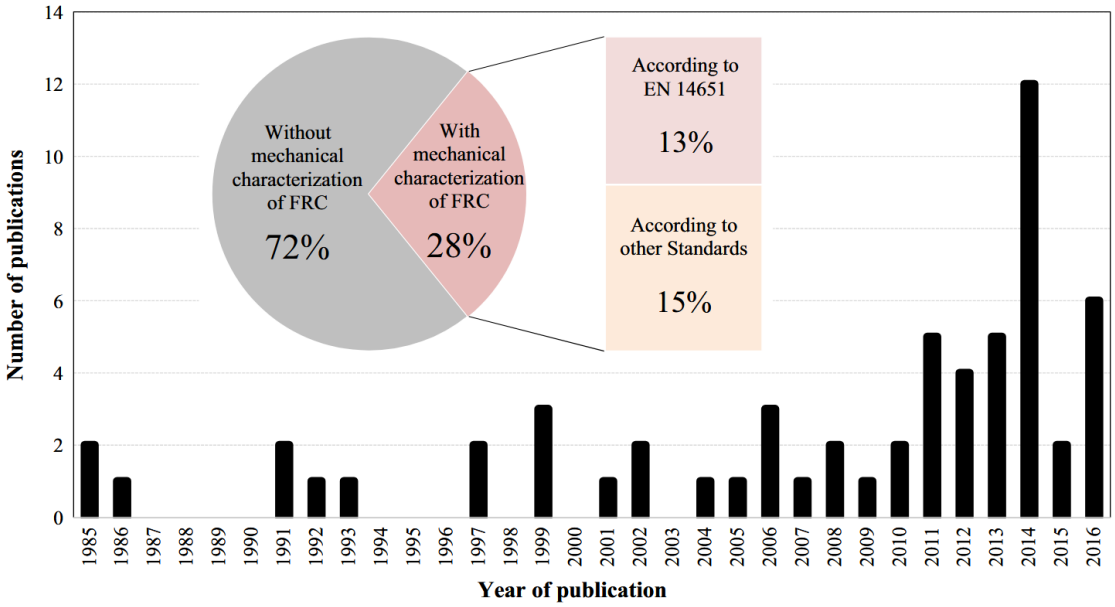



Figure 1.19. "Papers about shear behavior on FRC beams"
(Fig. 1, Cuenca et al., 2018)[65]

In 2025, the dataset compiled by Alcocer et al.[66] was employed to evaluate the validity of the shear design formula proposed in ACI 318-19[57,67]. Two major limitations were identified: the absence of explicit consideration of size-effects and the reliance on a relatively narrow database. Within this framework, 340 SFRC beams exhibiting pure shear failure were selected based on ten stringent criteria:

I. Deformed steel fibers conforming to ASTM A820[21]

II. Steel-fiber aspect ratio in the range 50 to 100

III. Nonprestressed rectangular cross sections

IV. *Shear-dominated specimens* (i.e. collapse due to shear) and no axial load applied

V. No shear reinforcement (e.g. stirrups)

VI. Concrete compressive strength $f'_c \leq 10{,}000\ psi$ $(69\ MPa)$

VII. Normal-Weigth Concrete (NWC) and Lightweight Concrete (LWC)

VIII. 4PBT, 3PBT and spcial load configurations

IX. Slender beams $(a/d \geq 2.5)$

X. Specimens loaded monotonically under quasi-static conditions

However, despite the identification of a relevant number of tests, notable limitations remained concerning with specific reference to points VI and IV. Additionally, the distribution across other variables revealed significant imbalances with particular reference to overall depth, $h$, and of the Fiber Volume Fraction, $V_f$ (Figure 1.20).

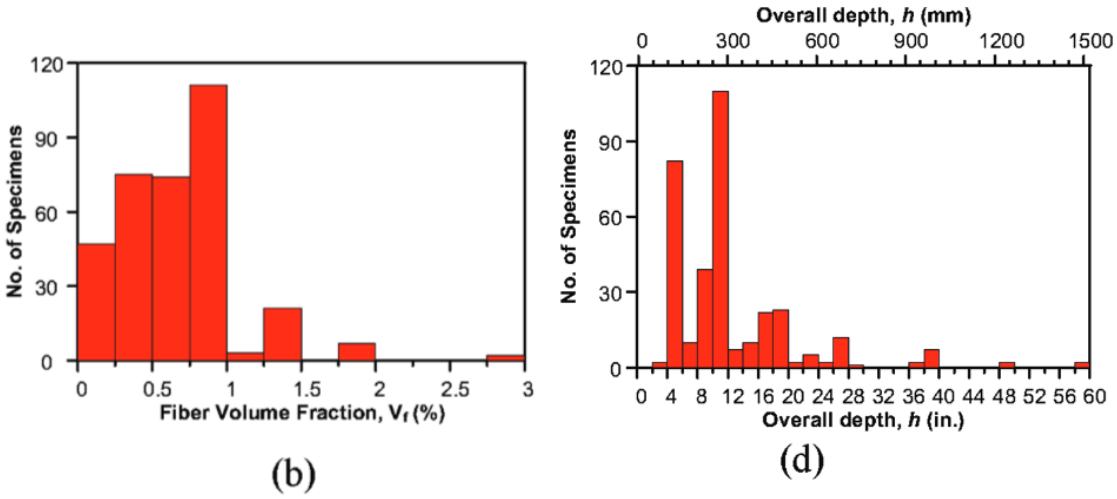



Figure 1.20. "Data set description; distribution of: [...] (b) steel fiber-volume ratio, $V_f$; [...](d) beam overall depth h"(Fig.1, Alcocer et al., 2025) [66]

The databases proposed by Cuenca et al.[65] and by Alcocer et al.[66] are taken as reference and filtered to only consider the beams characterized by shear failure mechanism resulting in 122 tests (58 FRC + 64 PC) from the first one and 340 FRC ones from the second one. All the tests considered are summarized in Figure 1.21 and Figure 1.22

The datasets are initially analyzed by examining their distribution with respect to variables deemed most relevant. This approach aims to identify sparsely populated regions, with the intention of contributing to their description through this experimental

campaign. Such enrichment enables a more robust evaluation of model performance across broader application scenarios. As indicated in Figure 1.23 from (a) to (l), the parameters considered include:

Effective depth $d$

Both the databases present a significantly higher concentration of tested beams at low value of this parameter. In particular in Alcocer et al.'s one the samples below 299 mm (11.8 in.) are 251 (74%) of which 106 below 199 mm (7.8 in.). Cuenca et al. presents instead a uniform distribution in the ranges 450-599 mm (17.7-23.6 in.), 300-449 mm (11.8-17.7 in.) and 200-299 mm (7.9-11.8 in.) respectively with 34, 34 and 33 results (83% of the total) without any lower value.

Maximum aggregate size $D_{max}$ and Compressive strength $f'_c$

The distribution of the maximum aggregate diameter and the compressive strength clearly describes the substantial deficiency of High-Performance Concretes (HPCs). With Cuenca et al., all the diameters are limited in the range 12-24 mm (0.5-0.9 in.) of which only 17% strictly lower then 16 mm whereas the second database reports 56 values lower then 12 mm (0.5 in.) of which 4 lower then 8 mm (0.3 in.). However, it should be noted that almost half of these Alcocer et al.'s data are not available (152 samples, 45%). The distribution is more uniform in terms of compressive strength, but with a concentration of values below 50 MPa (7.3 ksi) higher then 80% in both the series where only Cuenca et al. covers, albeit to a minimal extent, values higher then 70 MPa (10.2 ksi).

Type and Volume of steel fibers $V_f$

The choice of fiber type shows a strong preference, with both databases favoring a greater focus on Hooked-End (HE) fibers (Alcocer et al. 68%, Cuenca et al. 82% without considering the PC) followed by the crimped one (C) and then the other ones, metallic and non. The volume of fiber reinforcement is basically homogeneously distributed in both the systems up to a content of 1.25% corresponding to approximately 100 kg/m$^3$ (168.6 lb/yd$^3$) over which the populations drop significantly.

Longitudinal reinforcement ratio $\rho_S = A_S/(b_w \cdot d)$

To guarantee the shear failure respect to the bending failure the longitudinal flexural

reinforcement represents a fundamental condition to take into account. The longitudinal reinforcement ratio $\rho$ is expressed as the ratio between the transversal total area of the rebars $A_S$ and the effective cross section $(b_w \cdot d)$. Bearing in mind that the databases considered have already been purged of all unwanted type of failure, it is interesting to note a clear distinction between the two distributions. On the one hand, Alcocer et al. present a distribution centered in the range from 2 to 2.9% respect to Cuenca et al. that returns a clear peak in the lower range 1.0 to 1.9% with the 59% of the samples.

Flexural strength $\sigma_{fl}$ or $f$

Among all the parameters discussed, the flexural strength represents the most critical parameters in this analysis due to the systematic absence. An incomplete mechanical characterization according to both EN 14651[41] and ASTM C1609[42] makes it more difficult to establish a correlation between the regulatory models already presented. In the Alcocer et al.'s database only 18 results are characterized exclusively according to the European standard and 54 exclusively to the American one. None of them is characterized in both ways. Furthermore, only 4 out of the 18 present a value for both the $f_{R1}$ and $f_{R3}$ at least equal to 6 MPa (0.9 ksi) and 7 out of the 54 with both $f^D_{300}$ and $f^D_{150}$ at least equal to 6 MPa (0.9 ksi). The data reported by Cuenca et al. are limited to the only $f_{R1}$ and $f_{R3}$ for all the FRCs of which 12 with both the values at least equal to 6 MPa (0.9 ksi). No references to the other parameters and to the American norm are reported.

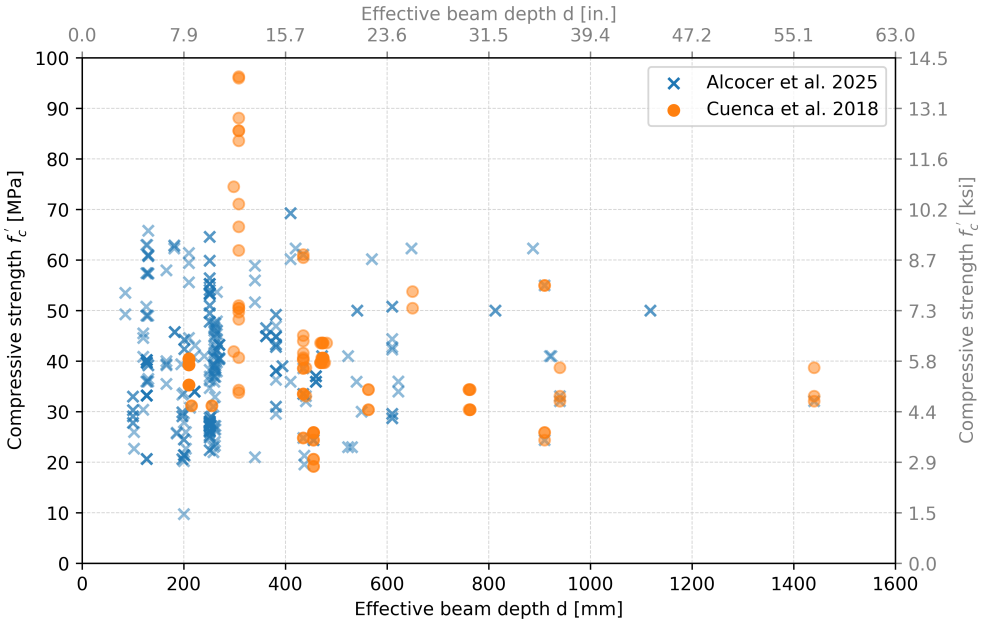



Figure 1.21. Shear-failure tests from Alcocer et al.[66] and Cuenca et al.[65]

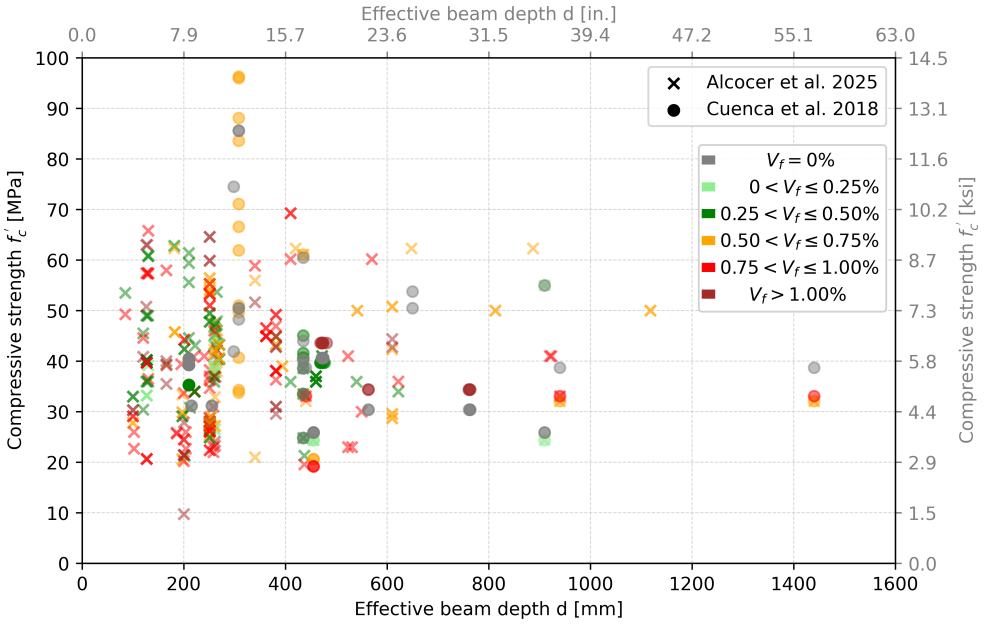
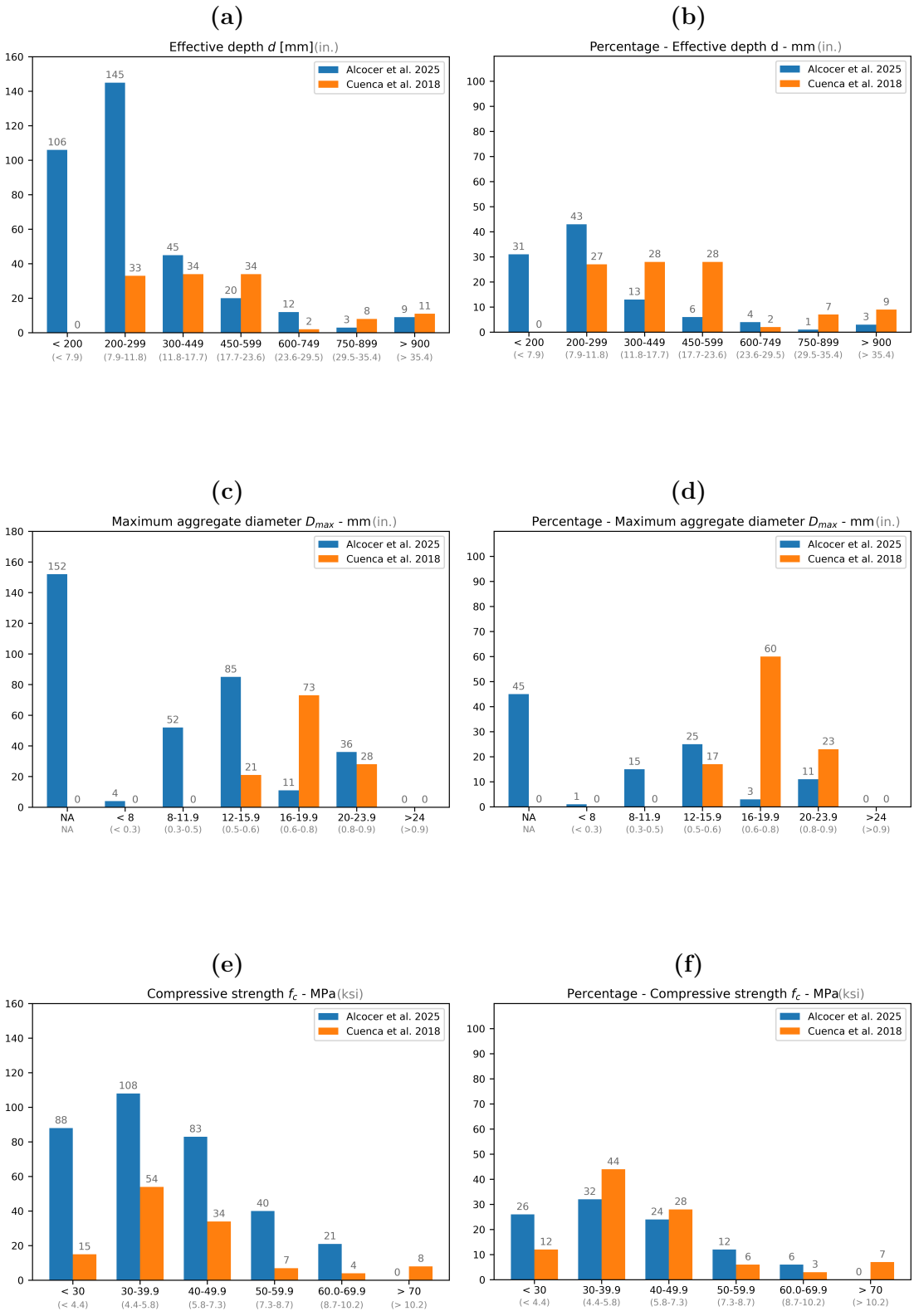



Figure 1.22. Shear-failure tests from Alcocer et al.[66] and Cuenca et al.[65] respect to $V_f$


(a)
Effective depth d [mm](in.)
Alcocer et al. 2025
Cuenca et al. 2018
106
0
145
33
45
34
20
34
12
2
3
8
9
11
< 200 (< 7.9)
200-299 (7.9-11.8)
300-449 (11.8-17.7)
450-599 (17.7-23.6)
600-749 (23.6-29.5)
750-899 (29.5-35.4)
> 900 (> 35.4)
(b)
Percentage - Effective depth d - mm (in.)
Alcocer et al. 2025
Cuenca et al. 2018
31
0
43
27
13
28
6
28
4
2
1
7
3
9
(c)
Maximum aggregate diameter $D_{max}$ - mm (in.)
Alcocer et al. 2025
Cuenca et al. 2018
152
0
4
0
52
0
85
21
11
73
36
28
0
0
NA NA
< 8 (< 0.3)
8-11.9 (0.3-0.5)
12-15.9 (0.5-0.6)
16-19.9 (0.6-0.8)
20-23.9 (0.8-0.9)
>24 (>0.9)
(d)
Percentage - Maximum aggregate diameter $D_{max}$ - mm (in.)
Alcocer et al. 2025
Cuenca et al. 2018
45
0
1
0
15
0
25
17
3
60
11
23
0
0
(e)
Compressive strength $f_c$ - MPa (ksi)
Alcocer et al. 2025
Cuenca et al. 2018
88
15
108
54
83
34
40
7
21
4
0
8
< 30 (< 4.4)
30-39.9 (4.4-5.8)
40-49.9 (5.8-7.3)
50-59.9 (7.3-8.7)
60.0-69.9 (8.7-10.2)
> 70 (> 10.2)
(f)
Percentage - Compressive strength $f_c$ - MPa (ksi)
Alcocer et al. 2025
Cuenca et al. 2018
26
12
32
44
24
28
12
6
6
3
0
7

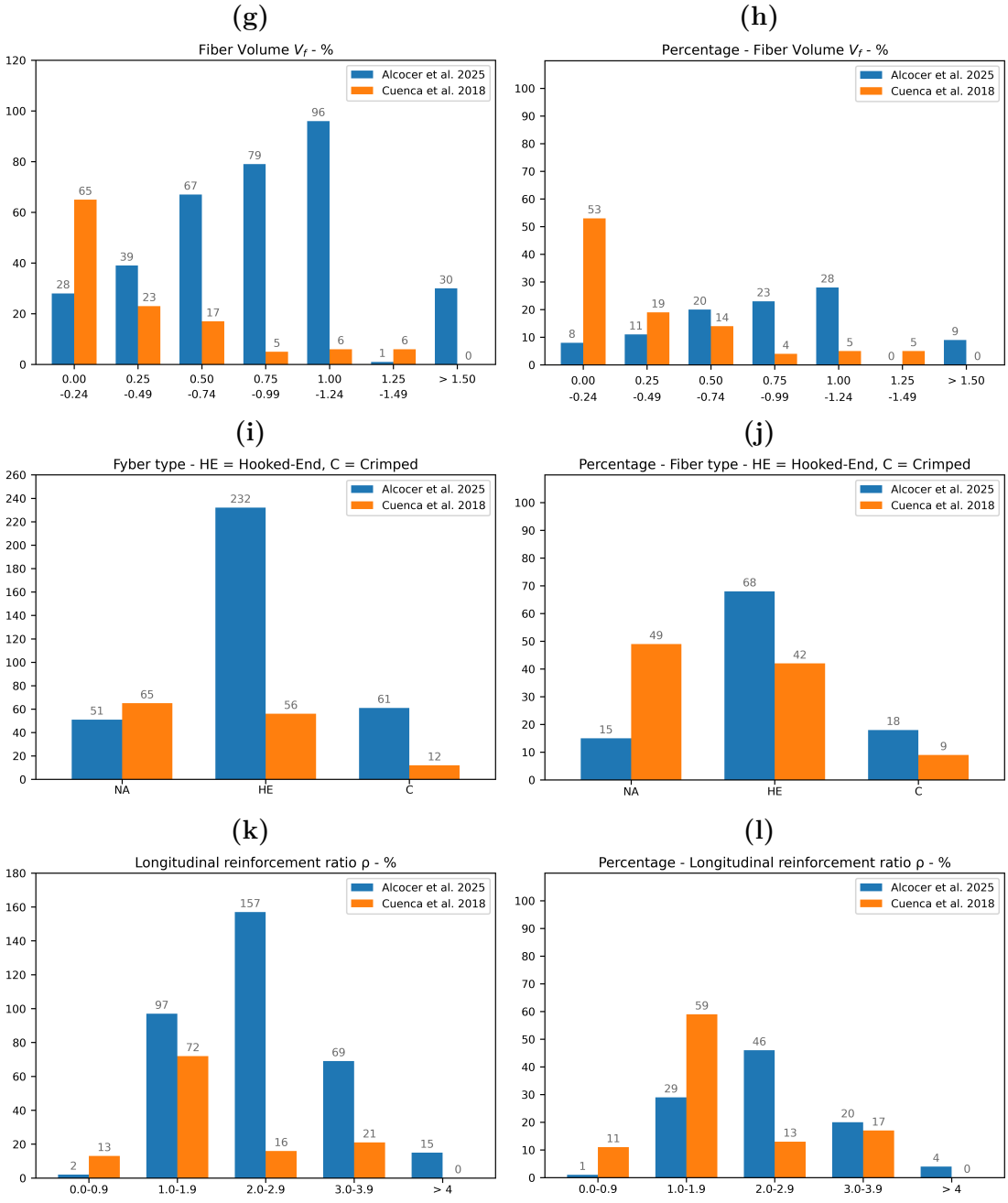



Figure 1.23. Distribution of shear-failure tests from Alcocer et al. and Cuenca et al. (Left) Effective total population, respectively, 340 and 122; (Right) Relative distribution respect to the corresponding effective population [65,66]

The size-effect previously described can be observed in Figure 1.24. The average shear strength $\tau$ is computed as the ratio between the shear force at failure (including the self-weight contribution) $V_u$ and the effective cross-sectional area ($b_w \cdot d$). For the sake of comparison, the outcomes are plotted on a color-scale based on the nominal fiber content with increments of 0.25% namely 20 kg/m$^3$ (33.7 lb/yd$^3$).

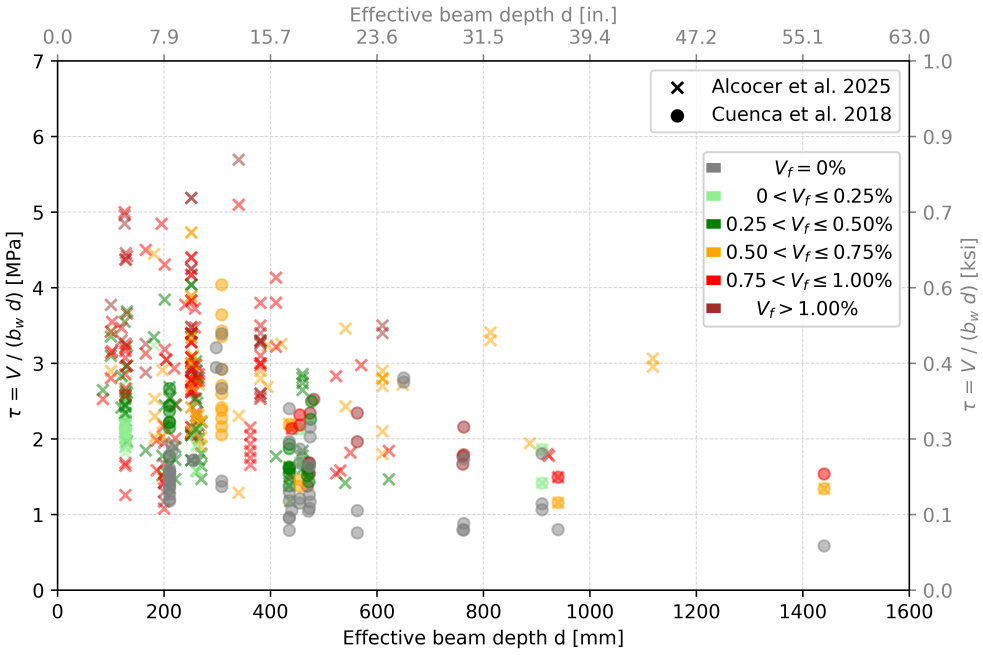



Figure 1.24. Average shear strength $\tau$ vs Effective beam depth $d$ from Alcocer et al.(2025) and Cuenca et al.(2018) [65,66]

## 1.4 Shear strength prediction models

Essential during the initial exploration of the topic and revisited throughout the discussion, the shear models provided by MC2020, CEN and ACI standards are now described in detail. The proposed analysis are presented in relation to the specific problem under investigation; consequently, scenarios deemed irrelevant or inapplicable are excluded, with appropriate justifications provided where necessary. All the following equations are expressed according to SI, unless otherwise specified.

### 1.4.1 *fib* Model Code 2020

MC2020[33] describes the shear in the Chapter *30.1.3 Shear*. The design value of resistance to shear force $V_{Rd}$ of a web or a slab in FRC without shear reinforcement is described in *30.1.3.4* as the sum of the design shear resistance attributed to the concrete $V_{Rd,C}$ and the design shear resistance attributed to fibre reinforced concrete $V_{Rd,FRC}$. The model identifies three Level of Approximation (LoA) depending on the level of detail that can be achieved.

$$V_{Rd} = V_{Rd,C} + V_{Rd,FRC} \tag{1.10}$$

$$V_{Rd,C} = k_{v,FRC} \frac{\sqrt{f_{ck}}}{\gamma_c} z_v \cdot b_w \tag{1.11}$$

$$V_{Rd,FRC} = \frac{k_s \cdot f_{FTU}}{\gamma_F} \cot(\theta_F) \cdot z_v \cdot b_w \tag{1.12}$$

where:

- $k_{v,FRC}$ is the design shear resistance for FRC coefficient (see LoA)
- $f_{ck}$ is the characteristic value of compressive strength of concrete
- $\gamma_c$ is the partial safety factor for concrete material properties
- $z_v$ is the effective shear depth
- $b_w$ is the width of the cross-section
- $k_s = 0.64$ is a parameter which considers the crack propagation and fibre orientation
- $f_{FTU}$ is the characteristic value of ultimate residual tensile strength (see LoA).
- $\gamma_F$ is the partial safety factor for fibre reinforced concrete
- $\theta_F$ is the inclination of the compressive stress field (see LoA)

The LoA I is applicable for members with no significant axial load, with $f_{ck} \leq 70$ MPa (10.2 ksi), $f_y \leq 500$ MPa (72.5 ksi) and with a maximum aggregate size of not less than 10 mm (0.4 in.):

$$f_{FTU} = \frac{f_{R3k}}{3} \tag{1.13}$$

$$k_{v,FRC} = \frac{0.4}{\left(1 + 750\frac{f_{yd}}{E_s}\right) + \zeta} \cdot \frac{1300}{1000 + 1.25 z_v} \tag{1.14}$$

$$\zeta = \left(20 - 7000\frac{f_{yd}}{E_s}\right) \cdot \frac{f_{FTU}}{f_{ck}} \geq 0 \tag{1.15}$$

$$\theta_F = 29^\circ + 3500\frac{f_{yd}}{E_s} \tag{1.16}$$

where:

- $f_{R3k}$ in the characteristic residual strength of fibre reinforced concrete significant for ultimate conditions
- $f_{yd}$ is the design yield strength of reinforcing steel in tension
- $E_S$ is the modulus of elasticity of reinforcing steel
- $\zeta$ is the reduction coefficient of the concrete component due to the increased crack width that occurs in the presence of fibres at ULS

The LoA II directly considers the aggregate size and the longitudinal strain in elastic analysis. $f_{FTU}$ is equivalent to LoA I and $\varepsilon_x$ is computed at the mid-depth of the effective shear depth:

$$k_{v,\mathrm{FRC}} = \frac{0.4}{(1 + 1500\varepsilon_x) + \zeta} \cdot \frac{1300}{1000 + k_{dg} \cdot z_v} \quad (z_v \text{ in mm}) \tag{1.17}$$

$$\zeta = (20 - 14000\varepsilon_x) \cdot \frac{f_{FTU}}{f_{ck}} \geq 0 \tag{1.18}$$

$$k_{dg} = \frac{32}{16 + d_g} \geq 0.75 \tag{1.19}$$

$$\theta_F = 29^\circ + 7000\varepsilon_x \tag{1.20}$$

where:

- $\epsilon_x$ is the average strain in x-direction at mid-depth of the effective depth
- $k_{dg}$ is the factor to account for roughness of critical shear crack
- $d_g$ is the aggregate size

The LoA III determines the crack width $w_u$ that has to be considered for the evaluation of $f_{FTU}$. The computation of $\varepsilon_x$, $\theta_F$ and $k_{dg}$ is analogous to LoA II:

$$k_{v,\mathrm{FRC}} = \frac{0.4}{1 + 1500\varepsilon_x} \cdot \frac{1300}{1000 + k_{dg} \cdot z_v} \quad (z_v \text{ in mm}) \tag{1.21}$$

$$w_u = (0.2 + 1000\varepsilon_x) \left( \frac{1000 + k_{dg} \cdot d_v}{1300} \right) / cos\theta_F \geq 0.5\,\mathrm{mm} \tag{1.22}$$

where:

- $w_u$ is the maximum crack opening accepted in structural design

### 1.4.2 Eurocode 2 - Annex L

The topic of shear for the FRC, as defined by CEN, is addressed with reference to the provisions of the *Eurocode 2: Design of Concrete Structures - Annex L – Steel Fibre Reinforced Concrete Structures - L.8.2 Shear* [56]. The design value of the shear strength for elements in FRC with longitudinal reinforcement bars in the tensile zone and without shear reinforcement (e.g. stirrups) must verify:

$$\tau_{Rd,cF} = \eta_c \cdot \tau_{Rd,c} + \eta_F \cdot f_{Ftud} \geq \eta_c \cdot \tau_{Rdc,\mathrm{min}} + \eta_F \cdot f_{Ftud} \tag{1.23}$$

for which:

$$\tau_{Rd,c} = \frac{0.66}{\gamma_V} \cdot \left( 100\rho_l \cdot f_{ck} \cdot \frac{d_{dg}}{d} \right)^{1/3} \geq \tau_{Rd,c,\mathrm{min}} \tag{1.24}$$

$$\tau_{Rdc,\min} = \frac{11}{\gamma_V} \cdot \sqrt{\frac{f_{ck}}{f_{yd}} \cdot \frac{d_{dg}}{d}} \tag{1.25}$$

$$f_{Ftu,ef} = k_O \cdot k_G \cdot 0.33 \cdot f_{R,3k} \tag{1.26}$$

$$f_{Ftud} = \frac{f_{Ftu,ef}}{\gamma_{SF}} \tag{1.27}$$

where:

- $\tau_{Rd,cF}$ is the design value of the shear strength of SFRC
- $\tau_{Rd,c}$ is the shear stress resistance of members without shear reinforcement
- $f_{Ftud}$ is the design value of residual tensile strength accounting for fibre orientation
- $\tau_{Rdc,min}$ is the minimum shear stress resistance to avoid a detailed verification for shear
- $\eta_c$ is the strength reduction coefficient for $\tau_{Rd,c}$
- $\eta_F$ is the strength reduction coefficient for $f_{Ftud}$
- $\gamma_V$ is a partial factors for shear resistance without shear reinforcement
- $\rho_l$ is the ratio between the tensile reinforcement and the considered section
- $f_ck$ is the characteristic concrete cylinder compressive strength
- $f_{yd}$ is the design yield strength of the flexural reinforcement
- $d_{dg}$ is the parameter describing the failure zone roughness. It depends on the concrete type and the aggregate properties and may be taken as:

$$\begin{aligned} &16\,\text{mm} + D_{\text{lower}} \leq 40\,\text{mm} && \text{for } f_{ck} \leq 60\,\text{MPa} \\ &16\,\text{mm} + D_{\text{lower}} \left(\frac{60}{f_{ck}}\right)^2 \leq 40\,\text{mm} && \text{for } f_{ck} > 60\,\text{MPa} \end{aligned} \tag{1.28}$$

- $d$ is the effective depth of the flexural reinforcement
- $f_{Ftu,ef}$ is the effective residual tensile strength of SFRC for given crack width accounting for fibre orientation and volume effect
- $k_0$ is the factor taking into account the orientation of the steel fibres in the concrete matrix in relation to the orientation of the principal tensile stress arising from the

action effects

- $k_G = 1.0 + A_{ct} \cdot 0.5 \leq 1.5$ is the factor taking into account the size of the tensile zone involved in the failure state. For shear, $A_{ct}$ is the area of the tension zone along the surface of the shear crack expressed in [$m^2$]
- $f_{R3,k}$ is the characteristic residual flexural strength at CMOD=2.5 mm.
- $\gamma_{SF}$ is the partial factor for SFRC in tension

### 1.4.3 ACI 544.4R-18

ACI addresses the issue of shear for FRC within both ACI 544.4R [16], specifically in *Section 4.8 - Design of FRC for shear*, and ACI 318-25 [57] in *22.5 - One-way shear strength.* For clarity of presentation, all the equations presented in this section are expressed in accordance with the United States Customary (USC).

ACI 544.4R is based on the model proposed by MC2010 [61,62] considering the flexural bheavior of the material through the parameter $f_{150}^D$, instead of the $f_{Ftuk}$ at $w_u$=1.5 mm:

$$V_{FRC} = \left\{ \frac{0.18}{\gamma_c} k_s \left[ 100\rho \left( 1 + 7.5 \frac{f_{ut-FRC}}{f_t} \right) f_c \right]^{\frac{1}{3}} + 0.15\sigma_{cp} \right\} \cdot b \cdot d \tag{1.29}$$

$$k_s = 1 + \sqrt{\frac{200}{d}} \leq 2.0 \tag{1.30}$$

$$\rho = \frac{A_s}{b \cdot d} \tag{1.31}$$

$$f_{ut-FRC} = 0.37 \cdot f_{150}^D \tag{1.32}$$

where:

- $V_{FRC}$ is the shear capacity
- $\gamma_c$ is the partial safety factor for plain concrete
- $k_s$ is the factor for size effect in shear calculations
- $\rho$ is the reinforcement ratio for longitudinal reinforcement

- $f_{ut-FRC}$ is the FRC ultimate tensile residual strength
- $f_t$ is the tensile strength of plain concrete
- $f_c$ is the compressive strength of plain concrete
- $\sigma_{cp}$ is the average normal stress acting on concrete cross section
- $b$ is the section width
- $d$ is the depth of reinforcement

### 1.4.4 ACI 318-25

The ACI 318-25 presents a different approach in *22.5 - One-way shear strength*. For the SFRC a set of compliance criteria is defined:

- 26.4.1.6.1(a) - Steel fiber reinforcement shall:
  - be deformed and conform to ASTM A820 [21]
  - have a length-to-diameter ratio between 50 and 100.
- 26.4.2.2 (h) - The minimum content of fibers shall:
  - conform to ASTM C1116 [68]
  - contain at least 41.5 kg/m$^3$ (70.0 lb/yd$^3$) for NWC
- 26.12.8.1(a) - the SFRC shall satify these minimum mechanical performance:
  - Compressive strength acceptance criteria for standard-cured specimens
  - Residual strength obtained from flexural testing in accordance with ASTM C1609 [42] at a midspan deflection of 1/300 of the span length is at least the greater of:
    - 90% of the measured first-peak strength obtained from a flexural test
    - 90% of the strength corresponding to $7.5\sqrt{f'_c[psi]}$
  - Residual strength obtained from flexural testing in accordance with ASTM C1609 [42] at a midspan deflection of 1/150 of the span length is at least the greater of:
    - 75% of the measured first-peak strength obtained from a flexural test
    - 75% of the strength corresponding to $7.5\sqrt{f'_c[psi]}$

If all the criteria are respected and in absence of shear reinforcement, the nominal shear strength, $V_n$, is coincident with the nominal shear strength of the concrete, $V_C$ that can be computed as:

$$V_c = \max\left(\left[2\lambda\sqrt{f'_c} + \frac{N_u}{6A_g}\right] b_w d \;;\; 1.3 \times \left[8\lambda(\rho_w)^{1/3}\sqrt{f'_c} + \frac{N_u}{6A_g}\right] b_w d\right) \tag{1.33}$$

$$\lambda_s = \frac{2}{1 + \frac{d}{10}} \leq 1 \tag{1.34}$$

where:

- $V_C$ is the nominal shear strength provided by concrete
- $\lambda$ is the modification factor to reflect the reduced mechanical properties of lightweight concrete relative to normalweight concrete of the same compressive strength
- $f_c$ is the specified compressive strength of concrete
- $N_u$ is the factored axial force normal to cross section
- $A_g$ is the gross area of concrete section
- $b_w$ is the section width
- $d$ is the depth of reinforcement
- $\rho_w$ is the ratio between the area of nonprestressed longitudinal tension reinforcement and $(b_w d)$

## 1.5 Research significance

Based on the above, it is clear that the assessment of the shear capacity of concrete, whether Plain Concrete (PC) or Fiber-Reinforced Concrete (FRC), remains far from being unambiguously defined. Over the years, various theoretical-empirical models have been proposed, each presenting clearly differences in approach and formulation. They are generally based on limited databases characterized by lower mechanical performances no longer in line with the current state-of-art (e.g., poor compressive strength, poor tensile strength of the fibers, poor residual flexural performances).

The performance of tests is crucial for populating databases and, consequently, for calibrating predictive models. Moreover, a comprehensive mechanical characterization enables meaningful comparisons among different interpretations, which is essential for assessing their reliability and for identifying the mechanisms that predominantly govern the behavior of FRC.

# Chapter 2

# Experimental Campaign

## 2.1 Experimental program

In this study, the experimental program proposed by Sneed and Ramirez [4] to evaluate the shear capacity of PC have been adapted and applied to the Fiber-Reinforced Concrete (FRC). To evaluate the shear strength capacity, a series of simply supported beams reinforced with only traditional flexural reinforcement (i.e., longitudinal rebars) and without shear reinforcement (i.e., stirrups) are tested under monotonic load in 3PBT and 4PBT configurations. Only the end zones, outside of the tested area, are reinforced with stirrups.
In the following sections, the formulations of the PCs and FRCs are not disclosed, as they are protected by patent [69].
The experimental program is divided into three phases:

- **Preliminary Investigation #1 - Small-Scale Beams (Phase 1)** - This phase involves the production and the testing of small-scale beams and Quality Control (QC) samples by means of laboratory-based production methods. Six different mixes with different dosage of fibers are considered - Batch size: 0.1 $m^3$ (3.5 $ft^3$).

- **Preliminary Investigation #2 - Full-Scale beams (Phase 2)** - This phase expands the study of the previous one to include full-scale structural elements, along

with additional small-scale beams, all produced through industrial-scale manufacturing. The objective is to examine the size-effect on shear strength capacity in FRC. Three different mixes are considered - Batch size: 3.5 $m^3$ (123.6 $ft^3$).

- **Comprehensive investigation - Size-effect of beams with variable heights (Phase 3)** - This phase marks a further advancement, in which beam specimens with different heights are casted and tested, all produced through industrial-scale manufacturing with the aim of better evaluating the contribute of the size-effect, with particular reference to the effective beam depth, $d$, on the shear strength of FRC. Three different mixes are considered - Batch size: 5.0 $m^3$ (176.6 $ft^3$).

## 2.2 Preliminary Investigation #1 - Small-Scale Beams

### 2.2.1 Test configuration - Setup #1

This preliminary phase focuses on evaluating the impact of steel fiber reinforcement on the shear capacity. A PC matrix with nominal class C40/50 - $f'_c = 40$ MPa (5.8 ksi) - at 14 days is selected as reference (*Ref*) for being compared to the same concrete matrix including different dosages of fibers namely 20, 40, 60 and 80 kg/$m^3$ (respectively 33.7, 67.4, 101.1 and 134.8 lb/$yd^3$). The maximum aggregate size is 11 mm (0.4 in.). Small adjustments of the plasticizer were needed to guarantee the same water-to-cement ratio and the desired consistency class (i.e., Self-Compacting Concrete (SCC) - class SF1 according to EN 206 [70] and EN 12350-8 [71]).
In addition, a further FRC having a nominal class C70/85 - $f'_c = 70$ MPa (10.1 ksi) - with a total fiber content of 100 kg/$m^3$ (168.6 lb/$yd^3$) is included in the study with maximum aggregate size of 8 mm (0.3 in.).
In all the mixes, high-strength Hooked-End steel fibers (HE) with maximum length of 50 mm (2.0 in.) and aspect ratio $L/\phi$ of 71 are used.
For each mix, a planetary concrete mixer with nominal capacity of 0.2 $m^3$ (7.1 $ft^3$) is used to produce more batches with a volume of 0.1 $m^3$ (3.5 $ft^3$) to avoid the overloading of the equipment and an improper mixing.

A series of small-scale beams measuring 200 mm (7.9 in.) by 200 mm (7.9 in.) by 1500 mm (59.1 in.), respectively width, height and length are produced. Hereinafter, this type of sample is called S1-0, similarly to the nomenclature adopted by Sneed and Ramirez [4]. The ends of the beam, located outside of the tested area, are shear reinforced (i.e., stirrups) to ensure safe handling and movement of the beam without introducing significant stresses in the sample. Conversely, the central zone subject to bending and shear effects is reinforced with only longitudinal reinforcement - namely 3Φ16 (3#5) with 25 mm (1.0 in.) net cover and classified as B500B corresponding to $f_{y,ks} = 500$ MPa (72.5 ksi) [72]. The overall geometry of the beam specimens is adjusted to fit within the geometry of the testing machine, its maximum load capacity and the available steel rebars in the market. A servo-hydraulic flexural testing machine by TESTING (made in Germany) with 300 kN (67.44 kips) capacity is used.

The final configuration is a 3PBT with a concentrated load applied in the center and a net span length between supports, $L_S$. of 1000 mm (39.4 in.), as shown in Figure 2.1.

The shear-span to effective depth ratio, $a/d$, is assumed equal to 3 accordingly to the *Valley of the critical failure* identified by Kani [5]. The geometrical properties of the samples S1-0 and the mechanical properties of the reinforcing steel are summarized in Table 2.1.

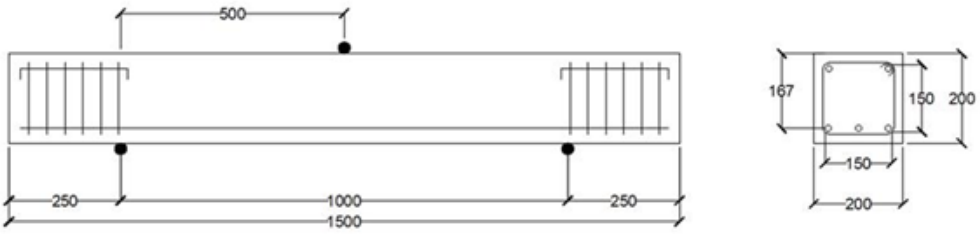



Figure 2.1. Phase1 - Setup of beam S1-0 (measures in mm)

Table 2.1. Phase1 - Geometrical properties and steel specifications for beam S1-0

| | | | |
|---|---|---|---|
| Width | $b_w$ | mm (in.) | 200 (7.9) |
| Height | $h$ | mm (in.) | 200 (7.9) |
| Depth | $d$ | mm (in.) | 167 (6.6) |
| Shear-span to Depth ratio | $a/d$ | - | 3.0 |
| Net span length | $L_s$ | mm (in.) | 1000 (39.4) |
| Longitudinal Reinforcement | $A_s$ | $mm^2$ ($in.^2$) | 603 (0.9) |
| Average steel yielding strength | $f_{ys}$ | MPa (ksi) | 545 (72.5) |
| Steel content | $\rho = A_s/b_w d$ | % | 1.81 |

### 2.2.2 Material properties

Hereinafter, the general nomenclature adopted is "XX-YY-ZZZh" where:

- XX: type of concrete (PC, FRC)
- YY: overall content of steel fibers expressed in $kg/m^3$ (0, 20, 40, 60, 80, 100)
- ZZZh: nominal height of the sample expressed in mm (200h)

All the tests are carried out at 14 days of curing on the same day as the shear tests on samples S1-0.
The following QC tests have been carried out:

- **Compression test** on Ø150 mm x 300 mm (Ø5.9 in. x 11.8 in.) cylinders with loading rate of 0.6 MPa/s (87.0 psi/s) according to EN 12390-3 [34]
- **Flexural test** on 150 mm x 150 mm x 550 mm (5.9 in. x 5.9 in. x 21.6 in.) prismatic beams according to EN 14651 [41]

- **Flexural test** on 150 mm x 150 mm x 550 mm (5.9 in. x 5.9 in. x 21.6 in.) prismatic beams according to ASTM C1609[42]
- **Splitting tensile test** on Ø150 mm x 300 mm (Ø5.9 in. x 11.8 in.) cylinders according to ASTM C496[73] for the only PC mix

In Table 2.2 and Table 2.3, the average values obtained from the tests mentioned are collected. Annex A reports all the tests completed in this phase from Table 3.3, to Table 3.11, in Figure 3.14 and in Figure 3.15.

For the sake of clarity, the values relative to the flexural parameters $f_L$ and $f_{1^{st}peak}$ reported in this section are relative to the average curve of the respective test. The values reported in Annex A are instead extracted from each single curve and then compared resulting, anyway, in non-significant differences.

The results of the shear tests will be discussed in the next Section.

Table 2.2. Phase1 - Mechanical properties according to EN 12390-3 and ASTM C496 [34,73]

| Beam ID | Days of curing | Density | $f_{cm}$ | $f_{T.Split}$ |
|---|---|---|---|---|
| | | $kg/m^3$ ($lb/yd^3$) | MPa (ksi) | MPa (ksi) |
| PC-0-200h | 14 | 2293 (3865) | 45.6 (6.6) | 2.9 (0.4) |
| FRC-20-200h | 14 | 2319 (3909) | 46.3 (6.7) | NA |
| FRC-40-200h | 14 | 2321 (3912) | 46.4 (6.7) | NA |
| FRC-60-200h | 14 | 2319 (3909) | 47.0 (6.8) | NA |
| FRC-80-200h | 14 | 2346 (3955) | 48.5 (7.0) | NA |
| FRC-100-200h | 14 | 2282 (3846) | 70.0 (10.2) | NA |

Table 2.3. Phase1 - Mechanical properties according to EN 14651 and ASTM C1609 [41,42]

| Beam ID | $f_{L,av}$ | $f_{R1,av}$ | $f_{R2,av}$ | $f_{R3,av}$ | $f_{R4,av}$ | $f_{1^{st}peak}$ | $f^D{}_{600}$ | $f^D{}_{300}$ | $f^D{}_{150}$ | $f_P$ |
|---|---|---|---|---|---|---|---|---|---|---|
| | MPa (ksi) | MPa (ksi) | MPa (ksi) | MPa (ksi) | MPa (ksi) | MPa (ksi) | MPa (ksi) | MPa (ksi) | MPa (ksi) | MPa (ksi) |
| PC-0-200h | NA | NA | NA | NA | NA | 4.1 (0.6) | NA | NA | NA | 4.1 (0.6) |
| FRC-20-200h | 4.0 (0.6) | 2.7 (0.4) | 3.4 (0.5) | 3.7 (0.5) | 3.8 (0.5) | 3.7 (0.5) | 2.3 (0.3) | 2.2 (0.3) | 2.0 (0.3) | 3.8 (0.5) |
| FRC-40-200h | 4.2 (0.6) | 4.5 (0.7) | 5.5 (0.8) | 5.5 (0.8) | 4.7 (0.7) | 4.7 (0.7) | 5.1 (0.7) | 4.8 (0.7) | 4.1 (0.6) | 5.6 (0.8) |
| FRC-60-200h | 4.6 (0.7) | 6.1 (0.9) | 6.7 (1.0) | 6.2 (0.9) | 6.2 (0.9) | 5.1 (0.7) | 5.3 (0.8) | 5.5 (0.8) | 4.9 (0.7) | 5.7 (0.8) |
| FRC-80-200h | 5.3 (0.8) | 7.8 (1.1) | 8.7 (1.3) | 8.1 (1.2) | 7.3 (1.1) | 5.3 (0.8) | 6.6 (1.0) | 6.0 (0.9) | 4.1 (0.6) | 7.2 (1.0) |
| FRC-100-200h | 4.9 (0.7) | 8.8 (1.3) | 9.3 (1.3) | 8.8 (1.3) | 8.0 (1.2) | 6.6 (1.0) | 9.4 (1.4) | 7.1 (1.0) | 5.0 (0.7) | 9.5 (1.4) |

### 2.2.3 Shear tests - Experimental results

As depicted in Figure 2.1, the shear test corresponds to a 3PBT of beams designed with only longitudinal reinforcement in order to reach a premature shear failure respect to bending. Considering the linear elastic behavior of the associated isostatic simply-supported beam describe through the Equations from 2.1 to 2.4, it is worth noting that the contribute of the self-weight is basically negligible and the representation of the stress distributions induced by only the actuator, without then considering the self-weight of the beam, is represented in Figure 2.2.

$$R_A = \frac{1}{L}\left(q\frac{(c+L)^2}{2} - q\frac{c^2}{2} + (L-a)P\right) \tag{2.1}$$

$$R_B = \frac{1}{L}\left(-q\frac{c^2}{2} + q\frac{(L+c)^2}{2} + aP\right) \tag{2.2}$$

$$V(x) = \begin{cases} qx & \text{if } x < c \\ qx + R_A & \text{if } c < x < c+a \\ qx + R_A + P & \text{if } c+a < x < c+a+b \\ qx + R_A + P + R_B & \text{otherwise} \end{cases} \tag{2.3}$$

$$M(x) = \begin{cases} q\frac{x^2}{2} & \text{if } x < c \\ q\frac{c^2}{2} + R_A(x-c) & \text{if } c < x < c+a \\ q\frac{c^2}{2} + R_A(x-c) + P(x-(c+a)) & \text{if } c+a < x < c+L \\ q\frac{c^2}{2} + R_A(x-c) + P(x-(c+a)) + R_B(x-(c+L)) & \text{otherwise} \end{cases} \tag{2.4}$$

where:

- $q$ homogeneous linear density of the beam
- $P$ load applied by the testing machine
- $R_A$ vertical reaction at hinged support A
- $R_B$ vertical reaction at hinged support B
- L Net span between supports = $\frac{5}{2}a$
- c Cantilever length

According to the Equations from 2.1 to 2.4 and considering the symmetrical configuration (a = L/2) it is then possible to estimate the shear and the bending moment at midspan, point of application of the load $P$, as:

$$V = \frac{P}{2} + \frac{qL_{tot}}{2} \tag{2.5}$$

$$M = \frac{P + qL_{tot}}{2}\frac{L}{2} + \frac{qc^2}{2} \tag{2.6}$$

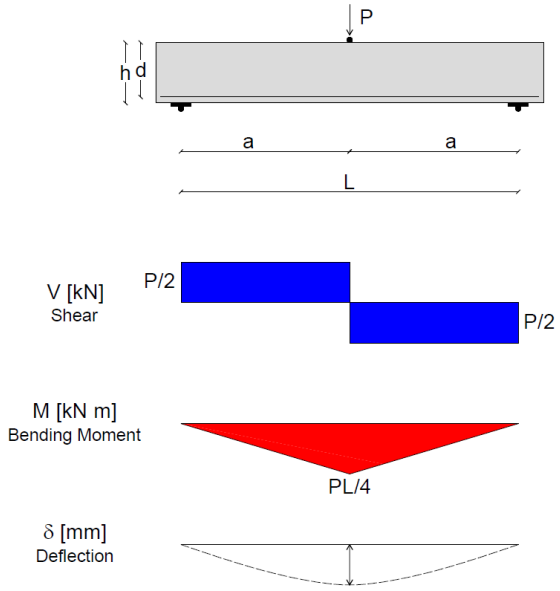



Figure 2.2. Phase1 - Test configuration and stress distribution along beam S1-0

The net deflection $\delta$ at the mid-span is obtained by subtracting the settlement of the supports from the displacement measured based on the disposition of the LVDTs.

Figure 2.3 and Figure 2.4 report the load-deflection curves obtained. More precisely, Figure 2.3 depicts the absolute values of the load respect to the net deflection at midspan, while Figure 2.4 shows the same curves normalized to the ultimate load achieved with the PC beam PC-0-200h, namely 95.6 kN (21.5 kips).

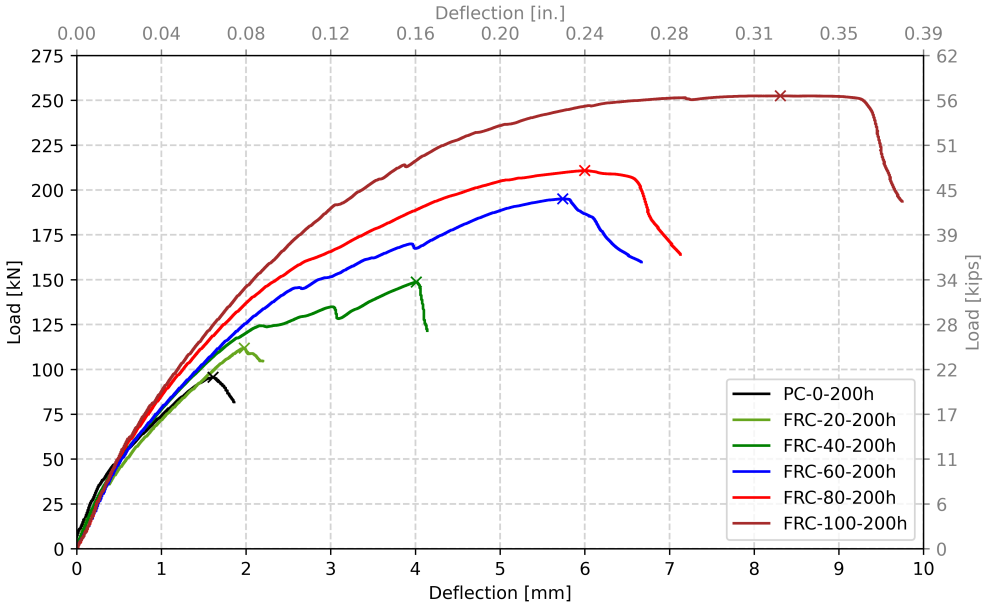



Figure 2.3. Phase1 - Load-deflection curves of all beams S1-0 under 3PBT

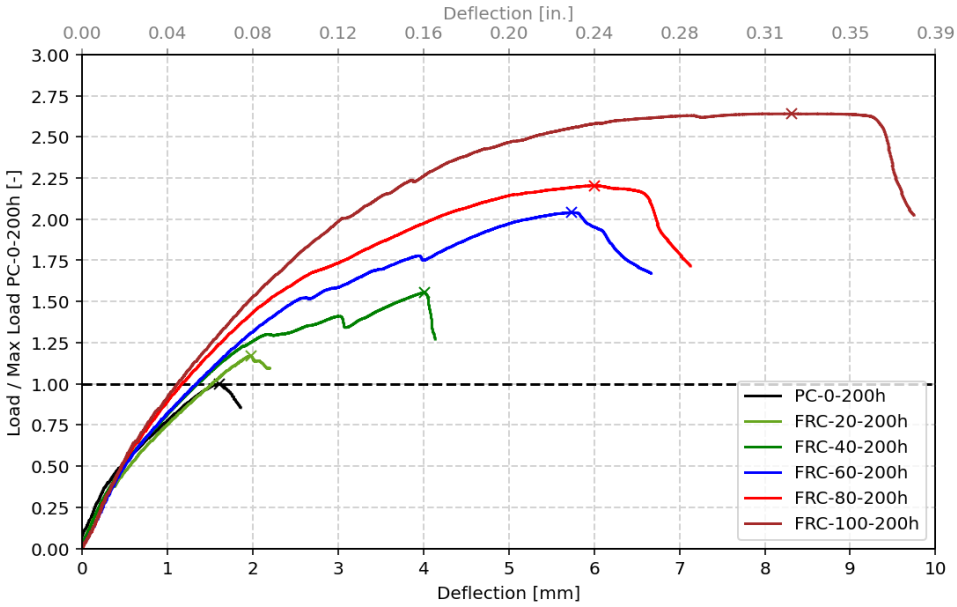



Figure 2.4. Phase1 - Load-deflection curves of all beams S1-0 under 3PBT normalized with respect to the ultimate load of PC, namely 95.6 kN (21.5 kips).

Table 2.4 summarizes the experimental load $P_u$ at failure, the corresponding peak deflection $\delta_{peak}$, the ultimate bending moment $M_u$, and the ultimate shear force $V_u$ calculated according to Equation 2.5 and Figure 2.1.

Table 2.4. Phase1 - Shear test results of beams S1-0

| **Beam ID** | **Days of curing** | $\delta_{\mathbf{peak}}$ | $P_u$ | $M_u$ | $M_{y,\mathrm{Fl}}^{num}$ | $M_u/M_{y,\mathrm{Fl}}^{num}$ | **Failure Mode** | $V_u$ | $V_u/V_{u,\mathrm{Ref}}$ |
|---|---|---|---|---|---|---|---|---|---|
| | | mm (in.) | kN (kips) | kN · m (kip-in.) | kN · m (kip-in.) | % | | kN (kips) | - |
| PC-0-200h | 14 | 1.62 (0.06) | 95.6 (21.5) | 24.0 (212.6) | 49.4 (437.3) | 49% | Sudden Shear | 48.3 (10.9) | *Ref* |
| FRC-20-200h | 14 | 2.12 (0.08) | 111.8 (25.1) | 28.1 (248.4) | 50.0 (442.5) | 56% | Shear | 56.4 (12.7) | 1.17 |
| FRC-40-200h | 14 | 4.45 (0.18) | 148.7 (33.4) | 37.3 (329.9) | 51.7 (457.9) | 72% | Shear | 74.8 (16.8) | 1.55 |
| FRC-60-200h | 14 | 5.74 (0.23) | 195.0 (43.8) | 48.9 (432.6) | 51.9 (459.4) | 94% | Shear + Bending | 98.0 (22.0) | 2.03 |
| FRC-80-200h | 14 | 6.00 (0.24) | 210.8 (47.4) | 52.8 (467.4) | 52.8 (466.9) | 100% | Shear + Bending | 105.9 (23.8) | 2.19 |
| FRC-100-200h | 14 | 8.31 (0.33) | 252.5 (56.8) | 63.2 (559.6) | 57.3 (507.1) | 110% | Bending + Shear | 126.7 (28.5) | 2.62 |

The bending capacity $M_{y,Fl}$ is computed at the yielding of the steel rebars considering equivalent rectangular compressive stress distribution (stress-block)[57] for the PC and referring to the Eurocode2 (EN1992)-Annex L[56] for the FRC mixes:

- PC : $M_{y,Fl} = 0.9\, A_s f_{ys} d$
- FRC : $M_{y,Fl} = f(f_{R1}, f_{R3}, f'_c, f_{ys})$

The safety factors are set equal to 1.00 (no reduction). Average values of the mechanical properties of concrete are assumed according to Table 2.2 and Table 2.3. The geometry of the cross-section and the mechanical properties of the steel correspond to

that described in Table 2.1.

In line with these premises, the numerical predictions $M_{y,Fl}$ are compared to the bending at failure experimentally obtained $M_u$ and expressed as a ratio $M_u/M_{y,Fl}$. If the ratio is below 100%, the failure is reached before reaching the (theoretical) yielding of the longitudinal steel rebars, otherwise it occurres with it. Expected pure-shear failures are reported in green, whereas mixed failure modes are reported in red.
In the column *Failure Mode*, the visual inspection carried out during and after the tests is described with a keyword for which a short explanation is reported below:

- I) **Sudden shear**: the failure occurs due to the sudden propagation of an arc-shaped crack along the diagonal between the load point and the support. In this case, no other visible and/or relevant cracks are observed before reaching the ultimate load.
- II) **Shear**: the failure occurs along the tensioned part of the beam under bending loading, with radial direction from the load point to the support.
- III) **Shear + Bending**: the failure occurs with a progressive opening and propagation of multiple shear cracking, but with the localization into the critical shear crack due to the achievement of the yielding strength of the steel reinforcement due to bending
- IV) **Bending + Shear**: the failure is governed by the yielding of the steel reinforcement and the consequent localization of the critical crack close to the midspan of the beam. Minor controlled shear crack occurs during the loading phase.
- V) **Shear + Local Failure**: Failure occurs with a progressive opening and propagation of multiple shear cracks, but with the sudden local failure in correspondence with the loading point.

In addition, the ratios between the shear strength $V_u$ obtained with the different FRC mixes respect to the reference PC-0-200h are shown in the last column. Figure 2.5 represent all the tested beams at the end of the respective shear test.

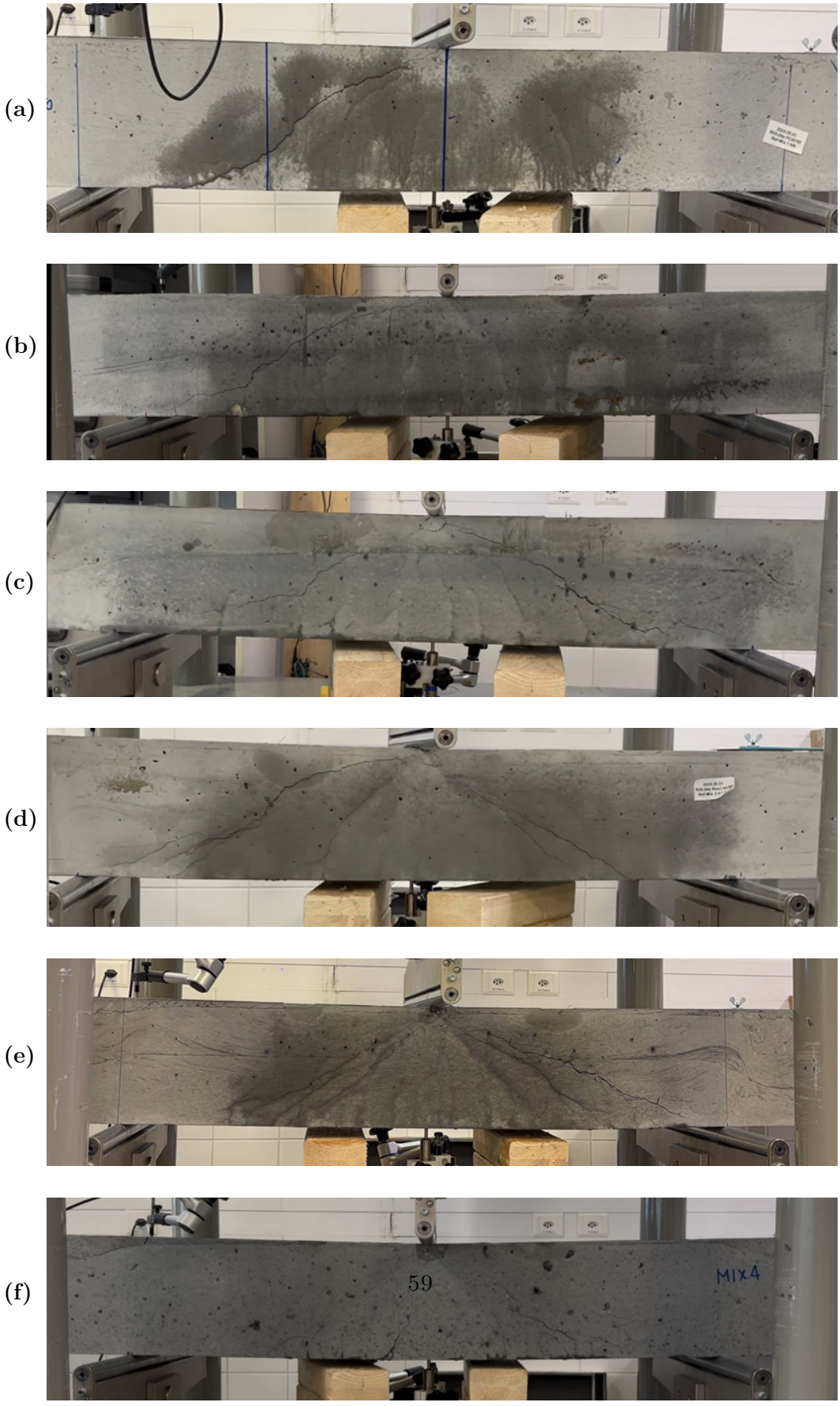



Figure 2.5. Phase1 - Pictures of all beams S1-0 at failure. (a) PC-0; (b) FRC-20; (c) FRC-40; (d) FRC-60; (e) FRC-80; (f) FRC-100

## 2.3 Preliminary Investigation #2 - Full-Scale beams

### 2.3.1 Test configuration - Setup #2

In the Phase 2 three mixes are selected to be replicated in a larger production by means of a concrete plant. The same concrete matrix with nominal strength C40/50 - $f'_c = 40$ MPa (5.8 ksi) - is used for the production of PC, the reference (*Ref*), and FRC with 60 kg/m$^3$ (101.1 lb/yd$^3$). Addionally, FRC with nominal class C70/85 - $f'_c = 70$ MPa (10.1 ksi) - and 100 kg/m$^3$ (168.6 lb/yd$^3$) is considered. All of them have a maximum aggregate size of 8 mm (0.3 in.) and they differ from the previous ones in terms of raw materials, whereas the additives and fibers remain unchanged. Small adjustments of the plasticizer were needed to guarantee the same water-to-cement ratio and the desired consistency class (i.e., SCC - class SF1 according to EN 206[70] and EN 12350-8[71]).
For each mix, a ready-mix truck with a batch volume of 3.5 m$^3$ (123.6 ft$^3$) is used.

One full-scale beam having dimensions 300 mm (11.8 in.) by 900 mm (35.4 in.) by 6000 mm (236.2 in.) - respectively width, height and length - is realized from each production and poured in the mold directly from the truck. Hereinafter, this sample is called S1-4 similarly to the nomenclature adopted by Sneed and Ramirez[4]. In addition two small-scale beams S1-0 and samples for the QC are casted as described in Section 2.2.1 and Section 2.2.2.

The full-scale beam S1-4 is realized in a manner analogous to small-scale one. The ends of the beam, located outside of the tested area, were reinforced with shear reinforcement (i.e., stirrups) to ensure safe handling and movement of the beam without introducing significant stresses. Conversely, the central zone subject to bending and shear stresses is reinforced with only longitudinal reinforcement, namely 4Φ34 (4#3) with 50 mm (2.0 in.) net cover and classified as B500B corresponding to $f_{y,ks} = 500$ MPa (72.5 ksi)[72].
Two rebars samples with a length of 800 mm (31.5 in.) are experimentally tested resulting in a mean yielding tensile strength $f_{y,ks} = 545$ MPa (79.0 ksi).

The small-scale and full-scale beams are tested in a 3PBT configuration with a net span length of respectively 1000 mm (39.4 in.) and 5000 mm (196.9 in.). For all the S1-0 samples and for the only PC and FRC S1-4, the setup is symmetric with a/d =

3.0 accordingly to the *Valley of the critical failure* identified by Kani[5] (Figure 2.1 and Figure 2.7a).

In contrast, the full-scale beam S1-4 for the FRC with 100 kg/m$^3$ (168.6 lb/yd$^3$) is designed with a reduced shear span-to-depth ratio of a/d = 1.6, due to the increased susceptibility to bending failure respect to the shear one. This configuration induces a constant shear force substantially equivalent to the symmetrical situation while effectively reducing the bending moment acting on the cross-section (Figure 2.6).

The geometrical properties of the samples S1-0 and S1-4 are summarized respectively in Table 2.5 and Table 2.6.

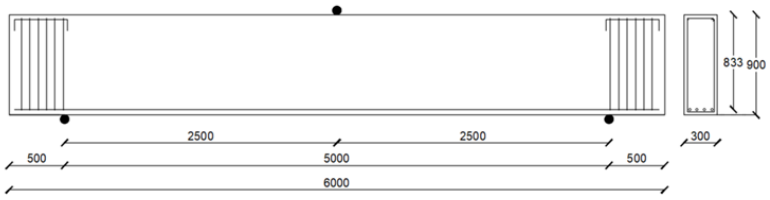



Figure 2.6. Phase2 - Setup of beam S1-4 for PC and FRC with 60 kg/m$^3$ (101.1 lb/yd$^3$)(measures in mm)

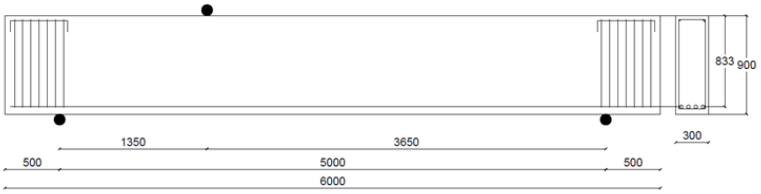



Figure 2.7. Phase2 - Setup of beam S1-4 for FRC with 100 kg/m$^3$ (168.6 lb/yd$^3$) (measures in mm)

Table 2.5. Phase2 - Geometrical properties and steel specifications for beam S1-0

| | | | |
|---|---|---|---|
| Width | $b_w$ | mm (in.) | 200 (7.9) |
| Height | $h$ | mm (in.) | 200 (7.9) |
| Depth | $d$ | mm (in.) | 167 (6.6) |
| Shear-span to Depth ratio | $a/d$ | - | 3.0 |
| Net span length | $L_s$ | mm (in.) | 1000 (39.4) |
| Longitudinal Reinforcement | $A_s$ | $mm^2$ ($in.^2$) | 603 (0.9) |
| Average steel yielding strength | $f_{ys}$ | MPa (ksi) | 545 (72.5) |
| Steel content | $\rho = A_s/b_w d$ | % | 1.81 |

Table 2.6. Phase2 - Geometrical properties and steel specifications for beam S1-4

| | | | |
|---|---|---|---|
| Width | $b_w$ | mm (in.) | 300 (11.8) |
| Height | $h$ | mm (in.) | 900 (35.4) |
| Depth | $d$ | mm (in.) | 833 (32.8) |
| Shear-span to Depth ratio | $a/d$ | - | 3.0 |
| Net span length | $L_s$ | mm (in.) | 5000 (196.9) |
| Longitudinal Reinforcement | $A_s$ | $mm^2$ ($in.^2$) | 3632 (5.7) |
| Average steel yielding strength | $f_{ys}$ | MPa (ksi) | 545 (79.0) |
| Steel content | $\rho = A_s/b_w d$ | % | 1.45 |

### 2.3.2 Material properties

As previously stated, the general nomenclature adopted is "XX-YY-ZZZh" where:

- XX: type of concrete (PC, FRC)
- YY: overall content of steel fibers expressed in kg/m$^3$ (0, 60, 100)
- ZZZh: nominal height of the sample expressed in mm (200h, 900h)

Preliminary shear tests on one of the two small-scale beams and QC, tests as those described in Section 2.2.2, are carried out after 14 days of curing with the aim of comparing the experimental outcomes derived from laboratory (Phase 1) and industrial (Phase 2) productions at the same age.
Shear tests on the full-scale beams S1-4 are conducted no earlier than 28 days after casting, in alignment with the scheduling availability of an external laboratory. On the same day, the respective small-scale beams S1-0 and the QC specimens are also investigated. Specifically, PC is tested at 36 day, FRC-60 at 33 days and FRC-100 at 29 days of curing.

The following QC tests were carried out:

- **Compression test** on Ø150 mm x 300 mm (Ø5.9 in. x 11.8 in.) cylinders with loading rate of 0.6 MPa/s (87.0 psi/s) according to EN 12390-3 [34]
- **Flexural test** on 150 mm x 150 mm x 550 mm (5.9 in. x 5.9 in. x 21.6 in.) prism according to EN 14651 [41] for all the FRC mixes
- **Flexural test** on 150 mm x 150 mm x 550 mm (5.9 in. x 5.9 in. x 21.6 in.) prism according to ASTM C1609 [42]
- **Splitting tensile test** on Ø150 mm x 300 mm (Ø5.9 in. x 11.8 in.) cylinders according to ASTM C496 [73] for the only PC mix
- **Tensile test** on 800 mm (31.5 in.) long reinforcing bars $\phi$34 (34 mm, 1.3 in.) according to EN 10027-1 [72,74]

In Table 2.7 and Table 2.8, the average values obtained from the tests mentioned are collected. Annex A reports all the tests completed in this phase from Table 3.12, to Table 3.25, and from Figure 3.16 to Figure 3.20.

For the sake of clarity, the values relative to the flexural parameters $f_L$ and $f_{1^{st}peak}$ reported in this section are relative to the average curve of the respective test. The values reported in Annex A are instead extracted from each single curve and then compared resulting, anyway, in non-significant differences.

The results of the shear tests will be discussed in the next Section.

Table 2.7. Phase2 - Mechanical properties according to EN 12390-3, EN 12390-13(A), ASTM C496 [34,36,73]

| Beam ID | Days of curing | Density | $f_{cm}$ | $R_{cm}$ | $E_{cm,28}$ | $f_{T.Split}$ |
|---|---|---|---|---|---|---|
| | | $kg/m^3$ ($lb/yd^3$) | MPa (ksi) | MPa (ksi) | GPa (msi) | MPa (ksi) |
| PC-0-200h | 14 | 2366 (3988) | 59.1 (8.6) | 62.5 (9.1) | NA | 4.4 (0.6) |
| FRC-60-200h | 14 | 2387 (4024) | 57.6 (8.4) | 61.7 (9.0) | NA | NA |
| FRC-100-200h | 14 | 2351 (3964) | 73.5 (10.7) | 79.6 (11.6) | NA | NA |
| PC-0-200h | 36 | 2353 (3966) | 61.7 (9.0) | 71.9 (10.4) | 35.4 (5.1) | 4.4 (0.6) |
| FRC-60-200h | 33 | 2369 (3993) | 66.5 (9.6) | 73.5 (10.7) | 34.6 (5.0) | NA |
| FRC-100-200h | 29 | 2302 (3880) | 86.3 (12.5) | 92.7 (13.4) | 31.9 (4.6) | NA |
| PC-0-900h | 36 | 2353 (3966) | 61.7 (9.0) | 71.9 (10.4) | 35.4 (5.1) | 4.4 (0.6) |
| FRC-60-900h | 33 | 2369 (3993) | 66.5 (9.6) | 73.5 (10.7) | 34.6 (5.0) | NA |
| FRC-100-900h | 29 | 2302 (3880) | 86.3 (12.5) | 92.7 (13.4) | 31.9 (4.6) | NA |

Table 2.8. Phase2 - Mechanical properties according to EN 14651 and ASTM C1609 [41,42]

| Beam ID | $f_{L,av}$ | $f_{R1,av}$ | $f_{R2,av}$ | $f_{R3,av}$ | $f_{R4,av}$ | $f_{1^{st}peak}$ | $f^{D}{}_{600}$ | $f^{D}{}_{300}$ | $f^{D}{}_{150}$ | $f_P$ |
|---|---|---|---|---|---|---|---|---|---|---|
| | MPa (ksi) | MPa (ksi) | MPa (ksi) | MPa (ksi) | MPa (ksi) | MPa (ksi) | MPa (ksi) | MPa (ksi) | MPa (ksi) | MPa (ksi) |
| PC-0-200h | 4.5 (0.7) | NA | NA | NA | NA | 7.2 (1.0) | NA | NA | NA | 7.2 (1.0) |
| FRC-60-200h | 8.6 (1.2) | 7.3 (1.1) | 8.4 (1.2) | 8.1 (1.2) | 7.4 (1.1) | 5.7 (0.8) | 8.0 (1.2) | 7.7 (1.1) | 5.7 (0.8) | 8.6 (1.2) |
| FRC-100-200h | 11.3 (1.6) | 11.0 (1.6) | 10.8 (1.6) | 10.1 (1.5) | 9.1 (1.3) | 5.5 (0.8) | 9.4 (1.4) | 7.1 (1.0) | 5.2 (0.8) | 9.5 (1.4) |
| PC-0-200h | 4.8 (0.7) | NA | NA | NA | NA | 6.2 (0.9) | NA | NA | NA | 6.2 (0.9) |
| FRC-60-200h | 8.6 (1.2) | 7.0 (1.0) | 8.5 (1.2) | 7.6 (1.1) | 6.8 (1.0) | 5.0 (0.7) | 7.3 (1.1) | 6.9 (1.0) | 4.8 (0.7) | 7.8 (1.1) |
| FRC-100-200h | 12.9 (1.9) | 12.7 (1.8) | 12.4 (1.8) | 11.5 (1.7) | 10.5 (1.5) | 6.2 (0.9) | 10.1 (1.5) | 8.3 (1.2) | 5.4 (0.8) | 10.7 (1.6) |
| PC-0-900h | 4.8 (0.7) | NA | NA | NA | NA | 6.2 (0.9) | NA | NA | NA | 6.2 (0.9) |
| FRC-60-900h | 8.6 (1.2) | 7.0 (1.0) | 8.5 (1.2) | 7.6 (1.1) | 6.8 (1.0) | 5.0 (0.7) | 7.3 (1.1) | 6.9 (1.0) | 4.8 (0.7) | 7.8 (1.1) |
| FRC-100-900h | 12.9 (1.9) | 12.7 (1.8) | 12.4 (1.8) | 11.5 (1.7) | 10.5 (1.5) | 6.2 (0.9) | 10.1 (1.5) | 8.3 (1.2) | 5.4 (0.8) | 10.7 (1.6) |

### 2.3.3 Shear tests - Experimental results

As depicted in Figure 2.6 and Figure 2.7, the shear test corresponds to 3PBT of beams designed with only longitudinal reinforcement in order to reach a premature shear failure respect to bending one.
The linear elastic behavior of the associated isostatic simply-supported beam can be described through Equations from 2.1 to 2.6 taking care to note that the symmetric model is applicable only to the first two mixes.

The net deflection $\delta$ is obtained by subtracting the settlement of the supports from the displacement measured at the mid-span based on the disposition of the LVDTs shown.

Figure 2.8 and Figure 2.9 report the load-deflection curves obtained for the small-scale S1-0 beams, respectively at 14 and 28 days of curing.
Figure 2.10 describe the load-deflection curves obtained for the full-scale S1-4 beams and Figure 2.11 the shear-deflection curves of S1-4 according to Equations from 2.1 to 2.6.

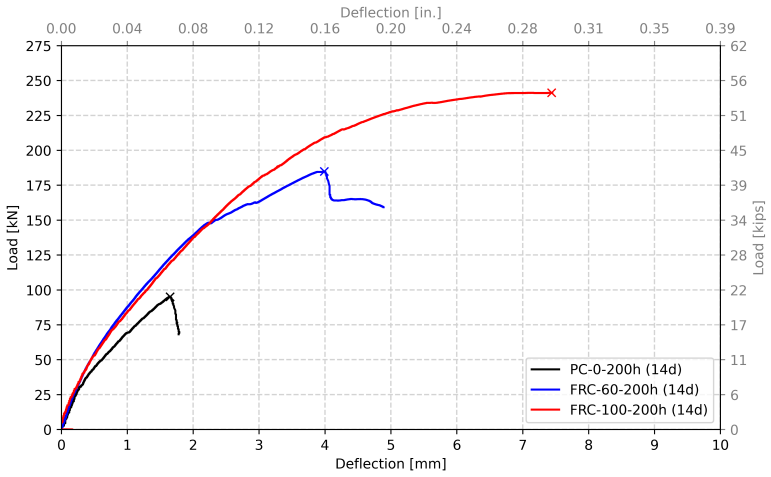



Figure 2.8. Phase2 - Load-deflection curves of PC-0-200h, FRC-60-200h and FRC-100-200h in 3PBT at 14 days of curing

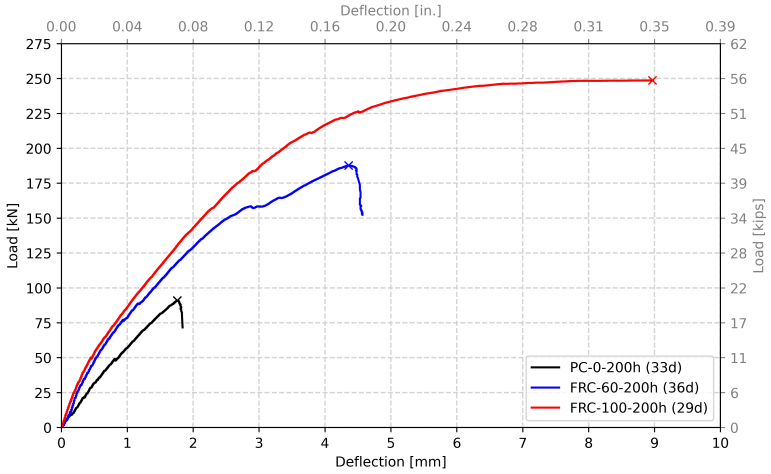



Figure 2.9. Phase2 - Load-deflection curves of PC-0-200h, FRC-60-200h and FRC-100-200h in 3PBT respectively at 36, 33, and 29 days of curing

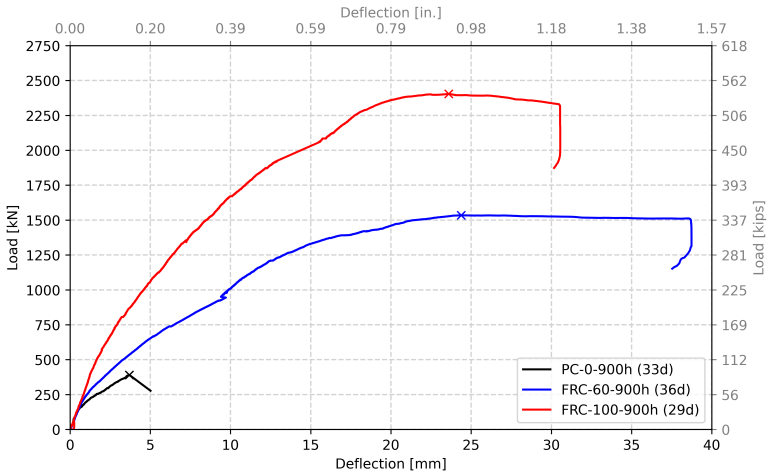



Figure 2.10. Phase2 - Load-deflection curves of PC-0-900h, FRC-60-900h and FRC-100-900h in 3PBT respectively at 36, 33, and 29 days of curing

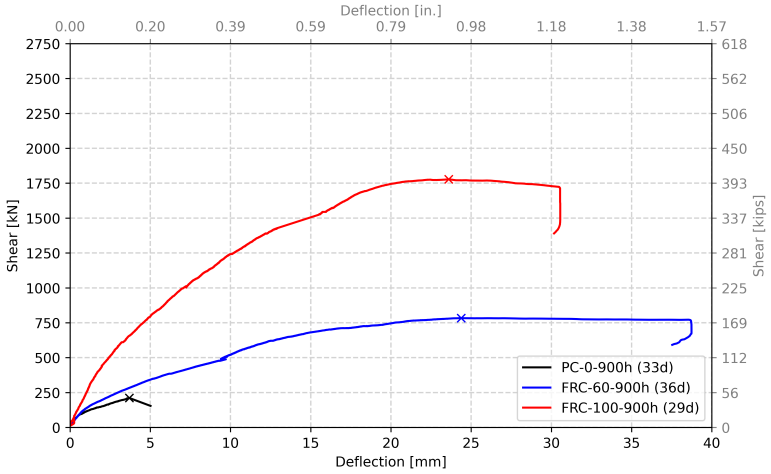



Figure 2.11. Phase2 - Shear-deflection curves of PC-0-900h, FRC-60-900h and FRC-100-900h in 3PBT respectively at 36, 33, and 29 days of curing

Table 2.9 summarizes the experimental load $P_u$ at failure, the corresponding peak deflection $\delta_{peak}$, the ultimate bending moment $M_u$, and the ultimate shear force $V_u$ calculated according to Equation 2.3 and Equation 2.5 specific for each setup.

Table 2.9. Phase2 - Shear test results of beams S1-0 adn S1-4

| **Beam ID** | **Days of curing** | $\delta_{peak}$ | $P_u$ | $M_u$ | $M_{y,Fl}^{num}$ | $M_u/M_{y,Fl}^{num}$ | **Failure Mode** | $V_u$ | $V_u/V_{u,Ref}$ |
|---|---|---|---|---|---|---|---|---|---|
| | | mm (in.) | kN (kips) | kN · m (kip-in.) | kN · m (kip-in.) | % | | kN (kips) | - |
| PC-0-200h | 14 | 1.65 (0.06) | 95.0 (21.4) | 23.9 (211.3) | 49.4 (437.3) | 48% | Shear | 48.0 (10.8) | *Ref* |
| FRC-60-200h | 14 | 3.99 (0.16) | 184.9 (41.6) | 46.3 (410.1) | 53.7 (475.3) | 86% | Shear | 92.9 (20.9) | 1.94 |
| FRC-100-200h | 14 | 7.46 (0.29) | 241.1 (54.2) | 60.4 (534.6) | 57.9 (512.5) | 104% | Bending | 121.0 (27.2) | 2.52 |
| PC-0-200h | 36 | 1.52 (0.06) | 90.9 (20.4) | 22.8 (202.2) | 49.4 (437.3) | 46% | Shear | 45.9 (10.3) | *Ref* |
| FRC-60-200h | 33 | 4.36 (0.17) | 187.6 (42.2) | 47.0 (416.2) | 53.7 (475.3) | 88% | Shear | 94.3 (21.2) | 2.05 |
| FRC-100-200h | 29 | 8.97 (0.35) | 248.6 (55.9) | 62.3 (551.1) | 60.1 (531.9) | 104% | Bending | 124.8 (28.1) | 2.72 |
| PC-0-900h | 36 | 3.70 (0.15) | 390.0 (87.7) | 498.6 (4412.6) | 1483.9 (13133.2) | 34% | Sudden Shear | 210.3 (47.3) | *Ref* |
| FRC-60-900h | 33 | 24.39 (0.96) | 1534.0 (344.9) | 1905.8 (16867.8) | 1533.2 (13570.0) | 124% | Shear + Bending | 782.4 (175.9) | 3.72 |
| FRC-100-900h | 29 | 23.61 (0.93) | 2403.8 (540.4) | 2389.5 (21149.1) | 1994.0 (17648.4) | 120% | Bending | 1770.0 (397.9) | 8.42 |

The bending capacity $M_{y,Fl}$ is computed at the yielding of the steel rebars considering equivalent rectangular compressive stress distribution (stress-block) [57] for the PC and referring to the EN1992-Annex L [56] for the FRC mixes:

- PC : $M_{y,Fl} = 0.9\, A_s f_{ys} d$
- FRC : $M_{y,Fl} = f(f_{R1}, f_{R3}, f'_c, f_{ys})$

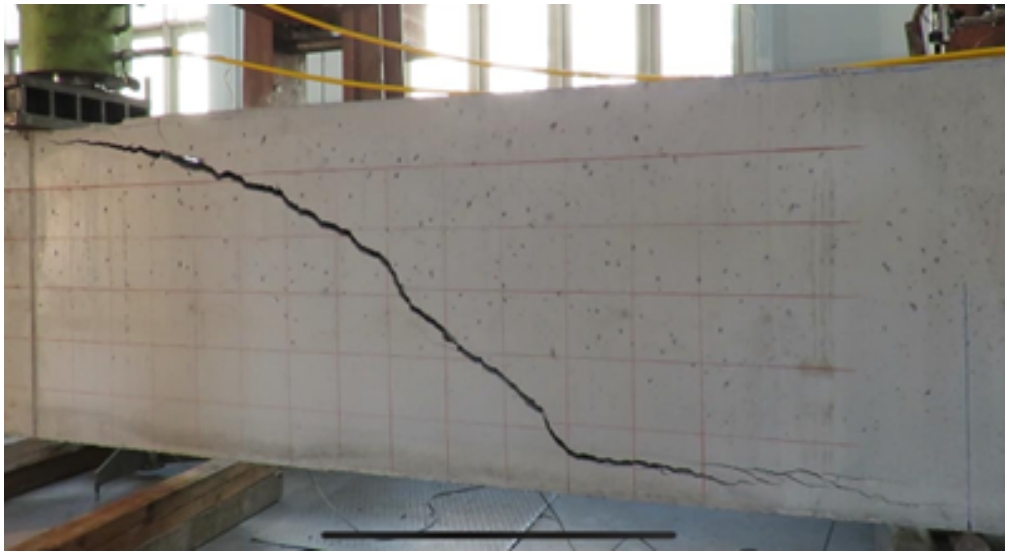
The safety factors are set equal to 1.00 (no reduction). Average values of the mechanical properties of concrete are assumed according to Table 2.7 and Table 2.8. The geometry of the cross-section and the mechanical properties of the steel correspond to

that described in Table 2.5 and Table 2.6.

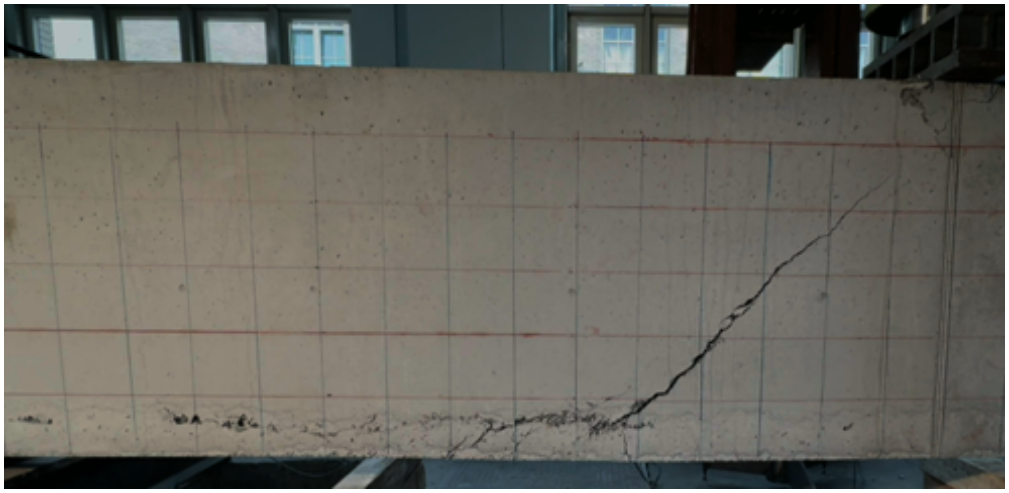
In line with these premises and in an analogous manner of Phase 1, the numerical predictions $M_{y,Fl}$ are compared to the bending at failure experimentally obtained $M_u$ and expressed as a ratio $M_u/M_{y,Fl}$. If the ratio is below 100%, the failure is reached before reaching the (theoretical) yielding of the longitudinal steel rebars, otherwise it occurrs with it. Expected Pure-shear failures are reported in green, whereas mixed failure modes are reported in red.
In the column *Failure Mode*, the visual inspection carried out during and after the tests is described with the same keywords used in Phase 1.
In addition, the ratios between the shear strength $V_u$ obtained with the different FRC mixes respect to the reference PC-0-200h are shown in the last column.

In Figure 2.12 are presented the three full-scale S1-4 beams at the end of the respective shear test.

**(a)**



**(b)**



**(c)**

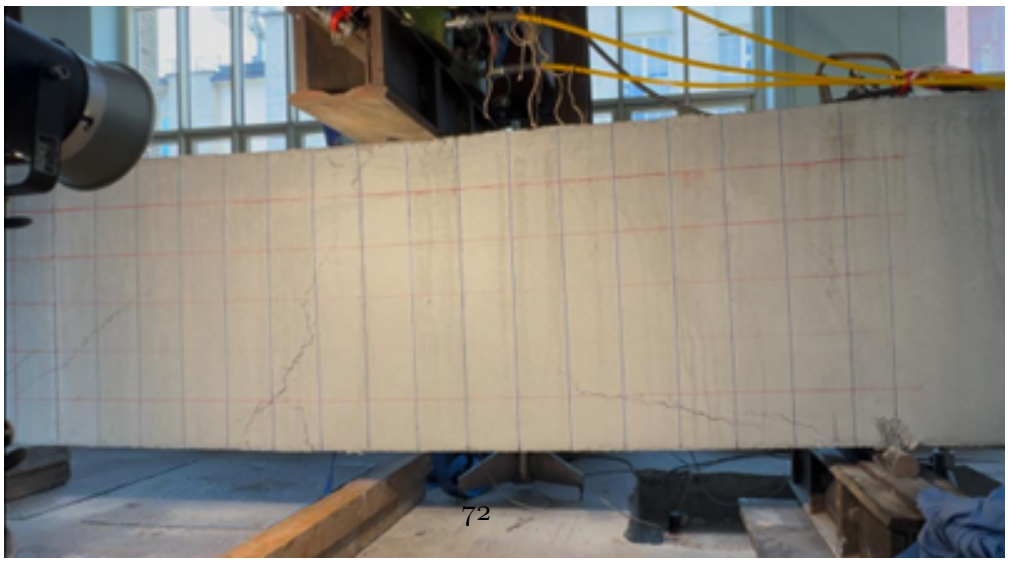




Figure 2.12. Phase2 - Pictures of all beams S1-4 at failure. (a) PC-0-900h; (b) FRC-60-900h;(c) FRC-100-900h

# 2.4 Comprehensive investigation - Size-effect of beams with variable heights

## 2.4.1 Test configuration - Setup #3

The objective of the third phase is to broaden both the quantity and diversity of available samples, thereby enabling a more robust analysis of the size-effect. The same concrete matrix with nominal strength C40/50 - $f'_c = 40$ MPa (5.8 ksi) - is used for the production of PC, the reference (*Ref*), and FRC with 60 kg/m$^3$ (101.1 lb/yd$^3$). Additionally, FRC with nominal class C70/85 - $f'_c = 70$ MPa (10.1 ksi) - and 80 kg/m$^3$ (134.8 lb/yd$^3$) is considered. All of them have a maximum aggregate size of 8 mm (0.3 in.) and they differ from the previous ones in terms of raw materials, whereas the additives and fibers remain unchanged. Small adjustments of the plasticizer were needed to guarantee the same water-to-cement ratio and the desired consistency class (i.e., SCC - class SF1 according to EN 206[70] and EN 12350-8[71]).
For each mix, a ready-mix truck with a batch volume of 5.0 m $^3$ (176.6 ft$^3$) is used.

Four different geometries are selected to be tested under shear loading realized in a manner analogous to that described in the previous phases. The ends of the beam, located outside of the tested area, are reinforced with shear reinforcement (i.e., stirrups) to ensure safe handling and movement of the beam without introducing significant stresses. Conversely, the central zone subject to bending and shear stresses is reinforced with only longitudinal reinforcement. Nominally, the longitudinal rebars are Grade42 according to the Mexican norm NMX-B-506[75] with a minimum yielding tensile strength of 4200 kg/cm$^2$ (411.9 MPa, 59.7 ksi) and experimental validation are performed. Dimensions and nomenclature proposed in this report of all the sizes are similar to those used by Sneed and Ramirez[4]:

- **S1-0**: 200 mm (7.9 in.) width × 200 mm (7.9 in.) height × 1625 mm (64.0 in.) length. Longitudinal reinforcement 4#6 (i.e., 4 x 19.1 mm, 4 x $\frac{6}{8}$in.) with net cover 10 mm (0.4 in.).

- **S1-1**: 200 mm (7.9 in.) width × 335 mm (13.2 in.) height × 2375 mm (93.5 in.) length. Longitudinal reinforcement 4#8 (i.e., 4 x 25.4 mm, 4 x $\frac{8}{8}$in.) with net cover 20 mm (0.8 in.).

- **S1-2**: 250 mm (9.8 in.) width × 600 mm (23.6 in.) height × 3845 mm (151.4 in.) length. Longitudinal reinforcement 6#10 (i.e., 6 x 31.8 mm, 6 x $\frac{10}{8}$in.) with net cover 30 mm (1.2 in.).

- **S1-3**: 250 mm (9.8 in.) width × 750 mm (29.5 in.) height × 4720 mm (185.8 in.) length. Longitudinal reinforcement 3#10 + 3#12 (i.e., 3 x 31.8 mm + 3 x 38.1 mm, 3 x $\frac{10}{8}$in. + 3 x $\frac{12}{8}$in.) with net cover 40 mm (1.6 in.).

- **S1-4**: 250 mm (9.8 in.) width × 900 mm (35.4 in.) height × 6000 mm (236.2 in.) length. Longitudinal reinforcement 6#12 (i.e., 6 x 38.1 mm, 6 x $\frac{12}{8}$in.) with net cover 50 mm (2.0 in.).

In addition specimens for QC are casted. These tests are performed no more then two days apart respect to when the respective shear test is carried out, except when explicitly stated.

Several measures are implemented to establish a defined margin between the shear failure of the PC beam and the predicted bending failure resulting from the yielding of longitudinal steel. Since the contribution of fibers to shear strength can exceed their contribution to bending, consistent with the findings from earlier phases, all sample geometries are designed to guarantee a ratio between the expected load causing yielding and the nominal load causing shear failure in PC beams at least equal to 4.
Firstly, the load configuration is modified by setting the shear-span to effective-depth ratio a/d = 2.5 differently from the value previously adopted (i.e, 3.0). This ratio is established to provide the minimum lever arm (i.e., distance $a$) necessary while still enabling the assessment of shear resistance under one of the most critical conditions, in accordance with Kani[5].
Additionally, the test setup is changed from a 3PBT to a 4PBT, as depicted in Figure 2.14.

According to Alcocer et al.[66], this test setup already accounts for 67% of shear-tested beams in their dataset. In this scenario, for a given load, the shear force remains substantially unchanged respect to the 3PBT (i.e., V = P/2), while the bending stresses decrease in the region with constant bending moment. A comparable longitudinal reinforcement ratio $\rho$, ranging from 3.18% to 3.56%, was applied across the various geometries to maintain the specified gap as previously detailed. Tables from 2.10 to 2.14 summarize the geometrical properties and the steel specifications of the specimens.

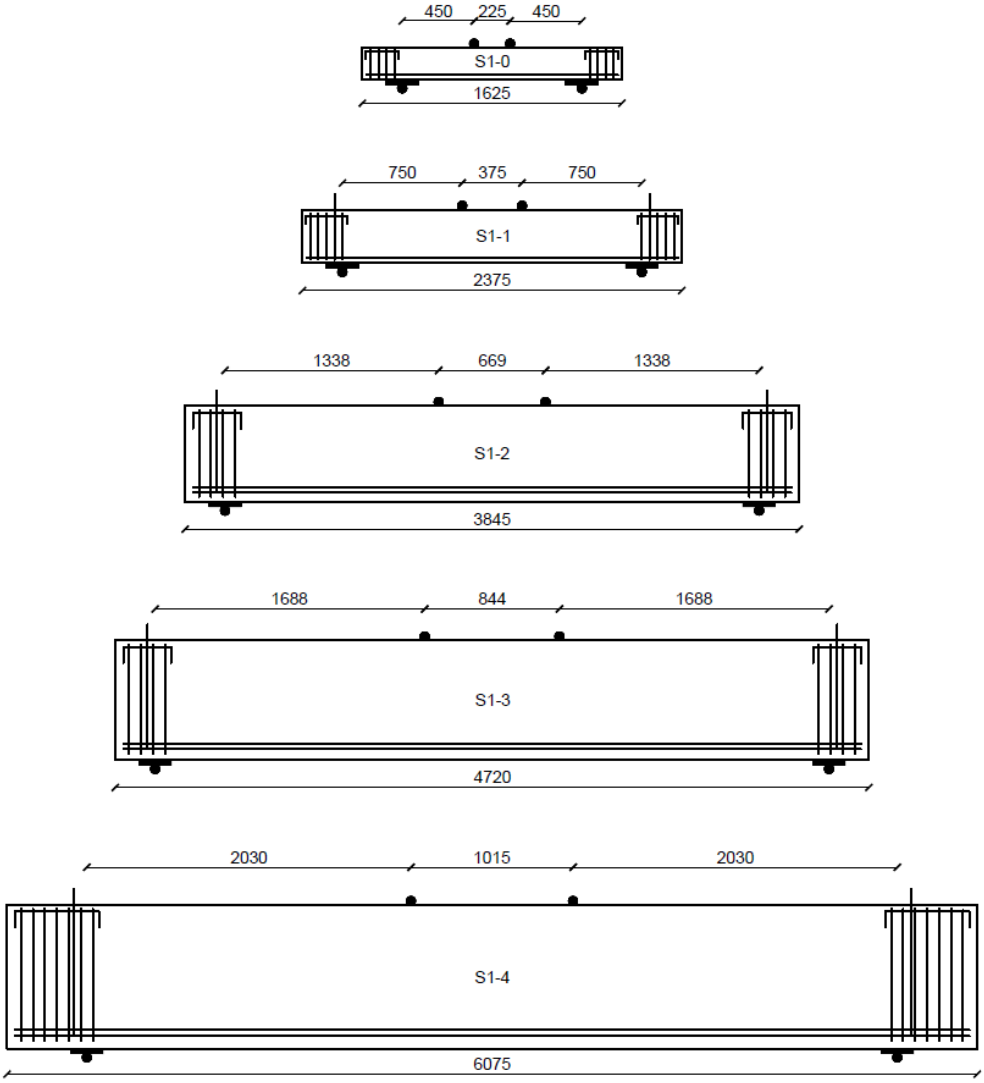



Figure 2.13. Phase3 - Setup of beams S1-0, S1-1, S1-2, S1-3, and S1-4 (measures in mm)

Table 2.10. Phase3 - Geometrical properties and steel specifications for beam S1-0

| | | | |
|---|---|---|---|
| Width | $b_w$ | mm (in.) | 200 (7.9) |
| Height | $h$ | mm (in.) | 200 (7.9) |
| Depth | $d$ | mm (in.) | 180 (7.1) |
| Shear-span to Depth ratio | $a/d$ | - | 2.5 |
| Net span length | $L_s$ | mm (in.) | 1125 (44.3) |
| Longitudinal Reinforcement | $A_s$ | $mm^2$ ($in.^2$) | 1140 (1.8) |
| Average steel yielding strength | $f_{ys}$ | MPa (ksi) | 476 (69.0) |
| Steel content | $\rho = A_s/b_w d$ | % | 3.17 |

Table 2.11. Phase3 - Geometrical properties and steel specifications for beam S1-1

| | | | |
|---|---|---|---|
| Width | $b_w$ | mm (in.) | 200 (7.9) |
| Height | $h$ | mm (in.) | 335 (13.2) |
| Depth | $d$ | mm (in.) | 302 (11.9) |
| Shear-span to Depth ratio | $a/d$ | - | 2.5 |
| Net span length | $L_s$ | mm (in.) | 1875 (73.8) |
| Longitudinal Reinforcement | $A_s$ | $mm^2$ ($in.^2$) | 2027 (3.1) |
| Average steel yielding strength | $f_{ys}$ | MPa (ksi) | 483 (70.0) |
| Steel content | $\rho = A_s/b_w d$ | % | 3.35 |

Table 2.12. Phase3 - Geometrical properties and steel specifications for beam S1-2

| | | | |
|---|---|---|---|
| Width | $b_w$ | mm (in.) | 250 (9.8) |
| Height | $h$ | mm (in.) | 600 (23.6) |
| Depth | $d$ | mm (in.) | 538 (21.2) |
| Shear-span to Depth ratio | $a/d$ | - | 2.5 |
| Net span length | $L_s$ | mm (in.) | 3345 (131.7) |
| Longitudinal Reinforcement | $A_s$ | $mm^2$ ($in.^2$) | 4750 (7.4) |
| Average steel yielding strength | $f_{ys}$ | MPa (ksi) | 482 (69.9) |
| Steel content | $\rho = A_s/b_w d$ | % | 3.53 |

Table 2.13. Phase3 - Geometrical properties and steel specifications for beam S1-3

| | | | |
|---|---|---|---|
| Width | $b_w$ | mm (in.) | 250 (9.8) |
| Height | $h$ | mm (in.) | 750 (29.5) |
| Depth | $d$ | mm (in.) | 675 (26.6) |
| Shear-span to Depth ratio | $a/d$ | - | 2.5 |
| Net span length | $L_s$ | mm (in.) | 4220 (166.1) |
| Longitudinal Reinforcement | $A_s$ | $mm^2$ ($in.^2$) | 5795 (9.0) |
| Average steel yielding strength | $f_{ys}$ | MPa (ksi) | 482 (69.9) |
| Steel content | $\rho = A_s/b_w d$ | % | 3.43 |

Table 2.14. Phase3 - Geometrical properties and steel specifications for beam S1-4

| | | | |
|---|---|---|---|
| Width | $b_w$ | mm (in.) | 250 (9.8) |
| Height | $h$ | mm (in.) | 900 (35.4) |
| Depth | $d$ | mm (in.) | 812 (32.0) |
| Shear-span to Depth ratio | $a/d$ | - | 2.5 |
| Net span length | $L_s$ | mm (in.) | 5075 (199.8) |
| Longitudinal Reinforcement | $A_s$ | $mm^2$ ($in.^2$) | 6841 (10.6) |
| Average steel yielding strength | $f_{ys}$ | MPa (ksi) | 482 (69.9) |
| Steel content | $\rho = A_s/b_w d$ | % | 3.37 |

### 2.4.2 Material properties

As previously stated, the general nomenclature adopted is "XX-YY-ZZZh" where:

- XX: type of concrete (PC, FRC)
- YY: overall content of steel fibers expressed in $kg/m^3$ (0, 60, 80)
- ZZZh: nominal height of the sample expressed in mm (200h, 335h, 600h, 750h, 900h)

The beams S1-0, S1-1, S1-2 and S1-3 are tested at 14±2 days of curing to accommodate the time required for modifications to the testing frame geometry. The beams S1-4 are tested at 116±2 days. The following QC tests are carried out in parallel to the corresponding shear tests date:

- **Compression test** on Ø150 mm x 300 mm (Ø5.9 in. x 11.8 in.) cylinders with loading rate of 0.6 MPa/s (87.0 psi/s) according to EN 12390-3 [34]
- **Compression test** on 150 mm x 150 mm x 150 mmm (5.9 in. x 5.9 in. x 5.9 in.) cubes with loading rate of 0.6 MPa/s (87.0 psi/s) according to EN 12390-3 [34]

- **Elastic modulus** on Ø150 mm x 300 mm (Ø5.9 in. x 11.8 in.) cylinders according to EN 12390-13 (Method A) based on the compression tests previously conducted [36]
- **Flexural test** on 150 mm x 150 mm x 550 mm (5.9 in. x 5.9 in. x 21.6 in.) prism according to EN 14651 [41] for all the FRC mixes
- **Flexural test** on 150 mm x 150 mm x 550 mm (5.9 in. x 5.9 in. x 21.6 in.) prisms according to ASTM C1609 [42]
- **Tensile test** on 800 mm (31.5 in.) long reinforcing bars #3 (9.5 mm, 0.4 in.), #4 (12.7 mm, 0.5 in.), #6 (19.1 mm, 0.8 in.), #8 (25.4 mm, 1.0 in.)and #10 (31.8 mm, 1.3 in.) according to NMX B506 [75]

In Table 2.15 and Table 2.16, the average values obtained from the tests mentioned are collected. Annex A reports all the tests completed in this phase from Table 3.26, to Table 3.35, and from Figure 3.21 to Figure 3.24.

For the sake of clarity, the values relative to the flexural parameters $f_L$ and $f_{1^{st}peak}$ reported in this section are relative to the average curve of the respective test. The values reported in Annex A are instead extracted from each single curve and then compared resulting, anyway, in non-significant differences.

The results of the shear tests will be discussed in the next Section.

Table 2.15. Phase3 - Mechanical properties according to EN 12390-3, EN 12390-13(A), ASTM C496[34,36,73]

| Beam ID | Days of curing | Density | $f_{cm}$ | $R_{cm}$ | $E_{cm,28}$ | $f_{T.Split}$ |
|---|---|---|---|---|---|---|
| | | $kg/m^3$ ($lb/yd^3$) | MPa (ksi) | MPa (ksi) | GPa (msi) | MPa (ksi) |
| PC-0-ZZZh | 14±2 | 2320 (3910) | 56.8 (8.2) | 50.6 (7.3) | 27.9 (4.1) | 4.4 (0.6) |
| FRC-60-ZZZh | 14±2 | 2349 (3959) | 52.1 (7.6) | 48.8 (7.1) | 27.3 (4.0) | NA |
| FRC-100-ZZZh | 14±2 | 2327 (3922) | 73.1 (10.6) | 70.0 (10.2) | 27.9 (4.0) | NA |
| PC-0-900h | 116±2 | 2320 (3910) | 62.1 9.0 | NA | NA | 4.4 (0.6) |
| FRC-60-900h | 116±2 | 2349 (3959) | 56.1 8.1 | NA | NA | NA |
| PC-0-900h | 116±2 | 2327 (3922) | 73.1 11.9 | NA | NA | NA |

Table 2.16. Phase3 - Mechanical properties according to EN 14651 and ASTM C1609[41,42]

| Beam ID | $f_{L,av}$ | $f_{R1,av}$ | $f_{R2,av}$ | $f_{R3,av}$ | $f_{R4,av}$ | $f_{1^{st}peak}$ | $f^D{}_{600}$ | $f^D{}_{300}$ | $f^D{}_{150}$ | $f_P$ |
|---|---|---|---|---|---|---|---|---|---|---|
| | MPa (ksi) | MPa (ksi) | MPa (ksi) | MPa (ksi) | MPa (ksi) | MPa (ksi) | MPa (ksi) | MPa (ksi) | MPa (ksi) | MPa (ksi) |
| PC-0-ZZZh | NA | NA | NA | NA | NA | 5.1 (0.7) | NA | NA | NA | 5.2 (0.8) |
| FRC-60-ZZZh | 4.7 (0.7) | 6.9 (1.0) | 8.6 (1.2) | 8.3 (1.2) | 7.7 (1.1) | 4.2 (0.6) | 7.6 (1.1) | 8.1 (1.2) | 6.4 (0.9) | 8.6 (1.3) |
| FRC-80-ZZZh | 5.3 (0.8) | 10.6 (1.5) | 12.2 (1.8) | 12.0 (1.7) | 11.4 (1.7) | 4.7 (0.7) | 9.3 (1.4) | 9.2 (1.3) | 6.6 (1.0) | 10.2 (1.5) |
| PC-0-900h | NA | NA | NA | NA | NA | 5.1 (0.7) | NA | NA | NA | 5.2 (0.8) |
| FRC-60-900h | 4.7 (0.7) | 8.8 (1.3) | 9.5 (1.4) | 9.5 (1.4) | 8.4 (1.2) | 5.3 (0.8) | 8.6 (1.2) | 9.8 (1.4) | 7.4 (1.1) | 9.9 (1.4) |
| FRC-80-900h | 4.6 (0.7) | 10.0 (1.5) | 11.2 (1.6) | 10.6 (1.5) | 9.9 (1.4) | 5.0 (0.7) | 8.2 (1.2) | 7.7 (1.1) | 5.6 (0.8) | 8.8 (1.3) |

### 2.4.3 Shear tests - Experimental results

As depicted in Figure 2.13, the shear test corresponds to a 4PBT of beams designed with only longitudinal reinforcement in order to reach a premature shear failure respect to bending. Considering the linear elastic behavior of the associated isostatic simply-supported beam describe through the Equations from 2.7 to 2.9, it is worth noting that the contribute of the self-weight is basically negligible and the representation of the stress distributions induced by only the actuator, without then considering the self-weigth of the beam, is represented in Figure 2.14.

$$R_A = R_B = \frac{1}{L}\left(q\frac{(c+L)^2}{2} - q\frac{c^2}{2} + a\frac{P}{2} + (\frac{3}{2}a)\frac{P}{2}\right) \tag{2.7}$$

$$V(x) = \begin{cases} -qx & \text{if } x < c \\ -qx + R_A & \text{if } c < x < c + a \\ -qx + R_A - \frac{P}{2} & \text{if } c + a < x < c + \frac{3}{2}a \\ -qx + R_A - P & \text{if } c + \frac{3}{2}a < x < c + L \\ -qx + R_A - P + R_B & \text{otherwise} \end{cases} \tag{2.8}$$

$$M(x) = \begin{cases} -q\frac{x^2}{2} & \text{if } x < c \\ -q\frac{c^2}{2} + R_A(x-c) & \text{if } c < x < c + a \\ -q\frac{c^2}{2} + R_A(x-c) - \frac{P}{2}(x-(c+a)) & \text{if } c + a < x < c + \frac{3}{2}a \\ -q\frac{c^2}{2} + R_A(x-c) - \frac{P}{2}(x-(c+a)) - \frac{P}{2}(x-(c+\frac{3}{2}a)) & \text{if } c + \frac{3}{2}a < x < c + L \\ -q\frac{c^2}{2} + R_A(x-c) - \frac{P}{2}(x-(c+a)) - \frac{P}{2}(x-(c+\frac{3}{2}a)) + R_B(x-(c+L)) & \text{otherwise} \end{cases} \tag{2.9}$$

where:

- q homogeneous linear density of the beam

- P total load applied by the testing machine
- $R_A$ vertical reaction at hinged support A
- $R_B$ vertical reaction at hinged support B
- L Net span between supports = $\frac{5}{2}a$
- c Cantilever length

According to the Equations from 2.7 to 2.9 and considering the symmetrical configuration described it is then possible to estimate the shear and the bending moment in correspondence of the actuator:

$$V = -q\ (c + a) + R_A \tag{2.10}$$

$$M = -q\frac{c^2}{2} + R_A\ a \tag{2.11}$$

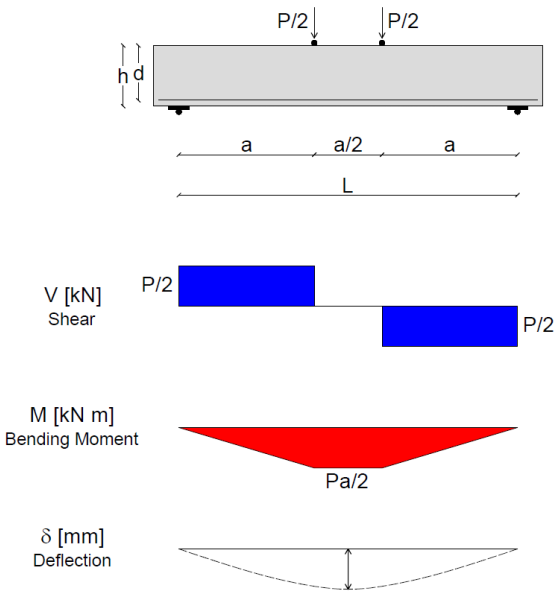



Figure 2.14. Phase3 - Test configuration and stress distribution along beams S1-0, S1-1, S1-2, S1-3, and S1-4

The net deflection $\delta$ is obtained by subtracting the settlement of the supports from the displacement measured at the mid-span based on the disposition of the LVDTs shown.

The Figures from 2.15 to 2.19 report the load-deflection curves for the beams S1-0, S1-1, S1-2, S1-3, and S1-4. The Y-axis presents load measurements neglecting self-weight contributions, accounting solely for the force applied by the actuator and the weight of the load transmission system (steel rollers, plates, and blocks). The X-axis displays net deflection values, calculated as the midspan gross deflection minus the mean support settlements.

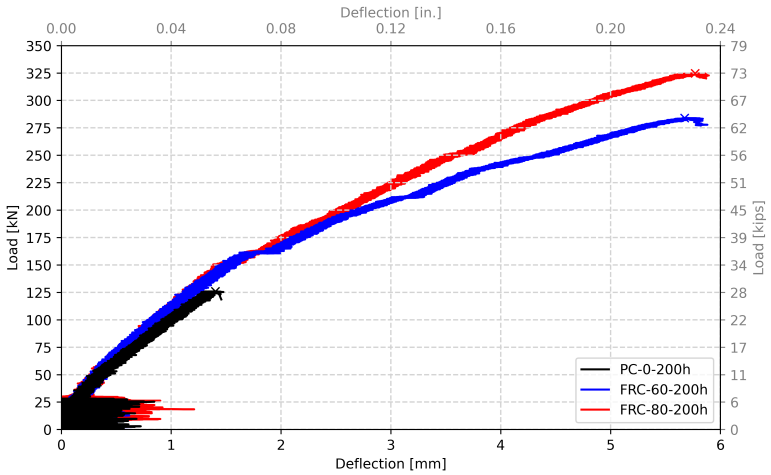



Figure 2.15. Phase3 - Load-deflection curves of PC-0-200h, FRC-60-200h and FRC-80-200h in 4PBT at 14±2 of curing

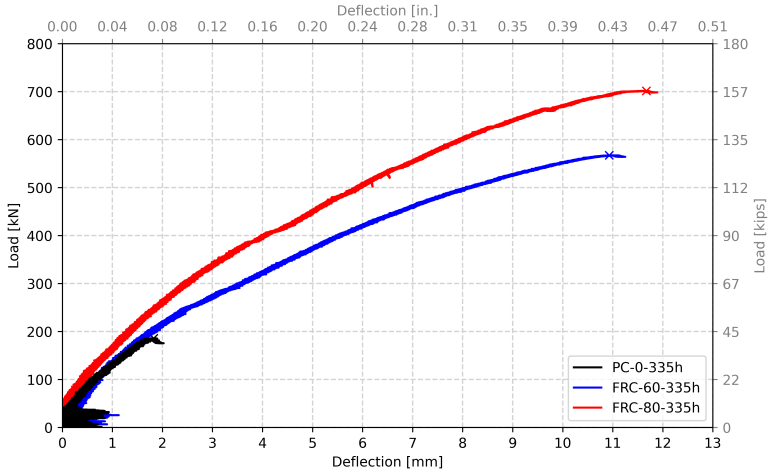



Figure 2.16. Phase3 - Load-deflection curves of PC-0-335h, FRC-60-335h and FRC-80-335h in 4PBT at 14±2 of curing

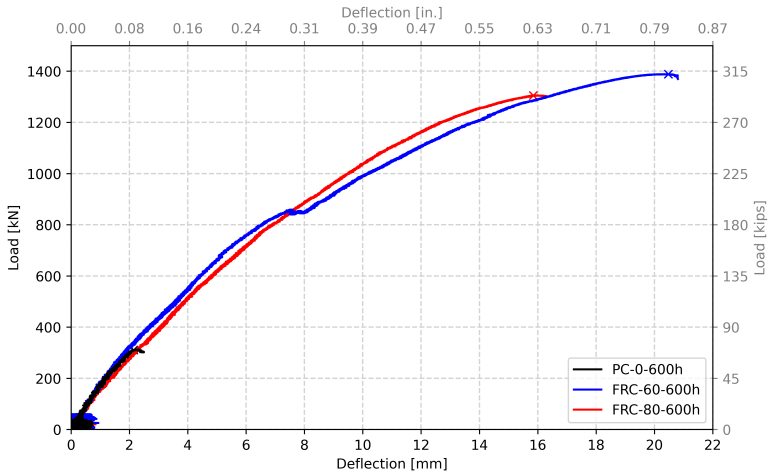



Figure 2.17. Phase3 - Load-deflection curves of PC-0-600h, FRC-60-600h and FRC-80-600h in 4PBT at 14±2 of curing

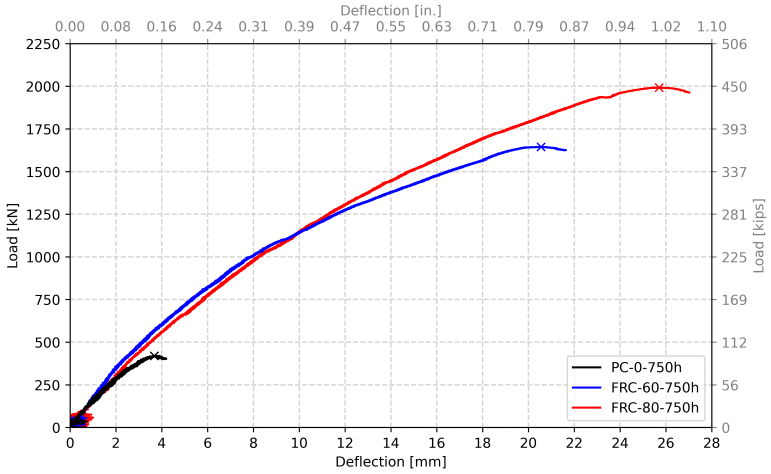



Figure 2.18. Phase3 - Load-deflection curves of PC-0-750h, FRC-60-750h and FRC-80-750h in 4PBT at 14±2 of curing

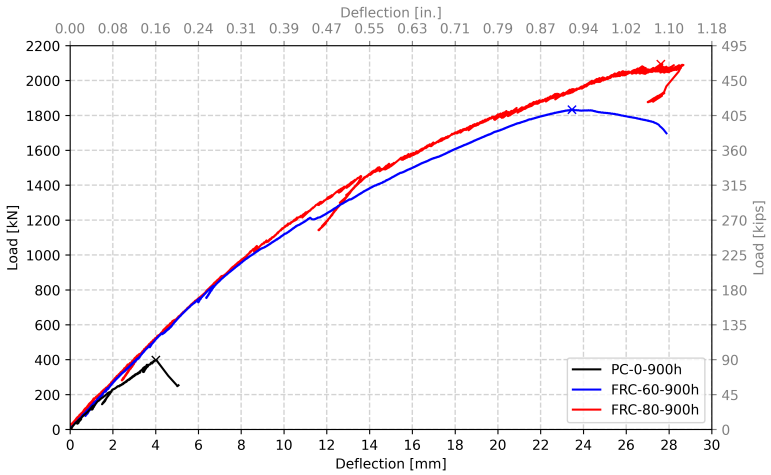



Figure 2.19. Phase3 - Load-deflection curves of PC-0-900h, FRC-60-900h and FRC-80-900h in 4PBT at 116±2 of curing

Table 2.17 summarizes the experimental load $P_u$ at failure, the corresponding peak deflection $\delta_{peak}$, the ultimate bending moment $M_u$, and the ultimate shear force $V_u$ calculated according to Equation 2.10.

Table 2.17. Phase1 - Shear test results of beams S1-0, S1-1, S1-2, S1-3 and S1-4

| **Beam ID** | **Days of curing** | $\delta_{peak}$ | $P_u$ | $M_u$ | $M_{y,Fl}^{num}$ | $M_u/M_{y,Fl}^{num}$ | **Failure Mode** | $V_u$ | $V_u/V_{u,Ref}$ |
|---|---|---|---|---|---|---|---|---|---|
| | | mm (in.) | kN (kips) | kN · m (kip-in.) | kN · m (kip-in.) | % | | kN (kips) | - |
| PC-0-200h | 14±2 | 1.40 (0.06) | 125.9 (28.3) | 28.1 (249.1) | 84.5 (748.2) | 33% | Shear | 63.4 (14.3) | *Ref* |
| FRC-60-200h | 14±2 | 5.67 (0.22) | 283.9 (63.8) | 63.5 (562.1) | 88.2 (780.9) | 72% | Shear | 142.5 (32.0) | 2.25 |
| FRC-80-200h | 14±2 | 5.77 (0.23) | 324.6 (73.0) | 73.2 (647.7) | 95.1 (841.8) | 77% | Shear | 162.8 (36.6) | 2.57 |
| PC-0-335h | 14±2 | 1.81 (0.07) | 185.7 (41.7) | 70.5 (624.4) | 249.1 (2204.5) | 28% | Shear | 94.3 (21.2) | *Ref* |
| FRC-60-335h | 14±2 | 10.93 (0.43) | 567.1 (127.5) | 213.3 (1888.3) | 258.6 (2288.4) | 83% | Shear | 285.0 (64.1) | 3.02 |
| FRC-80-335h | 14±2 | 11.75 (0.46) | 701.4 (157.7) | 262.2 (2320.7) | 279.1 (2469.8) | 94% | Shear | 352.1 (79.2) | 3.73 |
| PC-0-600h | 14±2 | 2.15 (0.08) | 310.1 (69.7) | 214.1 (1895.4) | 1042.3 (9225.1) | 21% | Shear | 160.8 (36.2) | *Ref* |
| FRC-60-600h | 14±2 | 20.48 (0.81) | 1388.0 (312.0) | 936.9 (8292.2) | 1073.8 (9504.2) | 87% | Shear | 699.8 (157.3) | 4.35 |
| FRC-80-600h | 14±2 | 15.85 (0.62) | 1304.9 (293.3) | 879.4 (7783.2) | 1168.2 (10339.5) | 75% | Shear | 658.2 (148.0) | 4.09 |
| PC-0-750h | 14±2 | 3.68 (0.14) | 419.0 (94.2) | 364.1 (3222.4) | 1487.5 (13165.7) | 24% | Shear | 218.5 (49.1) | *Ref* |
| FRC-60-750h | 14±2 | 20.55 (0.81) | 1644.3 (369.6) | 1401.0 (12400.2) | 1656.2 (14658.9) | 85% | Shear + Local | 831.2 (186.9) | 3.80 |
| FRC-80-750h | 14±2 | 25.71 (1.01) | 1991.3 (447.7) | 1679.6 (14865.5) | 1791.8 (15858.3) | 94% | Shear | 1004.5 (225.8) | 4.60 |
| PC-0-900h | 116±2 | 4.01 (0.16) | 397.7 (89.4) | 420.2 (3718.7) | 2352.3 (20819.6) | 18% | Shear | 211.8 (47.6) | *Ref* |
| FRC-60-900h | 116±2 | 23.47 (0.92) | 1832.7 (412.0) | 1876.9 (16611.8) | 2471.9 (21878.2) | 76% | Shear | 929.5 (209.0) | 4.39 |
| FRC-80-900h | 116±2 | 27.62 (1.09) | 2093.7 (470.7) | 2141.6 (18955.1) | 2695.4 (23856.3) | 79% | Shear | 1059.9 (238.3) | 5.00 |

The bending capacity $M_{y,Fl}$ is computed at the yielding of the steel rebars considering equivalent rectangular compressive stress distribution (stress-block) [57] for the PC and referring to the EN1992-Annex L [56] for the FRC mixes:

- PC : $M_{y,Fl} = 0.9\, A_s f_{ys} d$
- FRC : $M_{y,Fl} = f(f_{R1}, f_{R3}, f'_c, f_{ys})$

The safety factors are set equal to 1.00 (no reduction) and the size-effect $k_G$ - function of the area under tension due to bending - is considered for all the samples. Average values of the mechanical properties of concrete are assumed according to Table 2.7 and Table 2.8. The geometry of the cross-section and the mechanical properties of the steel correspond to that described from Table 2.10 to Table 2.13.

In line with the previous phases, the numerical predictions $M_{y,Fl}$ are compared to the bending at failure experimentally obtained $M_u$ and expressed as a ratio $M_u/M_{y,Fl}$. If the ratio is below 100%, the failure is reached before reaching the (theoretical) yielding of the longitudinal steel rebars, otherwise it occurres with it. Expected Pure-shear failures are reported in green, whereas mixed failure modes are reported in red.
In the column *Failure Mode*, the visual inspection carried out during and after the tests is described with the same keywords used in Phase 1.
In addition, the ratios between the shear strength $V_u$ obtained with the different FRC mixes respect to the reference PC-0-ZZZh are shown in the last column.

The Figures from 2.20 to 2.24 present all the samples divided according to the geometry at the end of the respective shear test.




Figure 2.20. Phase3 - Pictures of all beams S1-0 after failure. (a) PC-0-200h; (b) FRC-60-200h; (c) FRC-80-200h; (d) 4PBT setup

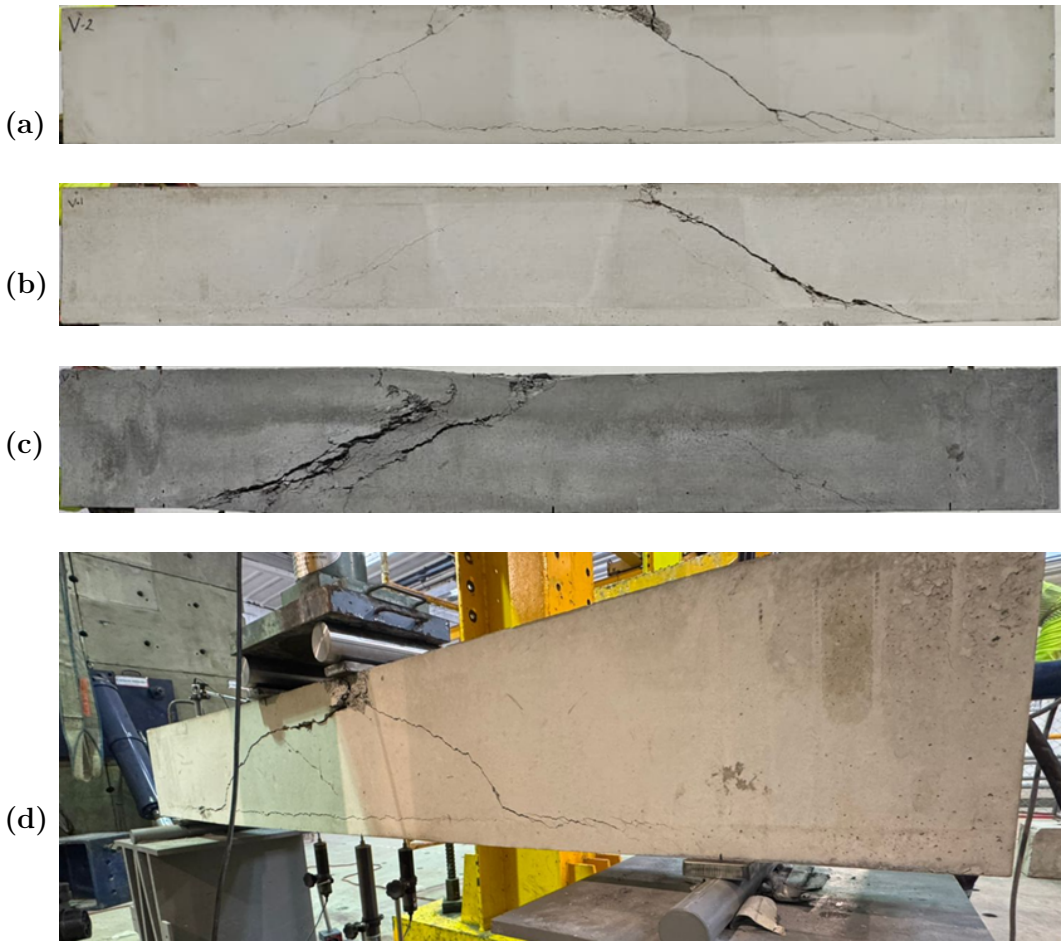
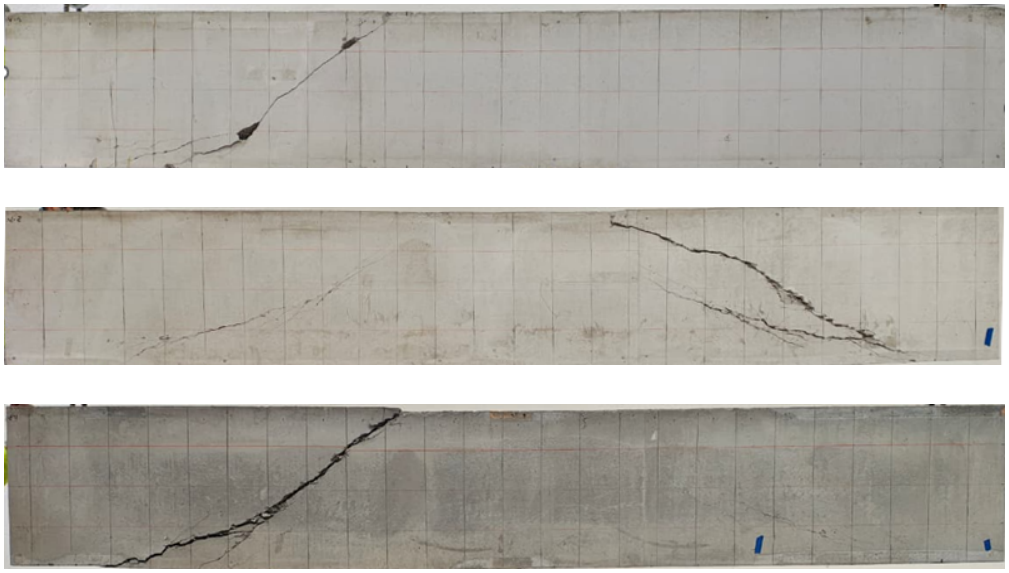



Figure 2.21. Phase3 - Samples S1-1 after failure. (a) PC-0-335h; (b) FRC-60-335h;(c) FRC-80-335h; (d) S1-1 setup



**(a)**



**(b)**



**(c)**



**(d)**

Figure 2.22. Phase3 - Samples S1-2 after failure. (a) PC-0-600h; (b) FRC-60-600h; (c) FRC-80-600h; (d) S1-2 setup

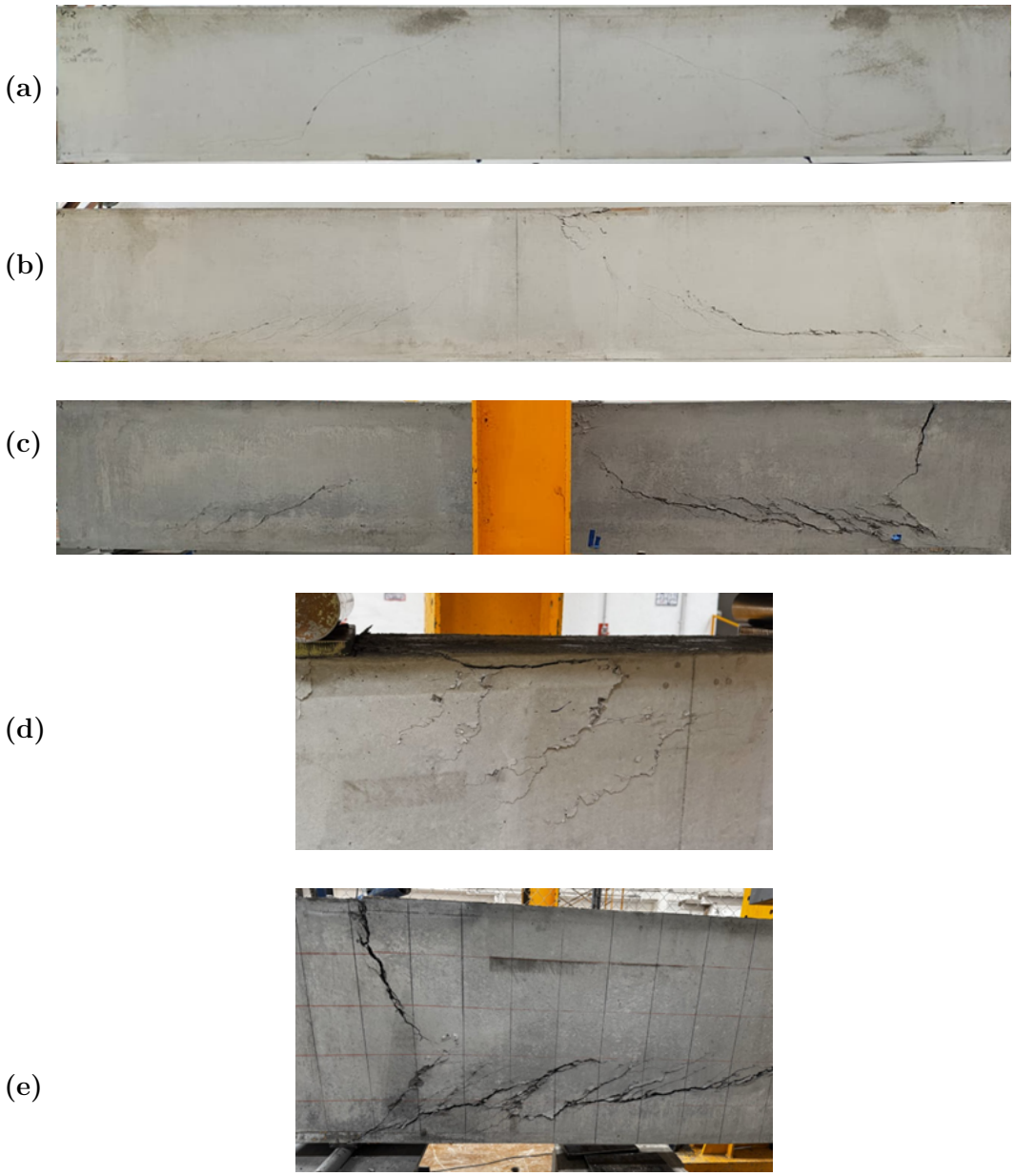



Figure 2.23. Phase3 - Samples S1-3 after failure. (a) PC-0-750h; (b) FRC-60-750h; (c) FRC-80-750h; (d) Detail of local failure of FRC-60-750h; (e) Detail of crack distribution of FRC-80-750h




Figure 2.24. Phase3 - Samples S1-4 after failure. (a) PC-0-900h; (b) FRC-60-900h; (c) FRC-80-900. (d) Size comparison of S1-0 to S1-4

# Chapter 3

# Discussion of test results

The investigations performed in Phase 1 and Phase 2 were used to optimize the design of the shear tests performed in Phase 3. Due to the multiple hybrid (i.e., shear and bending) failures observed in these phases, only the tests results of Phases 3 are analyzed below. In fact, as shown in Table 2.17 all tests presented a clear shear failure.

These tests, hereinafter identified as *"Present Study 2025"*, are compared with both the up-to-date databases provided by Alcocer et al.[66] and Cuenca et al.[65], respectively based on ASTM C1609[42] and EN 14651[41].

In addition, the experimental outcomes are compared to current prediction models according to Eurocode2[56], MC2020[33], ACI 318[57], and ACI 544.4R[16].

## 3.1 Experimental results vs Up-To-Date datasets

A summary of the Present Study is depicted in Figure 3.1. The dataset is then compared with the databases proposed by Alcocer et al. and Cuenca et al. from Figure 3.2 to Figure 3.5.

It is clear that an assessment of average shear strength based solely on fiber content, $V_f$, and without an actual assessment of flexural performance does not provide a clear

and, therefore, reliable result observing even counterintuitive results where low-content-fiber concretes perform better than the equivalent with more fibers (Figure 3.2).
Certainly more significant is what emerges from the comparison respect the flexural parameters $f_{R1}$, $f_{R3}$, $f^{D}_{600}$, and $f^{D}_{150}$ with an evident horizontal trend for fixed ranges of these variables which combines improved flexural performances with greater shear capacity. However, this last statement is severely limited by the poor characterization of the samples collected in the databases, drastically limiting the total population.

Some limitations of both the databases have already been presented. The key parameters considered in Section 1.3.3 are now are now being re-proposed with the addition of the Present Study in Figure 3.6 from (a) to (f). Albeit to a small extent, the contribution of the data provided is evident to ensure progressive expansion and therefore better calibration of the models based on them.

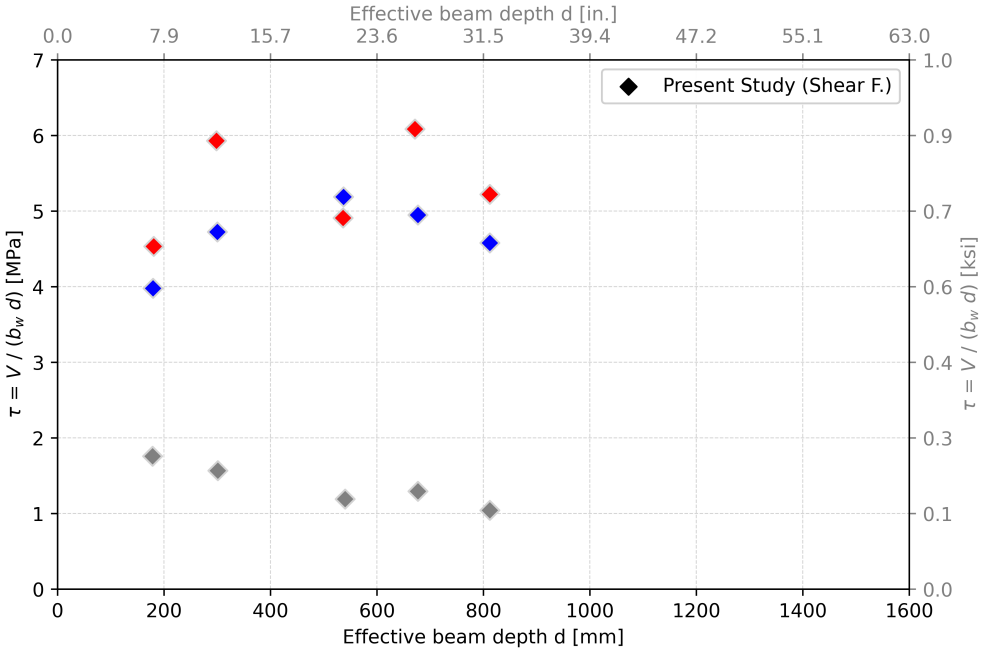



Figure 3.1. Dataset of shear tests from Present Study.

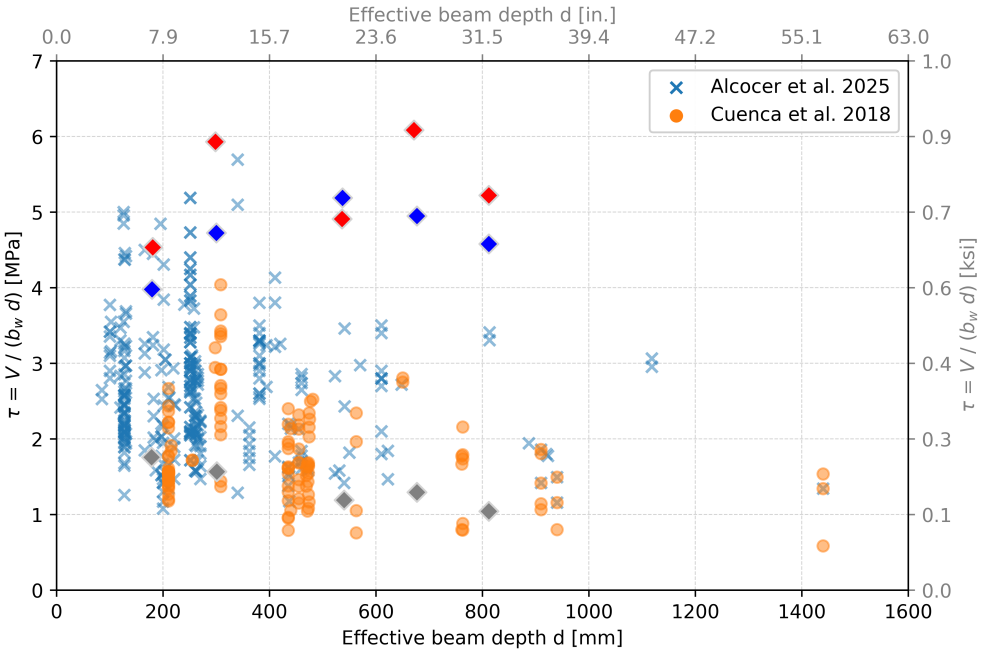



Figure 3.2. Dataset of shear tests from Present Study, Alcocer et al., Cuenca et al. [65,66]

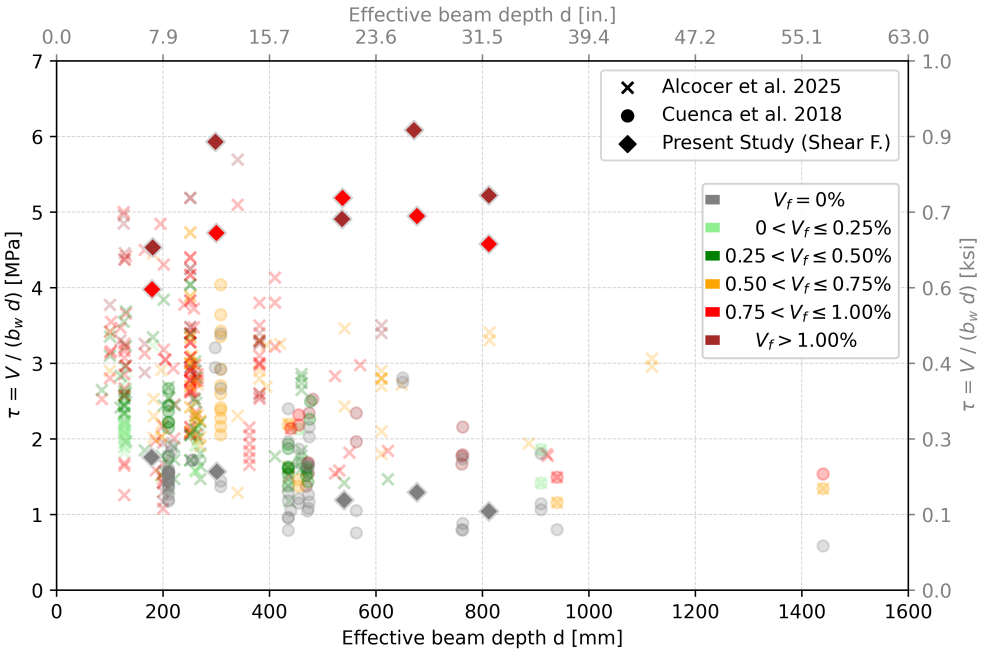



Figure 3.3. Dataset of shear tests from Present Study, Alcocer et al., Cuenca et al. [65,66] respect to the volume of steel fibers $V_f$

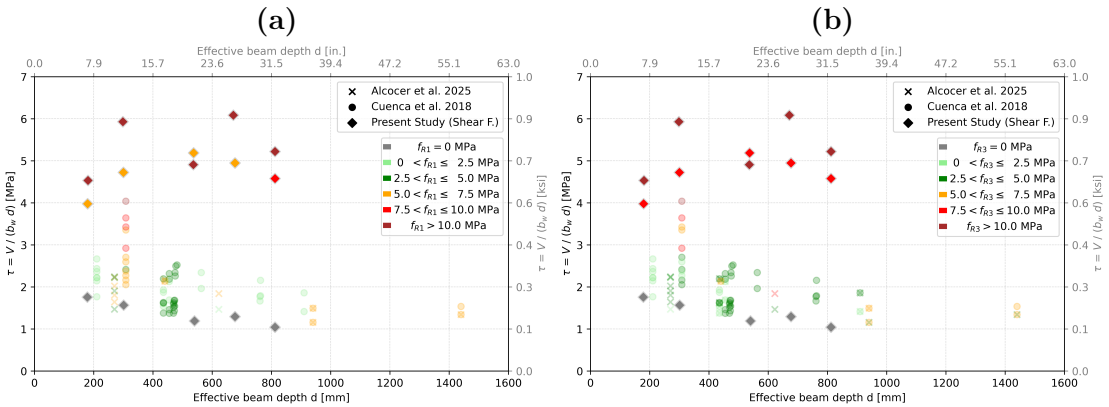



Figure 3.4. Dataset of shear tests from Present Study, Alcocer et al., Cuenca et al. [65,66] respect to $f_{R1}$ (left) and $f_{R3}$ (right)

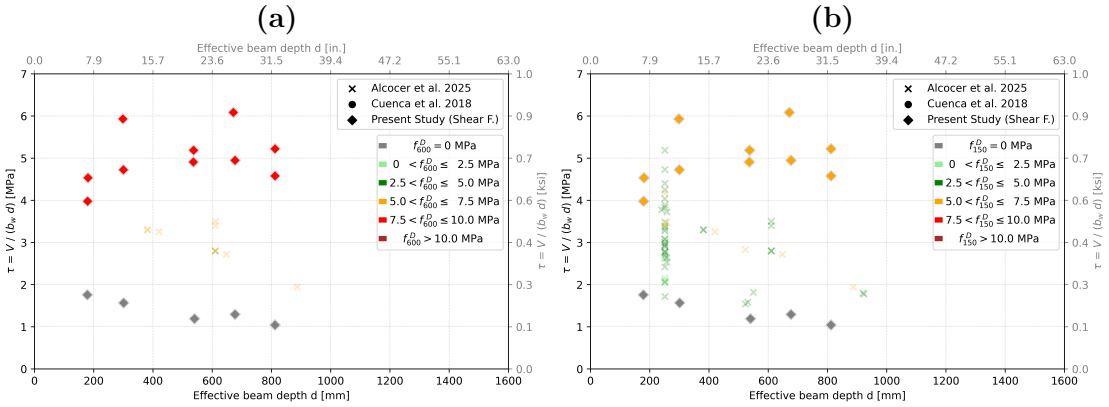



Figure 3.5. Dataset of shear tests from Present Study, Alcocer et al., Cuenca et al. [65,66] respect to $f'^{D}_{600}$ (left) and $f'^{D}_{150}$ (right)

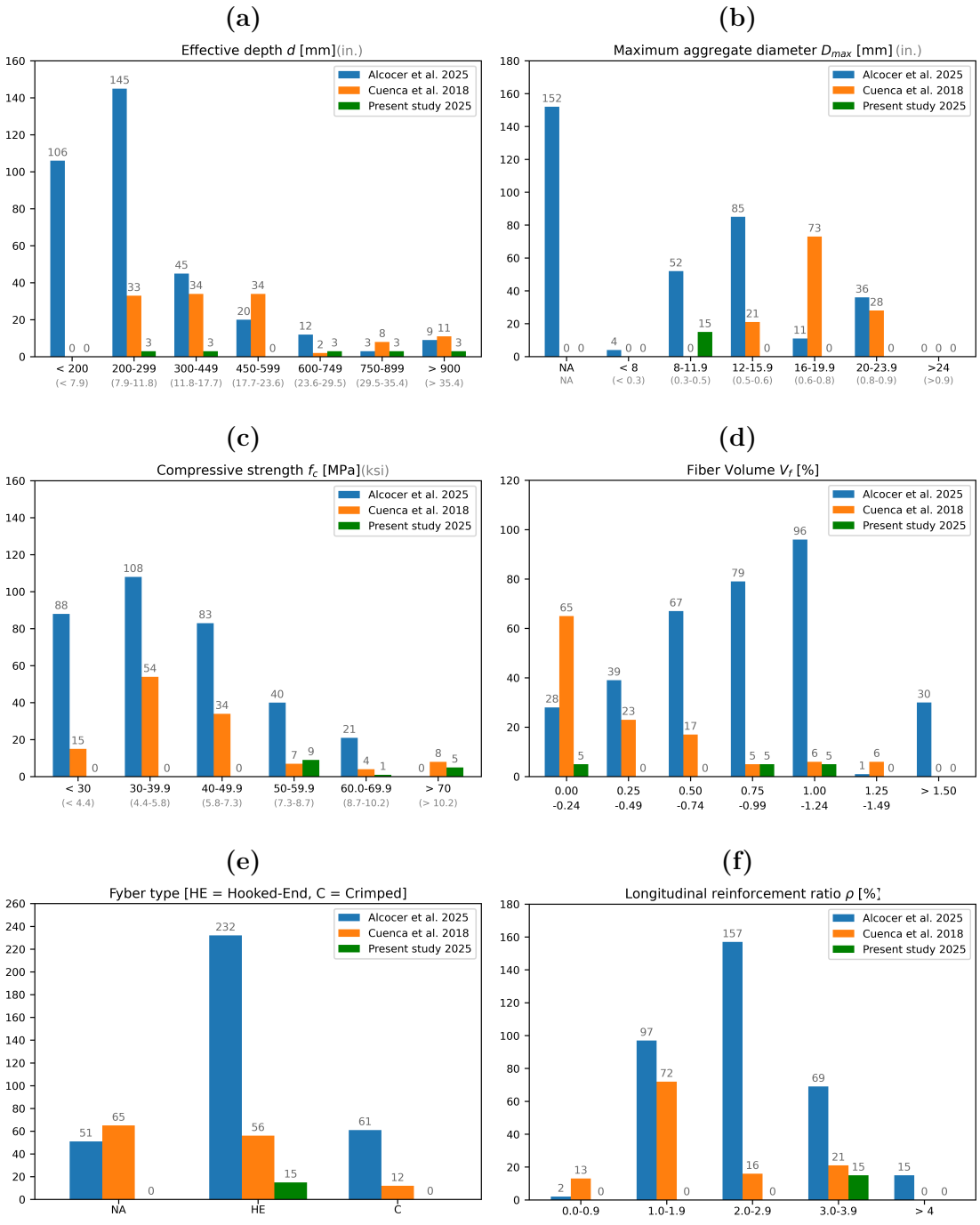



Figure 3.6. Distribution respect to main variables of shear tests from Present Study, Alcocer et al., Cuenca et al.[65,66] (respectively, 30, 340 and 122)

## 3.2 Experimental results vs prediction models

The considerations that follow are limited to all the Phase 3 because characterized by only shear failures, with the exception for the sample FRC-60-600h that, during the testing and after a clear shear cracks propagation, ends up in a local failure in correspondence of one of the two actuators. The other Phases are not considered due to the recurring bending mechanism. All the results are then refereed to a 4PBT configuration and a comparable longitudinal reinforcement ratio $\rho$ ranging from 3.18% to 3.56%. Furthermore, the PC mix is the same used for FRC with 60 kg/m$^3$ (101.1 lb/yd$^3$) of fibers, whereas the FRC with 80 kg/m$^3$ (134.8 lb/yd$^3$) is made with a slightly higher nominal compressive strength. Despite the first two concrete mixes being the same, PC achieved a slightly higher compressive strength (+8.2%).

The Figure 3.7 summarizes the ultimate shear force achieved by the single tests presented from Figure 2.15 to Figure 2.18 whereas the Figure 3.8 presents the same results in terms of average ultimate shear stress $\tau = V/(b_w\ d)$. All these result are plotted against the effective beam depth $d$, so the distance from the top of the beam to the geometrical center of the longitudinal reinforcement.

As shown in Figure 3.8, the FRC contribution is capable of mitigating the well-known size-effect of the PC under shear loading. In fact, whereas the ultimate shear stress of PC is lowering with the increase in height of the beam, the ultimate shear stress of the two FRC is maintaining a positive slope with the beam height when observing the linear interpolations of the experimental outcomes.

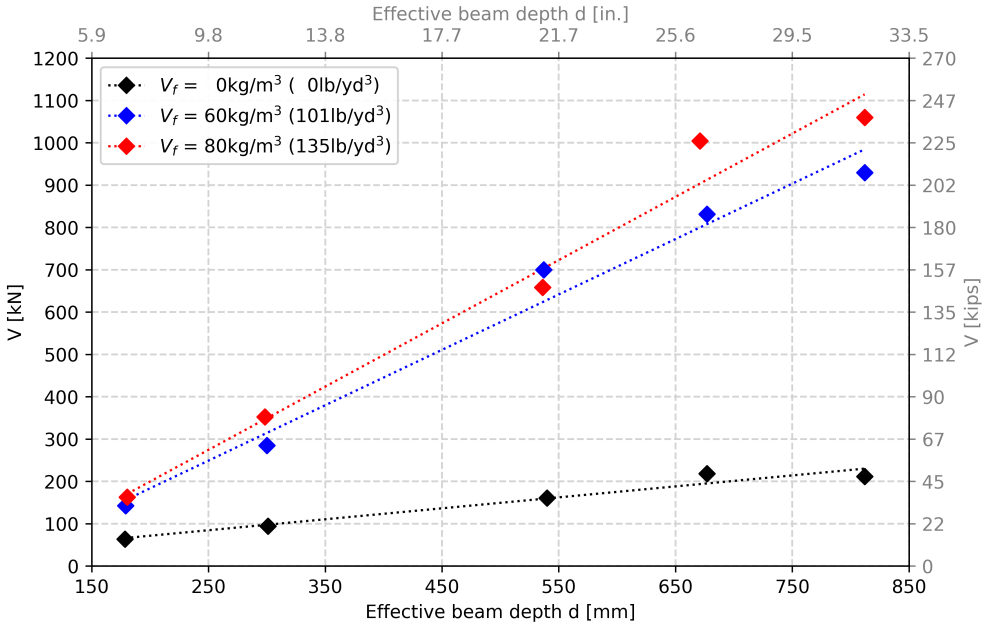



Figure 3.7. Present Study - Ultimate shear force results vs effective beam depth

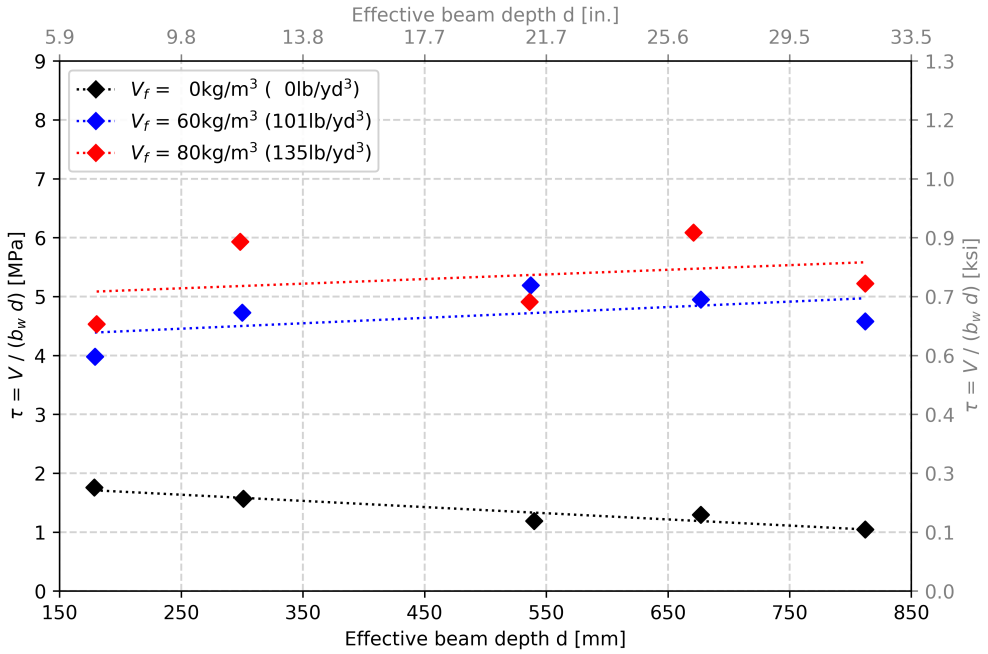



Figure 3.8. Present Study - Ultimate shear stress results vs effective beam depth

The results inherent to the only FRCs are then compared with the predictions obtained through the current prediction models aforementioned[16,33,56,57]. Furthermore, all the mixes are verified respect to the compliance criteria of the corresponding norm and the average values of any mechanical parameters obtained are considered.

The EN1992 imposes in Annex L the *Formula (L.1)*

$$f_{R1}/f_{ct;0.05} \geq 0.5 \tag{3.1}$$

where the $f_{ct;0.05}$ is computed considering the governing formulae reported in *"Table 5.1 - Compressive and tensile strength of concrete [MPa]"* of the code:

$$f_{ctm} = \begin{cases} 0.3 \cdot f_c^{2/3} & \text{if } f_c \leq 50 \;\; MPa \;\; (7.3 \;\; ksi) \\ 1.1 \cdot f_c^{1/3} & \text{if } f_c > 50 \;\; MPa \;\; (7.3 \;\; ksi) \end{cases} \tag{3.2}$$

$$f_{ct;0.05} = 0.7 \cdot f_{ctm} \tag{3.3}$$

For the MC2020, the conditions to be satisfied are two (Eq. 18.3-5 and Eq. 18.3-6):

$$f_{R1}/f_L > 0.4 \tag{3.4}$$

$$f_{R3}/f_{R1} > 0.5 \tag{3.5}$$

According to ACI 318, the following conditions must be verified for shear resistance:

- 26.4.1.6.1(a) - Steel fiber reinforcement shall:
  - be deformed and conform to ASTM A820[21]
  - have a length-to-diameter ratio between 50 and 100.

- 26.4.2.2 (h) - The minimum content of fibers shall:
  - conform to ASTM C1116 [68]
  - contain at least 41.5 kg/m$^3$ (70.0 lb/yd$^3$) for NWC
- 26.12.8.1(a) - the SFRC shall satify these minimum mechanical performance:
  - Compressive strength acceptance criteria for standard-cured specimens
  - Residual strength obtained from flexural testing in accordance with ASTM C1609 [42] at a midspan deflection of 1/300 of the span length is at least the greater of:
    - 90% of the measured first-peak strength obtained from a flexural test
    - 90% of the strength corresponding to $7.5\sqrt{f'_c[psi]}$
  - Residual strength obtained from flexural testing in accordance with ASTM C1609 [42] at a midspan deflection of 1/150 of the span length is at least the greater of:
    - 75% of the measured first-peak strength obtained from a flexural test
    - 75% of the strength corresponding to $7.5\sqrt{f'_c[psi]}$

The outcomes of these validations are presented in Table 3.2 for the first two codes, and in Table 3.1 for the latter. With the exception of the PCs, which clearly fail to meet any of the criteria, non-compliance is observed only for FRC-20 and FRC-40 under ACI 318. Nevertheless, the corresponding results are included in Section 2.2 to provide a more comprehensive description of the contribution of $V_f$, particularly in the context of a continuous distribution.

Table 3.1. Compliance with ACI 318-25 criteria[57]

| Beam ID | Days of curing | Fibers Aspect Ratio | 26.4.1.6.1(a) Fiber type | $V_f$ | 26.4.2.2(h) Minimum content | $f^D_{300}$ | 90%·$f_{1st.peak}$ | 90%·7.5·$\sqrt{f'_c}$ | 26.12.8.1(a) Performance criterium $f^D_{300}$ | $f^D_{150}$ | 75%·$f_{1st.peak}$ | 75%·7.5·$\sqrt{f'_c}$ | 26.12.8.1(a) Performance criterium $f^D_{150}$ | Final Acceptance |
|---|---|---|---|---|---|---|---|---|---|---|---|---|---|---|
| | | - | | kg/m³ (lb/yd³) | | MPa (ksi) | MPa (ksi) | MPa (ksi) | | MPa (ksi) | MPa (ksi) | MPa (ksi) | | |
| Ph1-PC-0 | 14 | - | NA | 0 (0.0) | No | 0.0 (0.0) | 3.68 (0.5) | 3.8 (0.5) | NA | 0.0 (0.0) | 3.1 (0.4) | 3.2 (0.5) | NA | No |
| Ph1-FRC-20 | 14 | 71.4 | Yes | 20 (33.7) | No | 2.2 (0.3) | 3.3 (0.5) | 3.8 (0.6) | No | 2.0 (0.3) | 2.8 (0.4) | 3.2 (0.5) | No | No |
| Ph1-FRC-40 | 14 | 71.4 | Yes | 40 (67.4) | No | 4.8 (0.7) | 4.1 (0.6) | 3.8 (0.6) | Yes | 3.9 (0.6) | 3.5 (0.5) | 3.2 (0.5) | Yes | No |
| Ph1-FRC-60 | 14 | 71.4 | Yes | 60 (101.1) | Yes | 5.5 (0.8) | 4.6 (0.7) | 3.8 (0.6) | Yes | 4.9 (0.7) | 3.8 (0.6) | 3.2 (0.5) | Yes | Yes |
| Ph1-FRC-80 | 14 | 71.4 | Yes | 80 (134.8) | Yes | 6.0 (0.9) | 4.8 (0.7) | 3.9 (0.6) | Yes | 4.1 (0.6) | 4.0 (0.6) | 3.3 (0.5) | Yes | Yes |
| Ph1-FRC-100 | 14 | 71.4 | Yes | 100 (168.6) | Yes | 7.1 (1.0) | 5.9 (0.9) | 4.7 (0.7) | Yes | 5.0 (0.7) | 5.0 (0.7) | 3.9 (0.6) | Yes | Yes |
| Ph2-PC-0 | 14 | - | NA | 0 (0.0) | No | 0.0 (0.0) | 6.5 (0.9) | 4.3 (0.6) | NA | 0.0 (0.0) | 5.4 (0.8) | 3.6 (0.5) | NA | No |
| Ph2-FRC-60 | 14 | 71.4 | Yes | 60 (101.1) | Yes | 7.7 (1.1) | 5.1 (0.7) | 4.3 (0.6) | Yes | 5.7 (0.8) | 4.2 (0.6) | 3.5 (0.5) | Yes | Yes |
| Ph2-FRC-100 | 14 | 71.4 | Yes | 100 (168.6) | Yes | 9.2 (1.3) | 4.8 (0.7) | 4.8 (0.7) | Yes | 6.7 (1.0) | 4.0 (0.6) | 4.0 (0.6) | Yes | Yes |
| Ph2-PC-0 | 36 | 71.4 | Yes | 0 (0.0) | No | 0.0 (0.0) | 5.6 (0.8) | 4.4 (0.6) | NA | 0.0 (0.0) | 4.6 (0.7) | 3.7 (0.5) | NA | No |
| Ph2-FRC-60 | 33 | 71.4 | Yes | 60 (101.1) | Yes | 6.9 (1.0) | 4.5 (0.7) | 4.6 (0.7) | Yes | 4.8 (0.7) | 3.8 (0.5) | 3.8 (0.6) | Yes | Yes |
| Ph2-FRC-100 | 29 | 71.4 | Yes | 100 (168.6) | Yes | 8.3 (1.2) | 5.6 (0.8) | 5.2 (0.8) | Yes | 5.4 (0.8) | 4.7 (0.7) | 4.3 (0.6) | Yes | Yes |
| Ph3-PC-0 | 14±2 | - | NA | 0 (0.0) | No | 0.0 (0.0) | 4.6 (0.7) | 4.2 (0.6) | NA | 0.0 (0.0) | 3.8 (0.6) | 3.5 (0.5) | NA | No |
| Ph3-FRC-60 | 14±2 | 71.4 | Yes | 60 (101.1) | Yes | 8.1 (1.2) | 3.8 (0.5) | 4.0 (0.6) | Yes | 6.4 (0.9) | 3.1 (0.5) | 3.4 (0.5) | Yes | Yes |
| Ph3-FRC-80 | 14±2 | 71.4 | Yes | 80 (134.8) | Yes | 9.2 (1.3) | 4.2 (0.6) | 4.8 (0.7) | Yes | 6.6 (1.0) | 3.5 (0.5) | 4.0 (0.6) | Yes | Yes |
| Ph3-PC-0 | 116±2 | - | NA | 0 (0.0) | No | NA | NA | 4.4 (0.6) | NA | 0.0 (0.0) | 3.8 (0.6) | 3.7 (0.5) | NA | No |
| Ph3-FRC-60 | 116±2 | 71.4 | Yes | 60 (101.1) | Yes | 9.8 (1.4) | 4.8 (0.7) | 4.2 (0.6) | Yes | 7.4 (1.1) | 4.0 (0.6) | 3.5 (0.5) | Yes | Yes |
| Ph3-FRC-80 | 116±2 | 71.4 | Yes | 80 (134.8) | Yes | 7.7 (1.1) | 4.5 (0.7) | 5.1 (0.7) | Yes | 5.6 (0.8) | 3.7 (0.5) | 4.2 (0.6) | Yes | Yes |

Table 3.2. Compliance with EN1992-1-1 - Annex L and *fib* Model Code 2020 criteria[33,56]

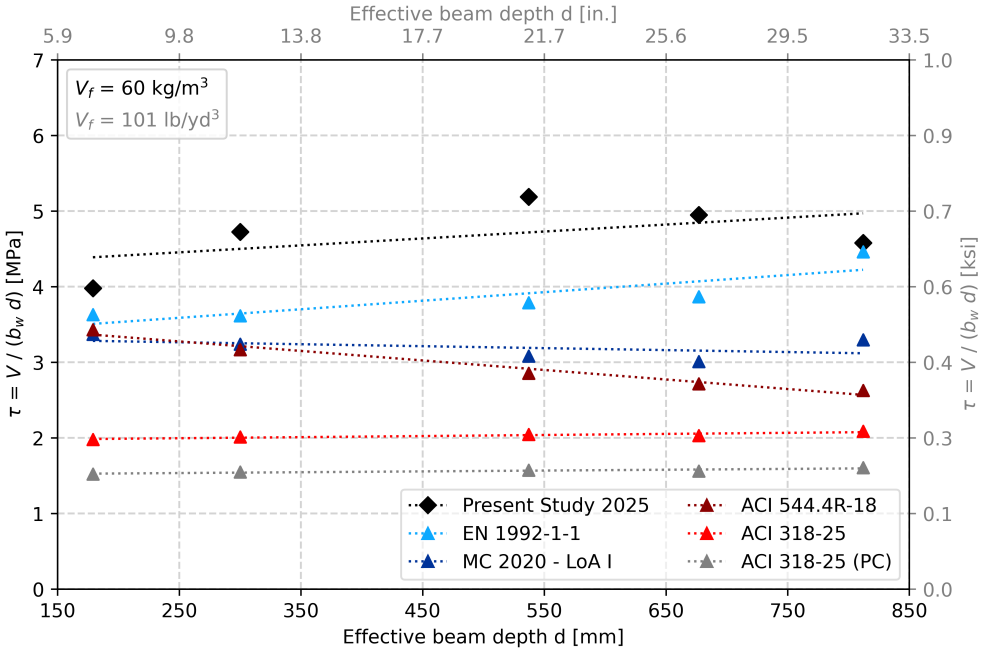
| Beam ID | Days of curing | $f_{R1}$ MPa (ksi) | $f_c$ MPa (ksi) | $f_{ct;0,05}$ MPa (ksi) | EN1992-1-1 Annex L Eq. L.1 | $f_L$ MPa (ksi) | $f_{R1}$ MPa (ksi) | $f_{R3}$ MPa (ksi) | MC 2020 Eq.18.3-5 | MC 2020 Eq.18.3-6 | MC2020 Final Acceptance |
|---|---|---|---|---|---|---|---|---|---|---|---|
| Ph1-PC-0 | 14 | NA | 45.6 (6.6) | 2.7 (0.4) | NA | NA | NA | NA | NA | NA | No |
| Ph1-FRC-20 | 14 | 2.7 (0.4) | 46.3 (6.7) | 2.7 (0.4) | Yes | 4.0 (0.6) | 2.7 (0.4) | 3.7 (0.5) | Yes | Yes | Yes |
| Ph1-FRC-40 | 14 | 4.7 (0.7) | 46.4 (6.7) | 2.7 (0.4) | Yes | 4.2 (0.6) | 4.7 (0.7) | 5.8 (0.8) | Yes | Yes | Yes |
| Ph1-FRC-60 | 14 | 6.1 (0.9) | 47.0 (6.8) | 2.7 (0.4) | Yes | 4.6 (0.7) | 6.1 (0.9) | 6.2 (0.9) | Yes | Yes | Yes |
| Ph1-FRC-80 | 14 | 7.8 (1.1) | 48.5 (7.0) | 2.8 (0.4) | Yes | 5.3 (0.8) | 7.8 (1.1) | 8.1 (1.2) | Yes | Yes | Yes |
| Ph1-FRC-100 | 14 | 8.8 (1.3) | 70.0 (10.2) | 3.2 (0.5) | Yes | 4.9 (0.7) | 8.8 (1.3) | 8.8 (1.3) | Yes | Yes | Yes |
| Ph2-PC-0 | 14 | 0.0 (0.0) | 59.1 (8.6) | 3.0 (0.4) | NA | 4.5 (0.7) | 0.0 (0.0) | 0.0 (0.0) | No | NA | No |
| Ph2-FRC-60 | 14 | 7.3 (1.1) | 57.6 (8.4) | 3.0 (0.4) | Yes | 8.6 (1.2) | 7.3 (1.1) | 8.1 (1.2) | Yes | Yes | Yes |
| Ph2-FRC-100 | 14 | 11.0 (1.6) | 73.5 (10.7) | 3.2 (0.5) | Yes | 11.3 (1.6) | 11.0 (1.6) | 10.1 (1.5) | Yes | Yes | Yes |
| Ph2-PC-0 | 36 | 0.0 (0.0) | 61.7 (9.0) | 3.0 (0.4) | NA | 5.0 (0.7) | 0.0 (0.0) | 0.0 (0.0) | No | NA | No |
| Ph2-FRC-60 | 33 | 7.0 (1.0) | 66.5 (9.6) | 3.1 (0.5) | Yes | 8.6 (1.2) | 7.0 (1.0) | 7.6 (1.1) | Yes | Yes | Yes |
| Ph2-FRC-100 | 29 | 12.7 (1.8) | 86.3 (12.5) | 3.4 (0.5) | Yes | 12.9 (1.9) | 12.7 (1.8) | 11.5 (1.7) | Yes | Yes | Yes |
| Ph3-PC-0 | 14±2 | NA | 56.8 (8.2) | 3.0 (0.4) | NA | NA | NA | NA | NA | NA | No |
| Ph3-FRC-60 | 14±2 | 6.9 (1.0) | 52.1 (7.6) | 2.9 (0.4) | Yes | 4.7 (0.7) | 6.9 (1.0) | 8.3 (1.2) | Yes | Yes | Yes |
| Ph3-FRC-80 | 14±2 | 10.6 (1.5) | 73.1 (10.6) | 3.2 (0.5) | Yes | 5.3 (0.8) | 10.6 (1.5) | 12.0 (1.7) | Yes | Yes | Yes |
| Ph3-PC-0 | 116±2 | NA | 62.1 (9.0) | 3.0 (0.4) | NA | NA | NA | NA | NA | NA | No |
| Ph3-FRC-60 | 116±2 | 10.2 (1.5) | 56.1 (8.1) | 2.9 (0.4) | Yes | 4.9 (0.7) | 10.2 (1.5) | 10.7 (1.6) | Yes | Yes | Yes |
| Ph3-FRC-80 | 116±2 | 10.7 (1.5) | 81.7 (11.8) | 3.3 (0.5) | Yes | 4.7 (0.7) | 10.7 (1.5) | 11.3 (1.6) | Yes | Yes | Yes |

More precisely, Figure 3.9a summarizes the results for the FRC with 60 kg/m$^3$ (101.1 lb/yd$^3$) of fibers, whereas the Figure 3.9b refers to the FRC with 80 kg/m$^3$ (134.8 lb/yd$^3$).

For the sake of clarity, all the predictions are calculated using the average values of any mechanical parameters – namely the compressive strength ($f'_c$) and the residual flexural strength ($f_{R3}$ or $f^D_{150}$), where required. Furthermore, neither partial safety factors or strength reduction factors were introduced.

All the prediction models maintain a certain degree of conservatism with respect to experimental outcomes and ACI 318 predictions provide the most conservative estimation.

a)



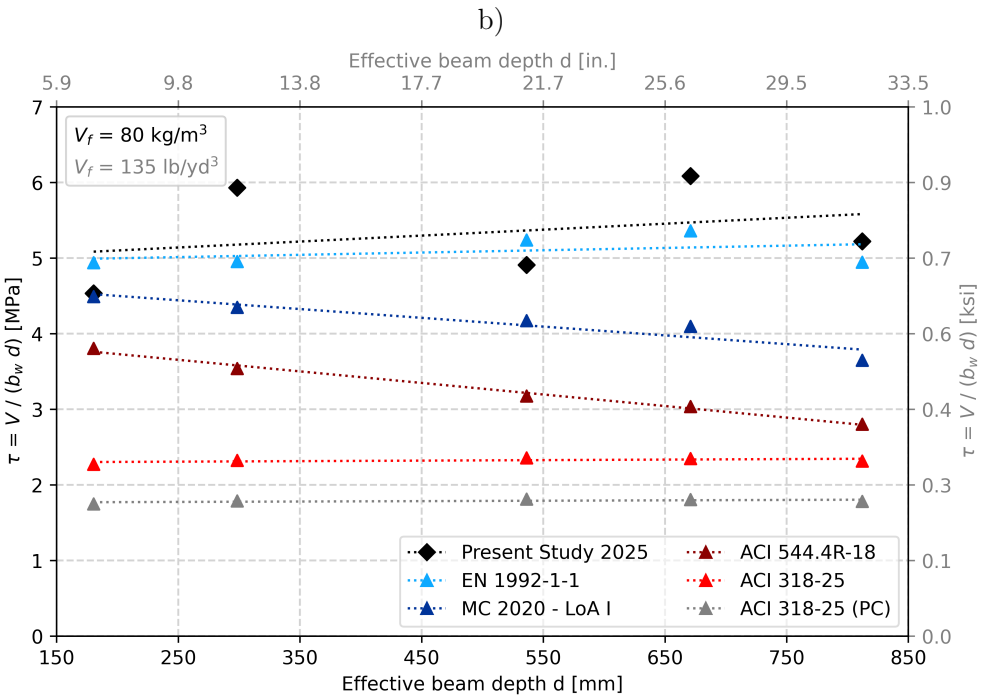



Figure 3.9. Present Study ultimate shear stress results vs numerical predictions[16,33,56,57]
(a) $V_f$=60 kg/m³ (101.1 lb/yd³); (b) $V_f$=80 kg/m³ (134.8 lb/yd³)

It is worth noting that this prediction labelled as "ACI 318-25" is not dependent on the effective residual flexural strength provided by the FRC, whereas it consists of the calculation equation given for PC (also reported and labelled as "ACI 318-25 (PC)") increased by a multiplier factor of 1.3, as explained in the Section *22.5.5.1.4* of the relative norm which states *"[...] $V_c$ shall be the greater of Eq.(a) and 1.3 times Equation (b) of Table 22.5.5.1."*[57] returning then to the two formulations already described in the introduction that refers to the geometry ($b_w$, $d$, $\rho_w$) but limit the mechanical analysis to the only compressive strength $f'_c$ and the type of concrete through the parameter $\lambda$. The tests conducted do not present axial forces so the term $\frac{N_u}{6A_g}$ is not taken into account in these considerations.

The predictions derived from MC2020 (LoA I) and EN1992 are capable to slightly better predict the shear strength. These calculations are based on the residual flexural strength $f_{R3}$ obtained by means of the testing method EN 14651[41].
Furthermore, in case of EN1992, an incremental trend in shear resistance is obtained as

the size of the beams increases. This is due to the coefficient $k_G$, function of the area of the tension zone $A_{ct}$, that increases according to the size of the beam's fracture surface under tension at failure. This allows for a trend consistent with that observed experimentally. Although this model is the closest to the values obtained, it should be highlighted that it refers to characteristic values (i.e. determined on the basis of both the mean and standard deviation) rather than just the mean values unlike American regulations. In order to evaluate and compare the models, as previously clarified, the average parameters are considered as well in this case.

ACI 544.4R, which is based on the calculation equation previously proposed by MC2010[61,62], provides an intermediate prediction between ACI 318 and the two other building codes. This method is a performance-based calculation which refers to the residual flexural strength $f_{150}^{D}$ obtained by means of ASTM C1609[42]. It is worth noting that these predictions, as for those elaborated for plain concrete elements, have a negative slope with the size of the element due to the size-effect coefficient ($k_s$) incorporated in the equation. If compared to the experimental outcomes, it's possible to observe that it is contrary to the effective observed behavior.

## 3.3 Considerations about ACI 318-25

Based on the results previously described, herein it is evaluated the difference between ACI 318[57] and the experimental results collected. In particular, it is evaluated the possibility, for the $\tau_{rb}$, to introduce a second multiplier $m \geq 1.3$ for FRCs which satisfy additional requirements.

Considering the plots reported in Figure 3.10, it is possible to address the matter by setting a multiplier m = 2.5. In fact, in both cases, the prediction models maintain a certain degree of conservativeness with all the experimental outcomes.

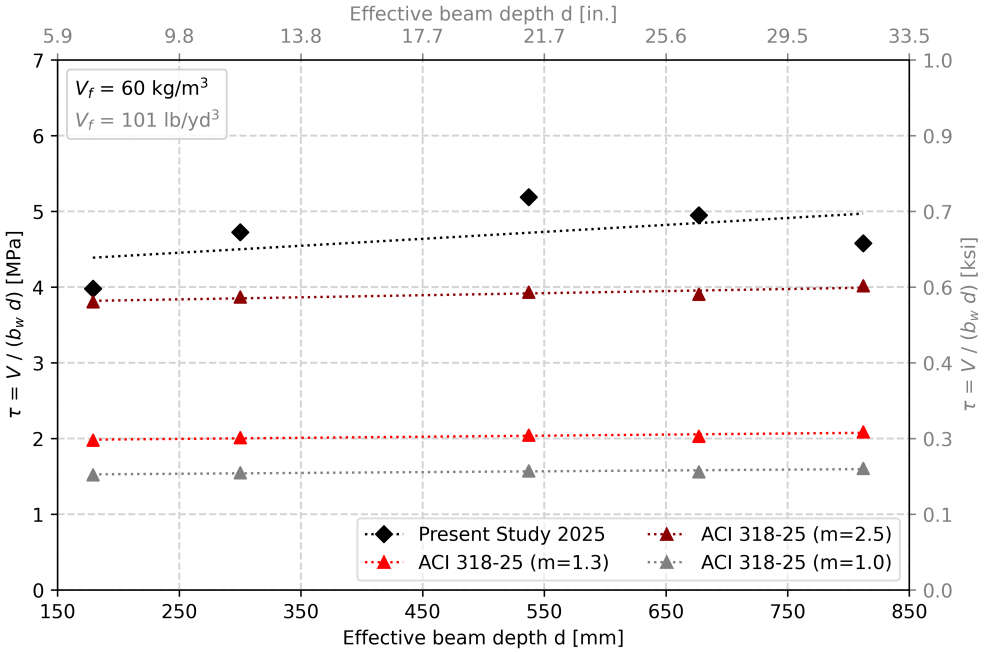
Furthermore, if considering as additional requirements $f'_c \geq 50$ MPa (7.3 ksi) and a minimum content of 60 kg/m$^3$ (101.1 lb/yd$^3$, ~0.75% by volume), it is possible to compare the experimental outcomes of the current study and those filtered from the dataset of Alcocer et al.[66]. It is indeed possible to extract 10 additional test results out of the

initial 340 samples all belonging to the study of Singh and Jain in 2014 [2]. None of the tests reported by Cuenca et al. [65] satisfies simultaneously both the criteria. In this way, a total of 20 outcomes (10 + 10, respectively) can be analyzed.

In Figure 3.11, the shear stresses achieved experimentally and those numerically obtained are normalized with respect to the numerical predictions evaluated with ACI 318 without applying any increasing multiplier (i.e., m = 1.0) corresponding to the condition for the PC. The results are presented as a function of increasing effective beam depth. A scaled distribution along the x-axis is not provided due to significant limitations associated with this parameter.

However, as shown, the outcomes of FRC mixes with similar nominal characteristics are not performing as those analyzed in the current study. In the same Figure, also the current multiplier m = 1.3 adopted from ACI 318 and a new multiplier m = 2.0 are plotted. As shown, m = 2.0 is needed to keep all the experimental values above the numerical predictions.

a)



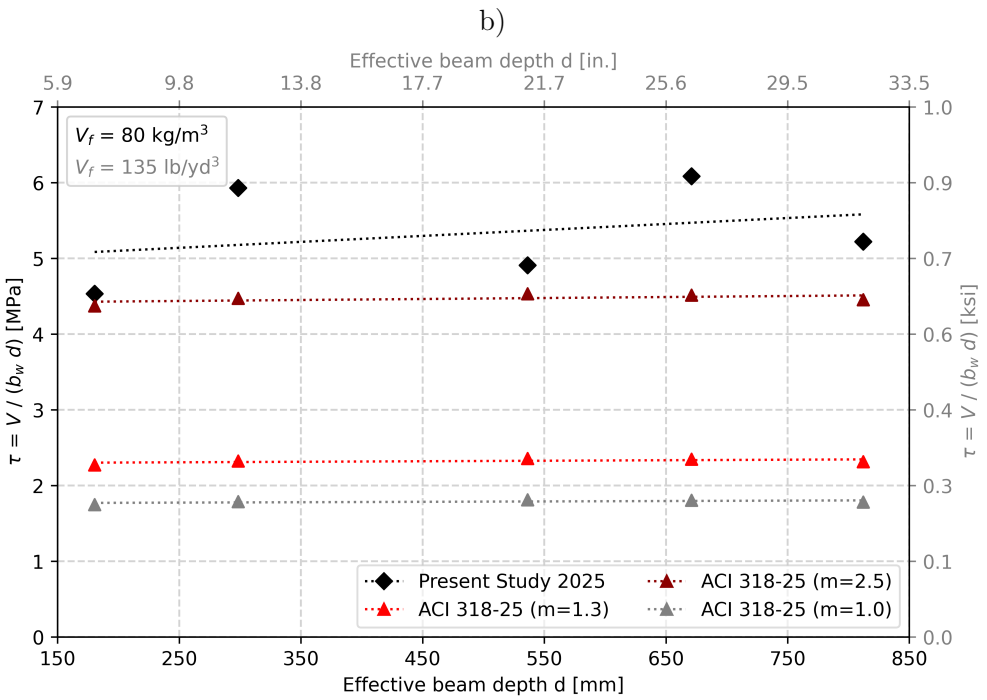



Figure 3.10. Present Study vs ACI 318 by setting different multipliers m. (a) $V_f$=60 kg/m$^3$ (101.1 lb/yd$^3$); (b) $V_f$=80 kg/m$^3$ (134.8 lb/yd$^3$) [57]

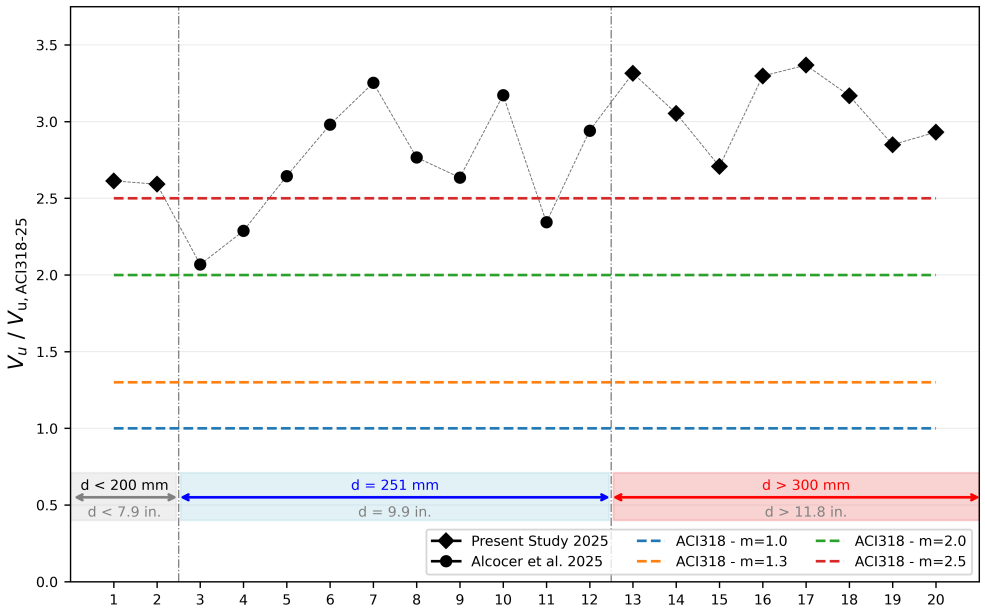



Figure 3.11. Present Study and Alcocer et al. filtered database - Ultimate shear force results vs actual ACI 318 by setting different multipliers m [2,57,66]

## 3.4 Considerations about ACI 544.4R-18

In this section, a similar analysis is conduced respect to ACI 544.4R [16].
Based on the observed mitigating effect provided by the fiber-reinforcement to the size-effect, it is evaluated the possibility of assuming $k_S = 2.0$ which is equivalent to assuming the current maximum value of this parameter, ignoring the negative effect of the size-effect assumed by the code in analysis.

As shown, the latest equation guarantees wide conservativeness with respect to the experimental outcomes despite the increase in shear strength prediction for higher beams.

Considering the database from Alcocer et al. [66] with the only shear failure, assuming $f_T = f_{1^{st}peak}$ due to the missing second data and imposing a minimum content of fibers $V_f = 0.5\%$ it is possible to consider only further 32 samples due to the limited amount of mechanically-characterized samples. All the filtered tests are attributable to the already mentioned study of Singh and Jain from 2014 [2] with a constant effective beam depth $d$ = 251 mm (9.9 in.), a span-to-depth ratio a/d = 3.5, a compressive strength $f'_c$ in the range between 24.9 to 64.6 MPa (from 3.6 to 9.4 ksi) and a fiber content between 0.5 and 1.5%. For this reason, in spite a significative distribution in terms of compressive strength and content of fibers, the results assume relatively little importance when assessing the contribute of the size-effect. None of the test from Cuenca et al. [65] can be consider due to the lack of data related to ASTM C1609 [42].

As shown in Figure 3.13, the calculation according to ACI 544.4R with the parameter $k_s$ function of the effective beam depth is conservative in all the cases unless for two samples for which predictions result above the experimental values (i.e., the ratio of measured-to-calculated shear strength is below 1. Only one ratio is below 0.95).

No significant changes are obtained if the modified equation with coefficient $k_S = 2.0$ is instead used. In other words, the coefficient which consider the member depth is fixed and no reduction due to the increasing depth is applied. In this case, five ratios are below 1 and 3 samples have a ratio measured-to-calculated shear strength below 0.95. On the contrary, the modified equation allows to reduce the gap between the measured values and the predicted ones of deeper beams.

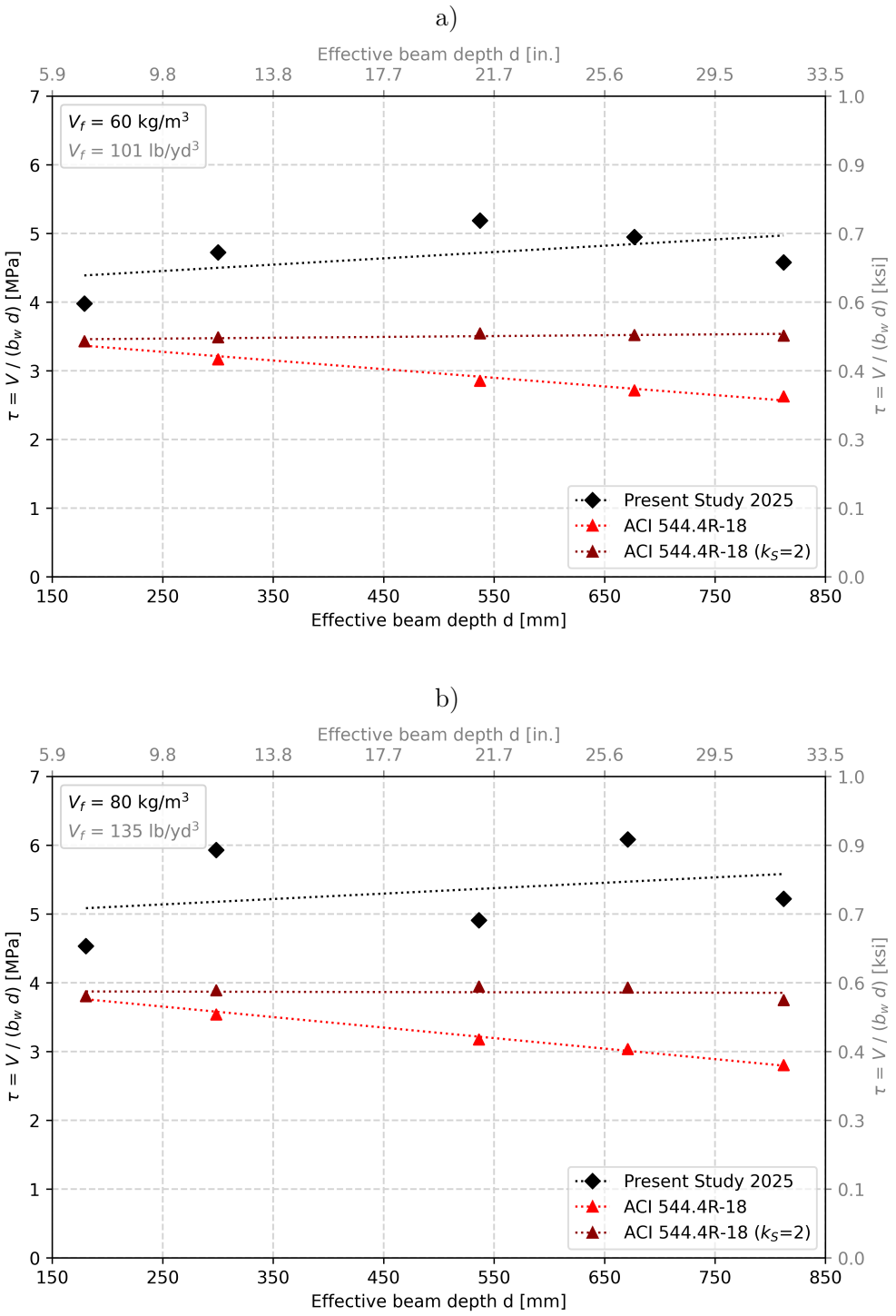



Figure 3.12. Present Study vs ACI 544.4R considering $k_S$ variable and constant. (a) $V_f$=60 kg/m$^3$ (101.1 lb/yd$^3$); (b) $V_f$=80 kg/m$^3$ (134.8 lb/yd$^3$)[16]

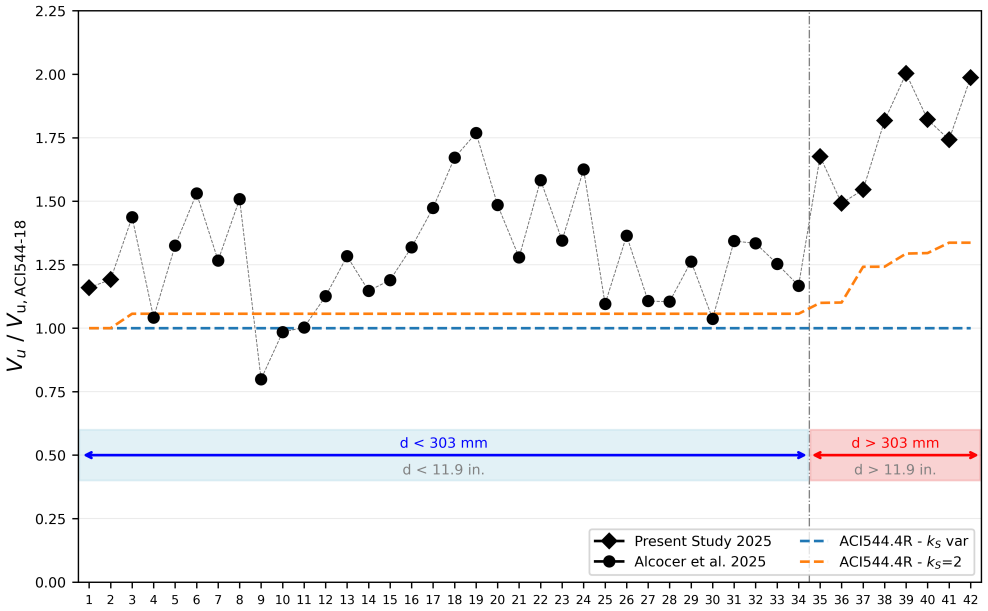



Figure 3.13. Present Study and Alcocer et al. filtered database - Ultimate shear force results vs ACI 544.4R considering $k_S$ variable and constant.[2,57,66]

# Conclusions

Based on the experimental results of the Present Study and their comparison with current prediction models, the following conclusions can be drawn:

- On the basis of the experimental outcomes, it has been observed that SFRC beams reinforced with only longitudinal reinforcement can achieve a shear strength up to five times greater then that of companion beams made with PC.
- All the beams of the Present Study, presenting varying heights between 200 to 900 mm (7.9 to 35.4 in.) and made of SFRC characterized by deflection-hardening residual flexural strength, exhibited remarkable ductility compared to the brittle behavior observed in those made of PC. More precisely, the SFRC beams have shown the contribution of the steel fibers in mitigating (and even overcoming) the well-known size effect associated with PC.
- By means of the mechanical characterization EN 14651, the experimental results were compared with numerical predictions calculated according to MC2020 and Eurocode 2. These performance-based models provided the most accurate estimates of the design shear strength of SFRC, albeit remaining conservative.
- By means of the mechanical characterization ASTM C1609, the experimental results were also compared with numerical predictions according to ACI 318-25 and ACI 544.4R-18:
  - The analyses of SFRC specimens presented in this thesis satisfy the compliance requirements of ACI 318-25, thereby allowing to calculate the shear strength

capacity increased by 30% respect to that calculated for an equivalent PC (i.e., concrete with the same compressive strength). Among all numerical models evaluated, ACI 318-25 provided the most conservative prediction. The numerical shear strength so determined was in the range 40–50% of the values obtained experimentally showing a severe conservativeness.

– The mechanical performance-based model proposed by ACI 544.4R-18, which is derived from the MC2010, provides intermediate results between those obtained from MC2020 and ACI 318-25. Moreover, by modifying the ACI 544.4R-18 equation to neglet the size-effect, it was possible to obtain more representative predictions even for beams with heights up to 900 mm (35.4 in.).

Following a comprehensive review of existing databases[65,66] on SFRC beams subjected to shear failure, together with the findings of the Present Study, it is recommended characterizing SFRC using current methodologies for residual flexural strength testing is crucial. Indeed, such characterization is necessary to calculate a more representative prediction of design shear strength in accordance with performance-based models. In addition, a common mechanical characterization of FRC is needed to collect consistent databases and to formulate a more-refined numerical prediction model.

# Acronyms

**ACI** American Concrete Institute . . . . . 8

**ASTM** American Society for Testing and Materials . . . . . 16

**CEN** European Committee for Standardization . . . . . 16

**CMOD** Crack Mouth Opening Displacement . . . . . 24

**DTT** Direct Tensile Test . . . . . 22

**EN1992** Eurocode2 . . . . . 57

**FRC** Fiber-Reinforced Concrete . . . . . 3

**HE** Hooked-End steel fibers . . . . . 48

**HPC** High-Performance Concrete . . . . . 33

**LoA** Level of Approximation . . . . . 39

**LOP** Limit of Proportionality . . . . . 24

**LVDT** Linear Variable Differential Transformer . . . . . 22

**LWC** Lightweight Concrete . . . . . 32

**MCFT** Modified Compression-Field Theory . . . . . 14

**MC2010** *fib* Model Code 2010 . . . . . 30

**MC2020** *fib* Model Code 2020 . . . . . 14

**NA** Not Applicable / Not Available . . . . . 102

**NWC** Normal-Weigth Concrete . . . . . 32

**PC** Plain Concrete . . . . . 6

**QC** Quality Control . . . . . 47

**RC** Reinforced Concrete . . . . . 14

**SCC** Self-Compacting Concrete . . . . . 48

**SF** Slump-flow . . . . . 119

**SFRC** Steel Fiber-Reinforced Concrete . . . . . 12

**SI** International System of Units . . . . . 4

**SW** Self-Weight . . . . . 119

**UHPFRC** Ultra High-Performance Fiber-Reinforced Concrete . . . . . 22

**USC** United States Customary . . . . . 43

**3PBT** 3-Points Bending Test . . . . . 11

**4PBT** 4-Points Bending Test . . . . . 8

# Notations and Conversions

## Symbology

$b_w$ ..... Base of the cross-section

$c$..... Length of the cantilever

$d$ ..... Effective depth of the cross-section

$f'_c$ or $f_c$ . Cylindrical compressive strength

$f_{1^{st}peak}$.. First-peak strength according to $f_1$ of ASTM C1609

$f^D_{600}$..... Residual strength at L/600 according to ASTM C1609

$f^D_{300}$..... Residual strength at L/300 according to ASTM C1609

$f^D_{150}$..... Residual strength at L/150 according to ASTM C1609

$f_{ct;0.05}$ .. Axial tensile strength of concrete (5% fractile)

$f_L$ ..... Strength at LOP

$f_{R1k}$ .... Residual flexural strength at CMOD = 0.5 mm (0.02 in.)

$f_{R2k}$ .... Residual flexural strength at CMOD = 1.5 mm (0.06 in.)

$f_{R3k}$ .... Residual flexural strength at CMOD = 2.5 mm (0.10 in.)

$f_{R4k}$ .... Residual flexural strength at CMOD = 3.5 mm (0.14 in.)

$f_P$ ..... Peak strength according to $f_P$ of ASTM C1609

$f_{T,Split}$ .. Splitting tensile strength

$f_{ys}$ ..... Average or Nominal steel yielding strength

$h$ ..... Height of the cross-section

$k_S$ ..... Size-effect coefficient

$m$ ..... Multiplier coefficient

$q$ ..... Homogeneous linear density of the beam

$A_g$ ..... Gross area of concrete section

$A_s$ ..... Area of longitudinal reinforcement

$D_{max}$ ... Maximum aggregate size

$E_{cm}$ .... Elastic modulus according to EN 12390-13 [36]

$L$ ..... Nominal length of the steel fiber

$L_S$ ..... Net span length

$L_{tot}$ ..... Total length of the beam as (span length + cantilevers)

$M_{y,Fl}^{num}$ .. Bending capacity according to EN 1992-1-1-Annex L [56]

$M_u$ ..... Ultimate bending moment

$N_u$ ..... Factored axial force normal to cross section

$P$ ..... Load applied by the actuator

$P_u$ ..... Load at failure

$R_A$ ..... Vertical reaction at hinged support A

$R_B$ ..... Vertical reaction at hinged support B

$SF_1$ ..... Consistence class 1 expressed by Slump-flow (SF)

$V$ ..... Shear force (Self-Weight (SW) contribute + actuator contribute)

$V_f$ ..... Volume of steel fibers (weight of steel fibers / weight of concrete matrix)

$V_u$ ..... Ultimate shear force

$V_{u,Ref}$ .. Ultimate shear force of the corresponding PC

$\delta$ ..... Density / Midspan deflection for shear test

$\delta_{peak}$ .... Deflection corresponding to $P_u$

$\lambda$ ..... Modification factor

$\rho$ ..... Steel content of longitudinal reinforcement ($= A_S/(b_w \cdot d)$

$\tau$ ..... Ultimate shear stress ($= V/(b_w \cdot d)$)

$\phi$ ..... Nominal diameter of the longitudinal reinforcing bar expressed in [mm]

$\#$ ..... Nominal diameter of the longitudinal reinforcing bar expressed in [in./8]

$\oslash$ ..... Diameter of cylindrical specimen

# Conversions from SI

| | | | | |
|---|---|---|---|---|
| 1 | $kg$ | = | 2.2046 | $lb$ |
| 1 | $mm$ | = | 0.0394 | $in.$ |
| 1 | $m$ | = | 3.2808 | $ft$ |
| 1 | $m$ | = | 1.0936 | $yd$ |
| 1 | $m^3$ | = | 35.3147 | $ft^3$ |
| 1 | $kg/m^3$ | = | 1.6856 | $lb/yd^3$ |

$$1 \quad MPa \quad = \quad 0.1450 \qquad ksi$$

$$1 \quad MPa \quad = \quad 10.1972 \quad kg/m^2$$

$$1 \; kN \cdot m \quad = \quad 8.8507 \; kips \cdot in.$$

# List of Figures

1.1 "Typical loading arrangement and cross sections of the four beam series" (Fig. 3a, Kani, 1967) [5] . . . . . 9

1.2 "Relative strength $r_u$ versus a/d reinforced concrete beams of various depths" (Fig. 5, Kani, 1967) [5] . . . . . 10

1.3 "Influence of beam width" (Details from Fig. 8, Kani, 1967) [5] . . . . . 10

1.4 Average shear strength vs Effective beam depth with $2.5 \leq a/d \leq 3.0$ for PC from Kani (1967), Sneed et al.(2010), Minelli et al.(2014) [4,5,8] . . . . . 11

1.5 "Alternative simplified size effect formula compared with: (a) complete ESDB; and (b) small-size portion of that database in expanded scale." (Fig. 2, Bažant et al., 2007) [6] . . . . . 12

1.6 "Shape of stirrups at end of 19th century" (Fig. 1.1, Ritter, *fib* Bulletin 57, 1899) [9,10] . . . . . 13

1.7 "Simple or multiple truss systems with bent-up bars and with stirrups (Mörsch, 1908)" (Fig. 1.4, *fib* Bulletin 57, 2010) [10,12] . . . . . 13

1.8 a)"Tensile stress vs elongation of various fibres" (Fig. 5, Pham, 2025); b)"Fibre tensile strength vs Young's modulus" (Fig. 6, Pham, 2025) [18,19] . 16

1.9 "Examples of some typical fibre geometries" (Figure 10, Löfgren, 2005) [17] . 17

1.10 "(a) A schematic illustrating some of the toughening effects and crack front debonding, the Cook-Gordon effect (Cook and Gordon, 1964), and debonding and sliding in the crack wake. (b) Matrix spalling and matrix cracking. (c) Plastic bending (deformation) of inclined fibre during pullout – both at the crack and at the end-anchor" (Figure 19, Löfgren, 2005) [17,22] . . . . . 18
1.11 "Fiber contribution to tensile/flexural performance, obtained from flexural test, showing softening and hardening behaviors" (Fig. 3.4b, ACI 544.4R, 2018) [16] . . . . . 19
1.12 "Main differences between plain and fibre reinforced concrete having both normal and high strength under uniaxial compression" (Figure 18.2-1, MC2020, 2012) [33] . . . . . 20
1.13 "Outline of uniaxial tension test" (Fig. T2.3.1, JSCE 2008, 2008) [38] . . . . 23
1.14 "Typical arrangement for measuring CMOD" (Figure 4, EN 14651, 2005) [41] 25
1.15 "Load-CMOD diagram and $F_j$" (Figure 7, EN 14651, 2005) [41] . . . . . 25
1.16 "Example of Parameter Calculations when Peak Load is Greater than First-Peak Load (Not to Scale)" (FIG. 5, ASTM C1609, 2024) [42] . . . . . 26
1.17 "Arrangement to Obtain Net Deflection by Using Two Transducers Mounted on Jig Secured to Specimen Directly Above Supports" (FIG. 2, ASTM C1609, 2024) [42] . . . . . 27
1.18 "Different response of structures made of FRC having a softening or hardening behaviour under uniaxial tension or bending loads" (Figure 18.2-11, MC2020, 2020) [33] . . . . . 28
1.19 "Papers about shear behavior on FRC beams" (Fig. 1, Cuenca et al., 2018) [65] 31
1.20 "Data set description; distribution of: [...] (b) steel fiber-volume ratio, $V_f$; [...](d) beam overall depth h"(Fig.1, Alcocer et al., 2025) [66] . . . . . 32
1.21 Shear-failure tests from Alcocer et al. [66] and Cuenca et al. [65] . . . . . 35
1.22 Shear-failure tests from Alcocer et al. [66] and Cuenca et al. [65] respect to $V_f$ 35
1.23 Distribution of shear-failure tests from Alcocer et al. and Cuenca et al. (Left) Effective total population, respectively, 340 and 122; (Right) Relative distribution respect to the corresponding effective population [65,66] . . . . . 37

1.24 Average shear strength $\tau$ vs Effective beam depth $d$ from Alcocer et al.(2025) and Cuenca et al.(2018)[65,66] . . . . . 38

2.1 Phase1 - Setup of beam S1-0 (measures in mm) . . . . . 49

2.2 Phase1 - Test configuration and stress distribution along beam S1-0 . . . . 55

2.3 Phase1 - Load-deflection curves of all beams S1-0 under 3PBT . . . . . 56

2.4 Phase1 - Load-deflection curves of all beams S1-0 under 3PBT normalized with respect to the ultimate load of PC, namely 95.6 kN (21.5 kips). . . . . 56

2.5 Phase1 - Pictures of all beams S1-0 at failure. (a) PC-0; (b) FRC-20; (c) FRC-40; (d) FRC-60; (e) FRC-80; (f) FRC-100 . . . . . 59

2.6 Phase2 - Setup of beam S1-4 for PC and FRC with 60 kg/m$^3$ (101.1 lb/yd$^3$)(measures in mm) . . . . . 61

2.7 Phase2 - Setup of beam S1-4 for FRC with 100 kg/m$^3$ (168.6 lb/yd$^3$) (measures in mm) . . . . . 61

2.8 Phase2 - Load-deflection curves of PC-0-200h, FRC-60-200h and FRC-100-200h in 3PBT at 14 days of curing . . . . . 67

2.9 Phase2 - Load-deflection curves of PC-0-200h, FRC-60-200h and FRC-100-200h in 3PBT respectively at 36, 33, and 29 days of curing . . . . . 68

2.10 Phase2 - Load-deflection curves of PC-0-900h, FRC-60-900h and FRC-100-900h in 3PBT respectively at 36, 33, and 29 days of curing . . . . . 68

2.11 Phase2 - Shear-deflection curves of PC-0-900h, FRC-60-900h and FRC-100-900h in 3PBT respectively at 36, 33, and 29 days of curing . . . . . 69

2.12 Phase2 - Pictures of all beams S1-4 at failure. (a) PC-0-900h; (b) FRC-60-900h;(c) FRC-100-900h . . . . . 72

2.13 Phase3 - Setup of beams S1-0, S1-1, S1-2, S1-3, and S1-4 (measures in mm) 75

2.14 Phase3 - Test configuration and stress distribution along beams S1-0, S1-1, S1-2, S1-3, and S1-4 . . . . . 82

2.15 Phase3 - Load-deflection curves of PC-0-200h, FRC-60-200h and FRC-80-200h in 4PBT at 14±2 of curing . . . . . 83

2.16 Phase3 - Load-deflection curves of PC-0-335h, FRC-60-335h and FRC-80-335h in 4PBT at 14±2 of curing . . . . . 84
2.17 Phase3 - Load-deflection curves of PC-0-600h, FRC-60-600h and FRC-80-600h in 4PBT at 14±2 of curing . . . . . 84
2.18 Phase3 - Load-deflection curves of PC-0-750h, FRC-60-750h and FRC-80-750h in 4PBT at 14±2 of curing . . . . . 85
2.19 Phase3 - Load-deflection curves of PC-0-900h, FRC-60-900h and FRC-80-900h in 4PBT at 116±2 of curing . . . . . 85
2.20 Phase3 - Pictures of all beams S1-0 after failure. (a) PC-0-200h; (b) FRC-60-200h; (c) FRC-80-200h; (d) 4PBT setup . . . . . 88
2.21 Phase3 - Samples S1-1 after failure. (a) PC-0-335h; (b) FRC-60-335h;(c) FRC-80-335h; (d) S1-1 setup . . . . . 89
2.22 Phase3 - Samples S1-2 after failure. (a) PC-0-600h; (b) FRC-60-600h; (c) FRC-80-600h; (d) S1-2 setup . . . . . 90
2.23 Phase3 - Samples S1-3 after failure. (a) PC-0-750h; (b) FRC-60-750h; (c) FRC-80-750h; (d) Detail of local failure of FRC-60-750h; (e) Detail of crack distribution of FRC-80-750h . . . . . 91
2.24 Phase3 - Samples S1-4 after failure. (a) PC-0-900h; (b) FRC-60-900h; (c) FRC-80-900. (d) Size comparison of S1-0 to S1-4 . . . . . 92

3.1 Dataset of shear tests from Present Study. . . . . 94
3.2 Dataset of shear tests from Present Study, Alcocer et al., Cuenca et al.[65,66] 95
3.3 Dataset of shear tests from Present Study, Alcocer et al., Cuenca et al.[65,66] respect to the volume of steel fibers $V_f$ . . . . . 95
3.4 Dataset of shear tests from Present Study, Alcocer et al., Cuenca et al.[65,66] respect to $f_{R1}$ (left) and $f_{R3}$ (right) . . . . . 96
3.5 Dataset of shear tests from Present Study, Alcocer et al., Cuenca et al.[65,66] respect to $f^D_{600}$ (left) and $f^D_{150}$ (right) . . . . . 96
3.6 Distribution respect to main variables of shear tests from Present Study, Alcocer et al., Cuenca et al.[65,66] (respectively, 30, 340 and 122) . . . . . 97

3.7 Present Study - Ultimate shear force results vs effective beam depth . . . . 99
3.8 Present Study - Ultimate shear stress results vs effective beam depth . . . 99
3.9 Present Study ultimate shear stress results vs numerical predictions [16,33,56,57] (a) $V_f$=60 kg/m$^3$ (101.1 lb/yd$^3$); (b) $V_f$=80 kg/m$^3$ (134.8 lb/yd$^3$) . . . . . 105
3.10 Present Study vs ACI 318 by setting different multipliers m. (a) $V_f$=60 kg/m$^3$ (101.1 lb/yd$^3$); (b) $V_f$=80 kg/m$^3$ (134.8 lb/yd$^3$) [57] . . . . . 108
3.11 Present Study and Alcocer et al. filtered database - Ultimate shear force results vs actual ACI 318 by setting different multipliers m [2,57,66] . . . . . 108
3.12 Present Study vs ACI 544.4R considering $k_S$ variable and constant. (a) $V_f$=60 kg/m$^3$ (101.1 lb/yd$^3$); (b) $V_f$=80 kg/m$^3$ (134.8 lb/yd$^3$) [16] . . . . . 110
3.13 Present Study and Alcocer et al. filtered database - Ultimate shear force results vs ACI 544.4R considering $k_S$ variable and constant. [2,57,66] . . . . . 111
3.14 Phase1 - ASTM C1609 [42] all tests . . . . . 143
3.15 Phase1 - EN 14651 [41] all tests . . . . . 144
3.16 Phase2 - ASTM C1609 [42] all tests at 14 days of curing . . . . . 151
3.17 Phase2 - ASTM C1609 [42] all tests at 36, 33 and 29 days of curing . . . . . 152
3.18 Phase2 - EN 14651 [41] all tests at 14 days of curing . . . . . 152
3.19 Phase2 - EN 14651 [41] all tests at 36, 33 and 29 days of curing . . . . . 153
3.20 Phase2 - EN 10027 [72] all tests . . . . . 153
3.21 Phase3 - ASTM C1609 [42] all tests at 14 days of curing . . . . . 159
3.22 Phase3 - ASTM C1609 [42] all tests at 120 days of curing . . . . . 159
3.23 Phase3 - EN 14651 [41] all tests at 14 days of curing . . . . . 160
3.24 Phase3 - EN 14651 [41] all tests at 120 days of curing . . . . . 160

# List of Tables


1.1 "Physical properties of some fibers" (Table 6, Löfgren, 2005)[17] . . . . . 15

1.2 "State of the art of shear testing method found in literature" (Table 1, Sahlab et al., 2024)[44] . . . . . 29

2.1 Phase1 - Geometrical properties and steel specifications for beam S1-0 . . . 50

2.2 Phase1 - Mechanical properties according to EN 12390-3 and ASTM C496[34,73] 52

2.3 Phase1 - Mechanical properties according to EN 14651 and ASTM C1609[41,42] 52

2.4 Phase1 - Shear test results of beams S1-0 . . . . . 57

2.5 Phase2 - Geometrical properties and steel specifications for beam S1-0 . . . 62

2.6 Phase2 - Geometrical properties and steel specifications for beam S1-4 . . . 62

2.7 Phase2 - Mechanical properties according to EN 12390-3, EN 12390-13(A), ASTM C496[34,36,73] . . . . . 65

2.8 Phase2 - Mechanical properties according to EN 14651 and ASTM C1609[41,42] 66

2.9 Phase2 - Shear test results of beams S1-0 adn S1-4 . . . . . 70

2.10 Phase3 - Geometrical properties and steel specifications for beam S1-0 . . . 76

2.11 Phase3 - Geometrical properties and steel specifications for beam S1-1 . . . 76

2.12 Phase3 - Geometrical properties and steel specifications for beam S1-2 . . . 77

2.13 Phase3 - Geometrical properties and steel specifications for beam S1-3 . . . 77

2.14 Phase3 - Geometrical properties and steel specifications for beam S1-4 . . . 78

2.15 Phase3 - Mechanical properties according to EN 12390-3, EN 12390-13(A), ASTM C496[34,36,73] . . . . . 80

2.16 Phase3 - Mechanical properties according to EN 14651 and ASTM C1609[41,42] 80

2.17 Phase1 - Shear test results of beams S1-0, S1-1, S1-2, S1-3 and S1-4 . . . . 86

3.1 Compliance with ACI 318-25 criteria[57] . . . . . 102
3.2 Compliance with EN1992-1-1 - Annex L and *fib* Model Code 2020 criteria[33,56] 103
3.3 Phase1 - ASTM C1609[42] for PC-0-200h . . . . . 139
3.4 Phase1 - ASTM C1609[42] and EN14651[41] for FRC-20-200h . . . . . 140
3.5 Phase1 - ASTM C1609[42] and EN14651[41] for FRC-40-200h . . . . . 140
3.6 Phase1 - ASTM C1609[42] and EN14651[41] for FRC-60-200h . . . . . 141
3.7 Phase1 - ASTM C1609[42] and EN14651[41] for FRC-80-200h . . . . . 141
3.8 Phase1 - ASTM C1609[42] and EN14651[41] for FRC-100-200h . . . . . 141
3.9 Phase1 - EN 12390-3[34] and ASTM C496[73] for PC-0-200h . . . . . 142
3.10 Phase1 - EN 12390-3[34] for FRC-20-200h and FRC-40-200h . . . . . 142
3.11 Phase1 - EN 12390-3[34] for FRC-60-200h and FRC-80-200h . . . . . 142
3.12 Phase2 - ASTM C1609[42] for PC-0-ZZZh at 14 and 36 days of curing . . . 144
3.13 Phase2 - ASTM C1609[42] for FRC-60-ZZZh at 14 and 33 days of curing . 145
3.14 Phase2 - ASTM C1609[42] for FRC-100-ZZZh at 14 and 29 days of curing . 145
3.15 Phase2 - EN 14651[41] for PC-0-ZZZh at 14 and 36 days of curing . . . . . 146
3.16 Phase2 - EN 14651[41] for FRC-60-ZZZh at 14 and 33 days of curing . . . . 146
3.17 Phase2 - EN 14651[41] for FRC-100-ZZZh at 14 and 29 days of curing . . . 147
3.18 Phase2 - EN 12390-13[36] for PC-0-ZZZh at 36 days of curing (left); 10027-1[72] for rebars nominaly B500B $\phi$34 (right) . . . . . 147
3.19 Phase2 - EN 12390-13[36] for FRC-60-ZZZh at 33 days of curing (left) and FRC-100-ZZZh at 29 days of curing . . . . . 148
3.20 Phase2 - EN 12390-3[34] for PC-0-ZZZh at 14 days of curing on cylinders (left) and cubes (right) . . . . . 148
3.21 Phase2 - EN 12390-3[34] for PC-0-ZZZh at 36 days of curing on cylinders (left) and cubes (right) . . . . . 149
3.22 Phase2 - EN 12390-3[34] for FRC-60-ZZZh at 14 days of curing on cylinders (left) and cubes (right) . . . . . 149

3.23 Phase2 - EN 12390-3[34] for FRC-60-ZZZh at 33 days of curing on cylinders (left) and cubes (right) . . . 150
3.24 Phase2 - EN 12390-3[34] for FRC-100-ZZZh at 14 days of curing on cylinders (left) and cubes (right) . . . 150
3.25 Phase2 - EN 12390-3[34] for FRC-100-ZZZh at 29 days of curing on cylinders (left) and cubes (right) . . . 151
3.26 Phase3 - ASTM C1609[42] for FRC-60-ZZZh (left) and FRC-80-ZZZh (right) 154
3.27 Phase3 - ASTM C1609[42] for FRC-60-900h (left) and FRC-80-900h (right) 154
3.28 Phase3 - EN 14651[41] for FRC-60-ZZZh (left) and FRC-80-ZZZh (right) . 155
3.29 Phase3 - EN 14651[41] for FRC-60-900h (left) and FRC-80-900h (right) . . 156
3.30 Phase3 - EN 12390-13[36] for PC-0-ZZZh . . . 156
3.31 Phase3 - EN 12390-13[36] for FRC-60-ZZZh (left) and FRC-100-ZZZh (right) 157
3.32 Phase3 - EN 12390-3[34] for PC-0-ZZZh on cylinders (left) and cubes (right) 157
3.33 Phase3 - EN 12390-3[34] for FRC-60-ZZZh on cylinders (left) and cubes (right) . . . 157
3.34 Phase3 - EN 12390-3[34] for FRC-100-ZZZh on cylinders (left) and cubes (right) . . . 158
3.35 Phase3 - NMX B506[75] for rebars respectively #3 (9.5 mm, 0.4 in.), #4 (12.7 mm, 0.5 in.), #6 (19.1 mm, 0.8 in.), #8 (25.4 mm, 1.0 in.), and #10 (31.8 mm, 1.3 in.) . . . 158

# Bibliography

[1] Amir A. Mirsayah and Nemkumar Banthia. Shear strength of steel fiber-reinforced concrete. 2002.

[2] Bhupinder Singh and Kranti Jain. Appraisal of steel fibers as minimum shear reinforcementin concrete beams. 2014.

[3] Rajesh Cherkupally and Rajesh K. Garje. A new shear test setup for determining shear strength of normal and high strength concrete. 2023.

[4] Lesley H. Sneed and Julio A. Ramirez. Influence of effective depth on shear strength of concrete beams - experimental study. 2010.

[5] G. N. J. Kani. How safe are our large reinforced concrete beams? 1967.

[6] Zdenek P. Bažant, Qiang Yu, Walter Gerstle, James Hanson, and J Woody Ju. Justification of ACI 446 proposal for updating ACI code provisions for shear design of reinforced concrete beams. 2007.

[7] Daniel A. Kuchma, Sihang Wei, David H. Sanders, Abdeldjelil Belarbi, and Lawrence C. Novak. Development of the one-way shear design provisions of ACI 318-19 for reinforced concrete. 2019.

[8] Fausto Minelli, Antonio Conforti, Estefanía Cuenca, and Giovanni A. Plizzari. Are steel fibres able to mitigate or eliminate size effect in shear? 2014.

[9] W. Ritter. Construction method of hennebique (die bauweise hennebique). Schweizerische Bauzeitung, 1899.

[10] *fib* Bulletin 57. Shear and punching shear in RC and FRC elements. 2010.

[11] György L. Balázs. A historical review of shear. *fib* Bulletin 57, 2010.

[12] E. Mörsch. Reinforced concrete - theory and application (der eisenbetonbau seine theorie und anwendung). Verlag von Konrad Wittwer, Stuttgart, pp. 146-215., 1908.

[13] H. Kupfer. Extension of truss model by mörsch by using the principle of minimal work of deformations (erweiterung der mörsch' schen fachwerkanalogie mit hilfe des prinzips vom minimum der formäderungarbeit). Schear-Colloquium Stuttgart, Manuscript, 1962.

[14] Frank J. Vecchio and Michael P. Collins. The modified compression-field theory for reinforced concrete elements subjected to shear. 1986.

[15] Joost C. Walraven. Fundamental analysis of aggregate interlock. 1981.

[16] ACI 544.4R. *ACI 544.4R-18 Guide to Design with Fiber-Reinforced Concrete*. American Concrete Institute, 2018.

[17] Ingemar Löfgren. Fibre-reinforced concrete for industrial construction- a fracture mechanics approach to material testing and structural analysis. 2005.

[18] Thong M. Pham. Fibre-reinforced concrete: State-of-the-art-review on bridging mechanism, mechanical properties, durability, and eco-economic analysis. 2025.

[19] D. Zhang, J. Yu, H. Wu, B. Jaworska, B. R. Ellis, and V. C. Li. Discontinuous micro-fibers as intrinsic reinforcement for ductile engineered cementitious composites (ECC). 2020.

[20] EN 14889-1. *EN 14889-1 Fibres for concrete - Part 1: Steel fibres - Definitions, specifications and conformity*. European Committee for Standardization, 2006.

[21] ASTM A820. *ASTM A820/A820M-22 Standard Specification for Steel Fibers for Fiber-Reinforced Concrete*. American Society for Testing and Materials, 2022.

[22] J. Cook and J. E. Gordon. A mechanism for the control of crack propagation in all brittle systems. Proc. Roy. Soc. 282A, pp. 508-520, 1964.

[23] Doo-Yeol Yoo, Thomas Gries, and Young-Soo Yoon. Comparative low-velocity impact response of textile-reinforced concrete and steel-fiber-reinforced concrete beams. 2015.

[24] Vivek Bindiganavile and Nemkumar Banthia. Polymer and steel fiber-reinforced cementitious composites under impact loading - part 1: Bond-slip response. 2001.

[25] Ruben P. Borg, Owen Baldacchino, and Liberato Ferrara. Early age performance and mechanical characteristics of recycled PET fibre reinforced concrete. 2016.

[26] Doo-Yeol Yoo and Nemkumar Banthia. Size-dependent impact resistance of ultra-high-performance fiber-reinforced concrete beams. 2017.

[27] A. Bentur, S. Diamond, and S. Mindess. The microstructure of the steel fibre-cement interface. 1985.

[28] Jang H. J. Kim, Chan G. Park, Si W. Lee, Sang W. Lee, and Jong P. Won. Effects of the geometry of recycled PET fiber reinforcement on shrinkage cracking of cement-based composites. 2008.

[29] Su J. Lee and Jong P. Won. Shrinkage characteristics of structural nano-synthetic fibre-reinforced cementitious composites. 2016.

[30] Zengzhi Sun and Qinwu Xu. Microscopic, physical and mechanical analysis of polypropylene fiber reinforced concrete. 527(1):198–204, 2009.

[31] Fallah Saber and Nematzadeh Mahdi. Mechanical properties and durability of high-strength concrete containing macro-polymeric and polypropylene fibers with nano-silica and silica fume. Construction and Building Materials, 132. 170-187.

[32] Eleonora Mondo. Shear capacity of steel fibre reinforced concrete beams without conventional shear reinforcement. 2011.

[33] *fib* Model Code 2020. *fib Model Code for concrete structures (2020).* Fédération Internationale du Béton, 2020.

[34] EN 12390-3. *EN 12390-3 Testing hardened concrete - Part 3: Compressive strength of test specimens.* European Committee for Standardization, 2019.

[35] ASTM C39. *ASTM C39/C39M-24 Standard Test Method for Compressive Strength of Cylindrical Concrete Specimens.* 2024.

[36] EN 12390-13. *EN 12390-13 Testing hardened concrete - Part 13 : determination of secant modulus of elasticity in compression.* European Committee for Standardization, 2021.

[37] ASTM C69. *ASTM C496-02 Standard Test Method for Static Modulus of Elasticity and Poisson's Ratio of Concrete in Compression.* American Society for Testing and Materials, 2002.

[38] JSCE 2008. *Recommendations for Design and Construction of High Performance Fiber Reinforced Cement Composites with Multiple Fine Cracks (HPFRCC).* Japan Society of Civil ENgineers, 2008.

[39] SIA 2052. *SIA 2052:2016 Beton fibre ultra-performant (BFUP) - Materiaux, dimensionnement et execution.* Swiss Society of Engineers and Architects, 2016.

[40] AASHTO 397. *AASHTO T397-22 Uniaxial Tensile Response of Ultra- High Performance Concrete.* American Association of State Highway and Transportation Officials, 2022.

[41] EN 14651. *EN 14651 Test method for metallic fibered concrete - Measuring the flexural tensile stength (limit of proportionality (LOP), residual).* European Committee for Standardization, 2005.

[42] ASTM C1609. *ASTM C1609/C1609M-24 Standard Test Method for Flexural Performance of Fiber-Reinforced Concrete (Using Beam With Third-Point Loading).* American Society for Testing and Materials, 2024.

[43] Abdoladel Shoaib. Shear in steel fiber reinforced concrete members without stirrups. 2012.

[44] Ziad N. Sahlab, Nicholas S. Burello, Alfredo A. Flores G., Jorge C. Diaz, and Davide Zampini. Exploring shear strength of concrete: A novel z-test for direct shear testing of hpfrc. 2024.

[45] Mariano Valle and Oral Buyukozturk. Behavior of fiber reinforced high-strength concrete under direct shear. 1993.

[46] Juliana Trindade, Sergio L. Garcia, and Humberto Torres. Shear strength of concrete with recycled aggregates reinforced with steel fibers. 2021.

[47] Fulvio Tonon. JSCE-SF6 limitations for shear tests and ASTM d5607 shear tests on fiber-reinforced concrete. 2021.

[48] Nagaratnam Sivakugan, B. M. Das, Julie Lovisa, and Chittaranjan Patra. Determination of c and 934; of rocks from indirect tensile strength and uniaxial compression tests. 2014.

[49] Bo Meng, Hongwen Jing, Shengqi Yang, Yingchao Wang, and Biao Li. Experimental study on the shear behavior of bolted concrete blocks with oblique shear test. 2018.

[50] Selimir Lelovic and Dejan Vasovic. Determination of mohr-coulomb parameters for modelling of concrete. 2020.

[51] B. Barr and Mohamed Derradj. Numerical study of a shear (mode II) type test specimen geometry. 1990.

[52] B. Barr and E. B. D. Hasso. Development of a compact cylindrical shear test specimen. 1986.

[53] D. J. De Souza, Leandro F. M. Sanchez, and Mayra T. De Grazia. Evaluation of a direct shear test setup to quantify AAR-induced expansion and damage in concrete. 2019.

[54] Mohammad R. Zarrinpour and Shih-Ho Chao. Shear strength enhancement mechanisms of steel fiber-reinforced concrete slender beams.

[55] Gustavo J. Parra-Montesinos. Shear strength of beams with deformed steel fibers. 2006.

[56] Eurocode 2. *FprEN_1992-1-1 CEN/TC 250/SC 2 "Eurocode 2: Design of concrete structures - Part 1-1: General rules and rules for buildings, bridges and civil engineering structures"*. European Committee for Standardization, 2022.

[57] ACI 318. *ACI CODE-318-25 Building Code for Structural Concrete - Code Requirements and Commentary*. American Concrete Institute, 2025.

[58] Fausto Minelli and Giovanni A. Plizzari. Steel fibers as shear reinforcement for beams. Proceedings of The Second Fib Congress, Naples, Italy, 5-8 June 2006, abstract on page 282-283, full length paper available on accompanied CD, 2006, pp.12., 2006.

[59] Fausto Minelli and Giovanni A. Plizzari. Shear strength of FRC members with little or no shear reinforcement: a new analytical model. *fib* Bulletin 57, 2010.

[60] Fausto Minelli and Giovanni A. Plizzari. On the effectiveness of steel fibers as shear reinforcement. 2013.

[61] *fib* Model Code 2010. *Model Code 2010 - Final draft - Volume 1*. Fédération Internationale du Béton, 2012.

[62] *fib* Model Code 2010. *Model Code 2010 - Final draft - Volume 2*. Fédération Internationale du Béton, 2012.

[63] Shih-Ho Chao. Size effect on ultimate shear strength of steel fiber- reinforced concrete slender beams. 2020.

[64] Abdoladel Shoaib, Adam S. Lubell, and Vivek S. Bindiganavile. Size effect in shear for steel fiber-reinforced concrete members without stirrups. 2014.

[65] Estefanía Cuenca, Antonio Conforti, Fausto Minelli, Giovanni Plizzari, Juan N. Gregori, and Pedro Serna. A material-performance-based database for FRC and RC elements under shear loading. 2018.

[66] Sergio M. Alcocer, Ghassan Almasabha, Julian Carrillo, Shih-Ho Chao, and Adam S. Lubell. Shear strength of steel fiber-reinforced concrete beams and one-way slabs. 2025.

[67] ACI 318. *Building Code Requirements for Structural Concrete (ACI318-19)*. American Concrete Institute, 2019.

[68] ASTM C1116. *ASTM C1116/C1116M-09 Standard specification for Fiber-Reinforced Concrete*. American Society for Testing and Materials, 2009.

[69] Davide Zampini, Alexandre Guerini, and Giovanni Volpatti. EP 3 307 692 b1 - ADVANCED FIBER REINFORCED CONCRETE MIX DESIGNS, 2016.

[70] EN 206. *EN 206 Concrete - Specification, performance, production and conformity*. European Committee for Standardization, 2021.

[71] EN 12350-8. *EN 12350-8 Testing fresh concrete - Part 8: Self-compacting concrete - Slumpflow test*. European Committee for Standardization, 2019.

[72] EN 10027-1. *EN 10027-1 Designation systems for steels - Part 1: Steel names*. European Committee for Standardization, 2005.

[73] ASTM C496. *ASTM C496/C496M-17 Standard Test Method for Splitting Tensile Strength of Cylindrical Concrete Specimens*. American Society for Testing and Materials, 2017.

[74] ISO 15630-1. *ISO 15630-1 - Steel for the reinforcement and prestressing of concrete - Test methods Part 1: Reinforcing bars, wire rod and wire (2nd edition)*. International Standard, 2010.

[75] NMX B506. *NMX-B-506-CANACERO-2019 INDUSTRIA SIDERÚRGICA- VARILLA CORRUGADA DE ACERO PARA REFUERZO DE CONCRETOESPECIFICACIONES Y MÉTODOS DE PRUEBA*. NORMA MEXICANA, 2019.

# Annex A – Summary of Quality Control test results

* = nominal values

## Phase 1 – Preliminary Investigation 1

Table 3.3. Phase1 - ASTM C1609 [42] for PC-0-200h

| Sample ID PC-0 | $f_{1^{st}peak}$ | $f^D_{600}$ | $f^D_{300}$ | $f^D_{150}$ | $f_P$ |
|---|---|---|---|---|---|
| | MPa (ksi) | MPa (ksi) | MPa (ksi) | MPa (ksi) | MPa (ksi) |
| [1] | 4.09 (0.59) | - - | - - | - - | 4.09 (0.59) |
| Average | 4.09 (0.59) | - - | - - | - - | 4.09 (0.59) |
| CV (%) | NA | NA | NA | NA | NA |

Table 3.4. Phase1 - ASTM C1609[42] and EN14651[41] for FRC-20-200h

| Sample ID FRC-20 | $f_{1^{st}peak}$ MPa (ksi) | $f^D_{600}$ MPa (ksi) | $f^D_{300}$ MPa (ksi) | $f^D_{150}$ MPa (ksi) | $f_P$ MPa (ksi) |
|---|---|---|---|---|---|
| [1] | 3.39 (0.49) | 1.74 (0.25) | 1.70 (0.25) | 1.41 (0.20) | 3.39 (0.49) |
| [2] | 4.43 (0.64) | 2.78 (0.40) | 2.67 (0.39) | 2.35 (0.34) | 4.43 (0.64) |
| [3] | 4.35 (0.63) | 2.30 (0.33) | 2.27 (0.33) | 2.13 (0.31) | 4.35 (0.63) |
| Average | 4.05 (0.59) | 2.27 (0.33) | 2.21 (0.32) | 1.96 (0.28) | 4.05 (0.59) |
| CV (%) | 11.64 | 18.60 | 18.00 | 20.64 | 11.64 |

| Sample ID FRC-20 | $f_L$ MPa (ksi) | $f_{R1k}$ MPa (ksi) | $f_{R2k}$ MPa (ksi) | $f_{R3k}$ MPa (ksi) | $f_{R4k}$ MPa (ksi) |
|---|---|---|---|---|---|
| [1] | 3.62 (0.53) | 2.25 (0.33) | 2.95 (0.43) | 3.22 (0.47) | 3.24 (0.47) |
| [2] | 3.88 (0.56) | 3.10 (0.45) | 3.89 (0.56) | 4.28 (0.62) | 4.43 (0.64) |
| [3] | 4.45 (0.64) | 2.69 (0.39) | 3.38 (0.49) | 3.60 (0.52) | 3.67 (0.53) |
| Average | 3.98 (0.58) | 2.68 (0.39) | 3.41 (0.49) | 3.70 (0.54) | 3.78 (0.55) |
| CV (%) | 8.7 | 12.9 | 11.2 | 11.9 | 13.0 |

Table 3.5. Phase1 - ASTM C1609[42] and EN14651[41] for FRC-40-200h

| Sample ID FRC-40 | $f_{1^{st}peak}$ MPa (ksi) | $f^D_{600}$ MPa (ksi) | $f^D_{300}$ MPa (ksi) | $f^D_{150}$ MPa (ksi) | $f_P$ MPa (ksi) |
|---|---|---|---|---|---|
| [1] | 4.79 (0.70) | 4.51 (0.65) | 4.43 (0.64) | 3.80 (0.55) | 6.00 (0.87) |
| [2] | 4.78 (0.69) | 5.72 (0.83) | 5.21 (0.75) | 4.50 (0.65) | 6.28 (0.91) |
| [3] | 4.64 (0.67) | 3.73 (0.54) | 3.68 (0.53) | 3.37 (0.49) | 4.64 (0.67) |
| [4] | 4.92 (0.71) | 5.99 (0.87) | 5.77 (0.84) | 3.83 (0.56) | 6.47 (0.94) |
| Average | 4.78 (0.69) | 4.99 (0.72) | 4.77 (0.69) | 3.88 (0.56) | 5.85 (0.85) |
| CV (%) | 2.4 | 20.2 | 18.5 | 11.9 | 14.1 |

| Sample ID FRC-40 | $f_L$ MPa (ksi) | $f_{R1k}$ MPa (ksi) | $f_{R2k}$ MPa (ksi) | $f_{R3k}$ MPa (ksi) | $f_{R4k}$ MPa (ksi) |
|---|---|---|---|---|---|
| [1] | 4.40 (0.64) | 5.47 (0.79) | 6.68 (0.97) | 6.79 (0.98) | 6.78 (0.98) |
| [2] | 3.81 (0.55) | 2.13 (0.31) | 2.75 (0.40) | 3.11 (0.45) | 3.09 (0.45) |
| [3] | 4.45 (0.65) | 5.80 (0.84) | 7.25 (1.05) | 7.14 (1.04) | 5.53 (0.80) |
| [4] | 4.61 (0.67) | 6.67 (0.97) | 8.12 (1.18) | 7.73 (1.12) | 6.58 (0.95) |
| [5] | 4.25 (0.62) | 3.57 (0.52) | 3.95 (0.57) | 3.99 (0.58) | 3.66 (0.53) |
| Average | 4.30 (0.62) | 4.73 (0.69) | 5.75 (0.83) | 5.75 (0.83) | 5.13 (0.74) |
| CV (%) | 6.3 | 34.8 | 35.6 | 32.0 | 29.3 |

Table 3.6. Phase1 - ASTM C1609[42] and EN14651[41] for FRC-60-200h

| Sample ID FRC-60 | $f_{1^{st}peak}$ MPa (ksi) | $f^D_{600}$ MPa (ksi) | $f^D_{300}$ MPa (ksi) | $f^D_{150}$ MPa (ksi) | $f_P$ MPa (ksi) |
|---|---|---|---|---|---|
| [1] | 5.48 (0.79) | 4.21 (0.61) | 4.21 (0.61) | 3.11 (0.45) | 5.48 (0.79) |
| [2] | 5.30 (0.77) | 5.60 (0.81) | 5.37 (0.78) | 5.02 (0.73) | 5.68 (0.82) |
| [3] | 4.61 (0.67) | 5.00 (0.73) | 5.59 (0.81) | 4.75 (0.69) | 5.62 (0.81) |
| Average | 5.13 (0.74) | 4.94 (0.72) | 5.05 (0.73) | 4.29 (0.62) | 5.59 (0.81) |
| CV (%) | 7.3 | 11.5 | 12.0 | 19.7 | 1.5 |

| Sample ID FRC-60 | $f_L$ MPa (ksi) | $f_{R1k}$ MPa (ksi) | $f_{R2k}$ MPa (ksi) | $f_{R3k}$ MPa (ksi) | $f_{R4k}$ MPa (ksi) |
|---|---|---|---|---|---|
| [1] | 4.81 (0.70) | 6.44 (0.93) | 6.59 (0.96) | 6.57 (0.95) | 6.13 (0.89) |
| [2] | 4.81 (0.70) | 7.72 (1.12) | 8.99 (1.30) | 7.37 (1.07) | 7.33 (1.06) |
| [3] | 4.42 (0.64) | 4.18 (0.61) | 4.60 (0.67) | 4.79 (0.69) | 5.00 (0.72) |
| Average | 4.68 (0.68) | 6.11 (0.89) | 6.73 (0.98) | 6.24 (0.91) | 6.15 (0.89) |
| CV (%) | 3.9 | 23.9 | 26.7 | 17.3 | 15.5 |

Table 3.7. Phase1 - ASTM C1609[42] and EN14651[41] for FRC-80-200h

| Sample ID FRC-80 | $f_{1^{st}peak}$ MPa (ksi) | $f^D_{600}$ MPa (ksi) | $f^D_{300}$ MPa (ksi) | $f^D_{150}$ MPa (ksi) | $f_P$ MPa (ksi) |
|---|---|---|---|---|---|
| [1] | 5.28 (0.77) | 6.71 (0.97) | 6.35 (0.92) | 4.83 (0.70) | 6.88 (1.00) |
| [2] | 5.88 (0.85) | 6.49 (0.94) | 5.60 (0.81) | 3.42 (0.50) | 7.52 (1.09) |
| Average | 5.58 (0.81) | 6.60 (0.96) | 5.98 (0.87) | 4.13 (0.60) | 7.20 (1.04) |
| CV (%) | 5.4 | 1.7 | 6.3 | 17.0 | 4.5 |

| Sample ID FRC-80 | $f_L$ MPa (ksi) | $f_{R1k}$ MPa (ksi) | $f_{R2k}$ MPa (ksi) | $f_{R3k}$ MPa (ksi) | $f_{R4k}$ MPa (ksi) |
|---|---|---|---|---|---|
| [1] | 5.65 (0.82) | 8.68 (1.26) | 9.14 (1.33) | 8.98 (1.30) | 7.95 (1.15) |
| [2] | 5.06 (0.73) | 6.84 (0.99) | 8.28 (1.20) | 7.16 (1.04) | 6.74 (0.98) |
| Average | 5.36 (0.78) | 7.76 (1.13) | 8.71 (1.26) | 8.07 (1.17) | 7.35 (1.07) |
| CV (%) | 5.5 | 11.8 | 4.9 | 11.3 | 8.3 |

Table 3.8. Phase1 - ASTM C1609[42] and EN14651[41] for FRC-100-200h

| Sample ID FRC-100 | $f_{1^{st}peak}$ MPa (ksi) | $f^D_{600}$ MPa (ksi) | $f^D_{300}$ MPa (ksi) | $f^D_{150}$ MPa (ksi) | $f_P$ MPa (ksi) |
|---|---|---|---|---|---|
| [1] | 4.96 (0.72) | 9.26 (1.34) | 6.61 (0.96) | 4.77 (0.69) | 9.28 (1.35) |
| [2] | 5.46 (0.79) | 9.61 (1.39) | 7.65 (1.11) | 5.31 (0.77) | 9.76 (1.42) |
| Average | 5.21 (0.76) | 9.44 (1.37) | 7.13 (1.03) | 5.04 (0.73) | 9.52 (1.38) |
| CV (%) | 4.8 | 1.9 | 7.3 | 5.4 | 2.5 |

| Sample ID FRC-100 | $f_L$ MPa (ksi) | $f_{R1k}$ MPa (ksi) | $f_{R2k}$ MPa (ksi) | $f_{R3k}$ MPa (ksi) | $f_{R4k}$ MPa (ksi) |
|---|---|---|---|---|---|
| [1] | 4.56 (0.66) | 7.55 (1.09) | 8.69 (1.26) | 8.38 (1.22) | 7.42 (1.08) |
| [2] | 5.15 (0.75) | 10.11 (1.47) | 9.89 (1.43) | 9.15 (1.33) | 8.64 (1.25) |
| Average | 4.86 (0.70) | 8.83 (1.28) | 9.29 (1.35) | 8.76 (1.27) | 8.03 (1.16) |
| CV (%) | 6.1 | 14.5 | 6.5 | 4.4 | 7.6 |

Table 3.9. Phase1 - EN 12390-3[34] and ASTM C496[73] for PC-0-200h

| Sample ID PC-0 | D | h | $F_{max}$ | $\delta$ | $f_C$ |
|---|---|---|---|---|---|
| | mm (in.) | mm (in.) | kN (kips) | $kg/m^3$ ($lb/yd^3$) | MPa (ksi) |
| [1] | 150* (5.9) | 300* (11.8) | 794.2 (178.5) | 2293* (3865) | 44.94 (6.52) |
| [2] | 150* (5.9) | 300* (11.8) | 819.2 (184.2) | 2293* (3865) | 46.36 (6.72) |
| | | | Average | 2293 (3865) | 45.65 (6.62) |
| | | | CV (%) | NA | 1.55 |

| Sample ID PC-0 | D | h | $F_{max}$ | $f_T$ |
|---|---|---|---|---|
| | mm (in.) | mm (in.) | kN (kips) | MPa (ksi) |
| [1] | 149.6 (5.9) | 303.4 (11.9) | 199.8 (44.9) | 2.80 (0.41) |
| | | Average | 199.8 (44.9) | 2.80 (0.41) |
| | | CV (%) | NA | NA |

Table 3.10. Phase1 - EN 12390-3[34] for FRC-20-200h and FRC-40-200h

| Sample ID FRC-20 | D | h | $F_{max}$ | $\delta$ | $f_C$ |
|---|---|---|---|---|---|
| | mm (in.) | mm (in.) | kN (kips) | $kg/m^3$ ($lb/yd^3$) | MPa (ksi) |
| [1] | 149.1 (5.9) | 287.9 (11.3) | 814.4 (183.1) | 2334 (3933) | 46.67 (6.77) |
| [2] | 149.3 (5.9) | 291.3 (11.5) | 804.8 (180.9) | 2304 (3884) | 45.99 (6.67) |
| | | | Average | 2319 (3908) | 46.33 (6.72) |
| | | | CV (%) | 0.64 | 0.73 |

| Sample ID FRC-40 | D | h | $F_{max}$ | $\delta$ | $f_C$ |
|---|---|---|---|---|---|
| | mm (in.) | mm (in.) | kN (kips) | $kg/m^3$ ($lb/yd^3$) | MPa (ksi) |
| [1] | 149.7 (5.9) | 291.9 (11.5) | 815.9 (183.4) | 2321 (3912) | 46.38 (6.73) |
| | | | Average | 2321 (3912) | 46.38 (6.73) |
| | | | CV (%) | NA | NA |

Table 3.11. Phase1 - EN 12390-3[34] for FRC-60-200h and FRC-80-200h

| Sample ID FRC-60 | D | h | $F_{max}$ | $\delta$ | $f_C$ |
|---|---|---|---|---|---|
| | mm (in.) | mm (in.) | kN (kips) | $kg/m^3$ ($lb/yd^3$) | MPa (ksi) |
| [1] | 150* (5.9) | 300* (11.8) | 841.3 (189.1) | 2319* (3909) | 47.61 (6.90) |
| [2] | 150* (5.9) | 300* (11.8) | 820.4 (184.4) | 2319* (3909) | 46.42 (6.73) |
| | | | Average | 2319 (3909) | 47.02 (6.82) |
| | | | CV (%) | NA* | 1.26 |

| Sample ID FRC-80 | D | h | $F_{max}$ | $\delta$ | $f_C$ |
|---|---|---|---|---|---|
| | mm (in.) | mm (in.) | kN (kips) | $kg/m^3$ ($lb/yd^3$) | MPa (ksi) |
| [1] | 149.6 (5.9) | 289.2 (11.4) | 832.3 (187.1) | 2367 (3990) | 47.38 (6.87) |
| [2] | 149.7 (5.9) | 287.4 (11.3) | 829.7 ((186.5) | 2363 (3983) | 47.16 (6.84) |
| | | | Average | 2365 (3986) | 47.27 (6.86) |
| | | | CV (%) | 0.10 | 0.23 |

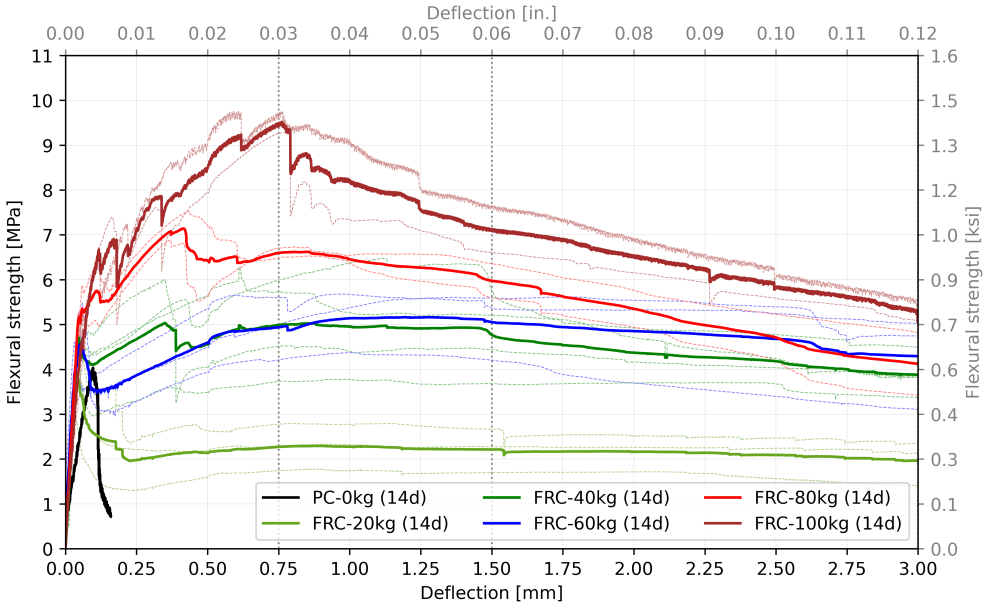



Figure 3.14. Phase1 - ASTM C1609[42] all tests

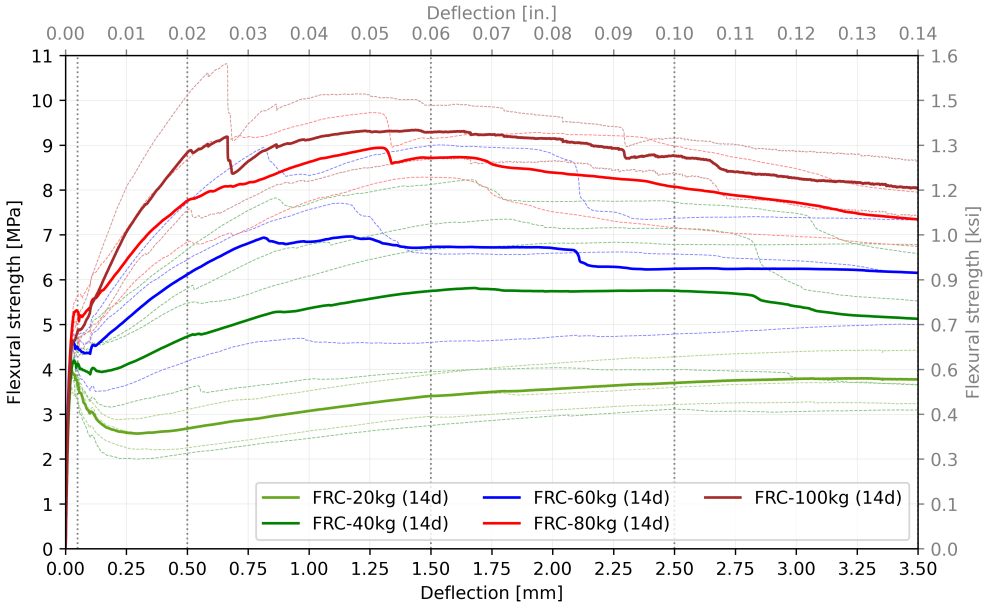



Figure 3.15. Phase1 - EN 14651[41] all tests

# Phase 2 – Preliminary Investigation 2

Table 3.12. Phase2 - ASTM C1609[42] for PC-0-ZZZh at 14 and 36 days of curing

| Beam ID PC-0 (14days) | $f_{1^{st}peak}$ | $f^D_{600}$ | $f^D_{300}$ | $f^D_{150}$ | $f_P$ |
|---|---|---|---|---|---|
| | MPa (ksi) | MPa (ksi) | MPa (ksi) | MPa (ksi) | MPa (ksi) |
| [1] | 6.91 (1.00) | - - | - - | - - | 6.91 (1.00) |
| [2] | 7.55 (1.10) | - - | - - | - - | 7.55 (1.10) |
| Average | 7.23 (1.05) | - - | - - | - - | 7.23 (1.05) |
| CV (%) | 4.47 | NA | NA | NA | 4.47 |

| Beam ID PC-0 (36days) | $f_{1^{st}peak}$ | $f^D_{600}$ | $f^D_{300}$ | $f^D_{150}$ | $f_P$ |
|---|---|---|---|---|---|
| | MPa (ksi) | MPa (ksi) | MPa (ksi) | MPa (ksi) | MPa (ksi) |
| [1] | 6.26 (0.91) | - - | - - | - - | 6.26 (0.91) |
| [2] | 6.09 (0.88) | - - | - - | - - | 6.09 (0.88) |
| Average | 6.18 (0.90) | - - | - - | - - | 6.18 (0.90) |
| CV (%) | 1.35 | NA | NA | NA | 1.35 |

Table 3.13. Phase2 - ASTM C1609[42] for FRC-60-ZZZh at 14 and 33 days of curing

| Beam ID FRC-60 (14days) | $f_{1^{st}peak}$ | $f^D_{600}$ | $f^D_{300}$ | $f^D_{150}$ | $f_P$ |
|---|---|---|---|---|---|
| | MPa (ksi) | MPa (ksi) | MPa (ksi) | MPa (ksi) | MPa (ksi) |
| [1] | 5.68 (0.82) | 7.88 (1.14) | 7.82 (1.13) | 6.27 (0.91) | 8.26 (1.20) |
| [2] | 6.15 (0.89) | 7.41 (1.07) | 5.77 (0.84) | 4.05 (0.59) | 7.87 (1.14) |
| [3] | 6.38 (0.93) | 8.71 (1.26) | 9.39 (1.36) | 6.92 (1.00) | 9.57 (1.39) |
| Average | 6.07 (0.88) | 8.00 (1.16) | 7.66 (1.11) | 5.75 (0.83) | 8.57 (1.24) |
| CV (%) | 4.79 | 6.72 | 19.34 | 21.39 | 8.48 |

| Beam ID FRC-60 (33days) | $f_{1^{st}peak}$ | $f^D_{600}$ | $f^D_{300}$ | $f^D_{150}$ | $f_P$ |
|---|---|---|---|---|---|
| | MPa (ksi) | MPa (ksi) | MPa (ksi) | MPa (ksi) | MPa (ksi) |
| [1] | 5.47 (0.79) | 6.25 (0.91) | 6.14 (0.89) | 4.19 (0.61) | 6.49 (0.94) |
| [2] | 5.80 (0.84) | 8.37 (1.21) | 7.62 (1.11) | 5.14 (0.75) | 9.16 (1.33) |
| [3] | 5.22 (0.76) | 8.81 (1.28) | 7.80 (1.13) | 5.29 (0.77) | 9.28 (1.35) |
| [4] | 5.17 (0.75) | 5.94 (0.86) | 6.83 (0.99) | 5.15 (0.75) | 6.90 (1.00) |
| [5] | 5.00 (0.72) | 6.89 (1.00) | 5.20 (0.75) | 3.53 (0.51) | 6.92 (1.00) |
| [6] | 5.19 (0.75) | 7.30 (1.06) | 7.56 (1.10) | 5.18 (0.75) | 7.85 (1.14) |
| Average | 5.31 (0.77) | 7.26 (1.05) | 6.86 (1.00) | 4.75 (0.69) | 7.77 (1.13) |
| CV (%) | 4.92 | 14.39 | 13.60 | 13.87 | 14.24 |

Table 3.14. Phase2 - ASTM C1609[42] for FRC-100-ZZZh at 14 and 29 days of curing

| Beam ID FRC-100 (14days) | $f_{1^{st}peak}$ | $f^D_{600}$ | $f^D_{300}$ | $f^D_{150}$ | $f_P$ |
|---|---|---|---|---|---|
| | MPa (ksi) | MPa (ksi) | MPa (ksi) | MPa (ksi) | MPa (ksi) |
| [1] | 5.55 (0.80) | 11.72 (1.70) | 10.29 (1.49) | 7.91 (1.15) | 8.26 (1.20) |
| [2] | 5.53 (0.80) | 8.19 (1.19) | 8.16 (1.18) | 5.51 (0.80) | 7.87 (1.14) |
| Average | 5.54 (0.80) | 9.96 (1.44) | 9.23 (1.34) | 6.71 (0.97) | 8.07 (1.17) |
| CV (%) | 0.15 | 17.72 | 11.51 | 17.90 | 2.43 |

| Beam ID FRC-100 (29days) | $f_{1^{st}peak}$ | $f^D_{600}$ | $f^D_{300}$ | $f^D_{150}$ | $f_P$ |
|---|---|---|---|---|---|
| | MPa (ksi) | MPa (ksi) | MPa (ksi) | MPa (ksi) | MPa (ksi) |
| [1] | 5.90 (0.86) | 9.85 (1.43) | 9.40 (1.36) | 5.13 (0.74) | 11.61 (1.68) |
| [2] | 7.43 (1.08) | 10.16 (1.47) | 9.10 (1.32) | 5.62 (0.81) | 10.54 (1.53) |
| [3] | 6.51 (0.94) | 10.20 (1.48) | 7.90 (1.15) | 5.32 (0.77) | 10.29 (1.49) |
| [4] | 7.05 (1.02) | 10.15 (1.47) | 8.50 (1.23) | 5.95 (0.86) | 10.59 (1.54) |
| [5] | 6.64 (0.96) | 9.99 (1.45) | 6.62 (0.96) | 4.32 (0.63) | 10.40 (1.51) |
| [6] | 6.42 (0.93) | 10.20 (1.48) | 8.25 (1.20) | 5.89 (0.85) | 10.81 (1.57) |
| Average | 6.67 (0.97) | 10.00 (1.45) | 9.25 (1.34) | 5.38 (0.78) | 11.08 (1.61) |
| CV (%) | 11.46 | 1.53 | 1.62 | 4.50 | 4.85 |

Table 3.15. Phase2 - EN 14651[41] for PC-0-ZZZh at 14 and 36 days of curing

| Beam ID PC-0 (14days) | $f_L$ | $f_{R1k}$ | $f_{R2k}$ | $f_{R3k}$ | $f_{R4k}$ |
|---|---|---|---|---|---|
| | MPa (ksi) | MPa (ksi) | MPa (ksi) | MPa (ksi) | MPa (ksi) |
| [1] | 4.78 (0.69) | - - | - - | - - | - - |
| [2] | 4.26 (0.62) | - - | - - | - - | - - |
| Average | 4.52 (0.66) | - - | - - | - - | - - |
| CV (%) | 5.7 | - | - | - | - |

| Beam ID PC-0 (36days) | $f_L$ | $f_{R1k}$ | $f_{R2k}$ | $f_{R3k}$ | $f_{R4k}$ |
|---|---|---|---|---|---|
| | MPa (ksi) | MPa (ksi) | MPa (ksi) | MPa (ksi) | MPa (ksi) |
| [1] | 5.04 (0.73) | - - | - - | - - | - - |
| [2] | 4.66 (0.68) | - - | - - | - - | - - |
| Average | 4.85 (0.70) | - - | - - | - - | - - |
| CV (%) | 3.9 | - | - | - | - |

Table 3.16. Phase2 - EN 14651[41] for FRC-60-ZZZh at 14 and 33 days of curing

| Beam ID FRC-60 (14days) | $f_L$ | $f_{R1k}$ | $f_{R2k}$ | $f_{R3k}$ | $f_{R4k}$ |
|---|---|---|---|---|---|
| | MPa (ksi) | MPa (ksi) | MPa (ksi) | MPa (ksi) | MPa (ksi) |
| [1] | 4.64 (0.67) | 6.91 (1.00) | 8.39 (1.22) | 8.01 (1.16) | 7.35 (1.07) |
| [2] | 4.72 (0.68) | 6.24 (0.90) | 8.01 (1.16) | NA NA | NA NA |
| [3] | 5.36 (0.78) | 8.87 (1.29) | 8.77 (1.27) | 8.26 (1.20) | 7.40 (1.07) |
| Average | 4.90 (0.71) | 7.34 (1.06) | 8.39 (1.22) | 8.14 (1.18) | 7.38 (1.07) |
| CV (%) | 6.6 | 15.2 | 3.7 | 1.5 | 0.4 |

| Beam ID FRC-60 (33days) | $f_L$ | $f_{R1k}$ | $f_{R2k}$ | $f_{R3k}$ | $f_{R4k}$ |
|---|---|---|---|---|---|
| | MPa (ksi) | MPa (ksi) | MPa (ksi) | MPa (ksi) | MPa (ksi) |
| [1] | 4.98 (0.72) | 7.80 (1.13) | 8.83 (1.28) | 6.89 (1.00) | 6.14 (0.89) |
| [2] | 5.10 (0.74) | 7.38 (1.07) | 8.70 (1.26) | 8.22 (1.19) | 7.30 (1.06) |
| [3] | 4.88 (0.71) | 6.34 (0.92) | 8.16 (1.18) | 6.90 (1.00) | 6.27 (0.91) |
| [4] | 4.79 (0.69) | 6.47 (0.94) | 8.38 (1.21) | 8.51 (1.23) | 7.28 (1.06) |
| Average | 4.94 (0.72) | 6.99 (1.01) | 8.52 (1.24) | 7.63 (1.11) | 6.75 (0.98) |
| CV (%) | 2.4 | 8.8 | 3.1 | 9.7 | 8.0 |

Table 3.17. Phase2 - EN 14651 [41] for FRC-100-ZZZh at 14 and 29 days of curing

| Beam ID FRC-100 (14days) | $f_L$ | $f_{R1k}$ | $f_{R2k}$ | $f_{R3k}$ | $f_{R4k}$ |
|---|---|---|---|---|---|
| | MPa (ksi) | MPa (ksi) | MPa (ksi) | MPa (ksi) | MPa (ksi) |
| [1] | 5.11 (0.74) | 10.84 (1.57) | 10.56 (1.53) | 9.45 (1.37) | 8.31 (1.21) |
| [2] | 5.87 (0.85) | 11.59 (1.68) | 11.38 (1.65) | 11.20 (1.62) | 10.31 (1.50) |
| [3] | 5.35 (0.78) | 10.45 (1.52) | 10.46 (1.52) | 9.73 (1.41) | 8.75 (1.27) |
| Average | 5.44 (0.79) | 10.96 (1.59) | 10.80 (1.57) | 10.13 (1.47) | 9.12 (1.32) |
| CV (%) | 5.8 | 4.3 | 3.8 | 7.6 | 9.4 |

| Beam ID FRC-100 (29days) | $f_L$ | $f_{R1k}$ | $f_{R2k}$ | $f_{R3k}$ | $f_{R4k}$ |
|---|---|---|---|---|---|
| | MPa (ksi) | MPa (ksi) | MPa (ksi) | MPa (ksi) | MPa (ksi) |
| [1] | 5.82 (0.84) | 12.54 (1.82) | 11.90 (1.73) | 11.18 (1.62) | 10.14 (1.47) |
| [2] | 6.17 (0.89) | 13.27 (1.92) | 12.31 (1.79) | 10.62 (1.54) | 9.60 (1.39) |
| [3] | 6.91 (1.00) | 14.86 (2.16) | 15.95 (2.31) | 15.39 (2.23) | 14.35 (2.08) |
| [4] | 5.20 (0.75) | 10.98 (1.59) | 10.63 (1.54) | 9.74 (1.41) | 8.26 (1.20) |
| [5] | 6.75 (0.98) | 12.02 (1.74) | 11.99 (1.74) | 11.27 (1.64) | 10.27 (1.49) |
| [6] | 6.13 (0.89) | 12.77 (1.85) | 11.67 (1.69) | 10.87 (1.58) | 10.16 (1.47) |
| Average | 6.17 (0.89) | 12.74 (1.85) | 12.41 (1.80) | 11.51 (1.67) | 10.46 (1.52) |
| CV (%) | 9.3 | 9.3 | 13.5 | 15.7 | 17.9 |

Table 3.18. Phase2 - EN 12390-13 [36] for PC-0-ZZZh at 36 days of curing (left); 10027-1 [72] for rebars nominaly B500B $\phi$34 (right)

| Beam ID PC-0 (36days) | D | h | $\delta$ | $E_{C,0}$ | $E_{C,S}$ |
|---|---|---|---|---|---|
| | mm (in.) | mm (in.) | $kg/m^3$ ($lb/yd^3$) | GPa (msi) | GPa (msi) |
| [1] | 149.5 (5.9) | 294.3 (11.6) | 2373 (3999) | 32.40 (4.70) | 34.61 (5.02) |
| [2] | 149.6 (5.9) | 287.4 (11.3) | 2377 (4007) | 34.61 (5.02) | 36.19 (5.25) |
| | Average | | 2375 (4003) | 33.51 (4.86) | 35.40 (5.13) |
| | CV (%) | | 0.10 | 3.30 | 2.23 |

| Rebar ID B500B | D | $A_S$ | $F_y$ | $F_t$ |
|---|---|---|---|---|
| | mm (in.) | $mm^2$ ($in.^2$) | MPa (ksi) | MPa (ksi) |
| [1] | 34.0 (1.3) | 907.9 (1.4) | 541.16 (78.49) | 639.05 (92.69) |
| [2] | 34.0 (1.3) | 907.9 (1.4) | 542.30 (78.65) | 630.85 (91.50) |
| Average | 34.0 (1.3) | 907.9 (1.4) | 541.73 (78.57) | 634.95 (92.09) |
| CV (%) | 0.00 | 0.00 | 0.11 | 0.65 |

Table 3.19. Phase2 - EN 12390-13[36] for FRC-60-ZZZh at 33 days of curing (left) and FRC-100-ZZZh at 29 days of curing

| Beam ID FRC-60 (33days) | D | h | $\delta$ | $E_{C,0}$ | $E_{C,S}$ |
|---|---|---|---|---|---|
| | mm (in.) | mm (in.) | $kg/m^3$ ($lb/yd^3$) | GPa (msi) | GPa (msi) |
| [1] | 149.8 (5.9) | 294.6 (11.6) | 2332 (3931) | 32.60 (4.73) | 34.30 (4.97) |
| [2] | 150.0 (5.9) | 293.7 (11.6) | 2394 (4036) | 33.58 (4.87) | 34.86 (5.06) |
| | | Average | 2363 (3983) | 33.09 (4.80) | 34.58 (5.01) |
| | | CV (%) | 1.31 | 1.48 | 0.81 |

| Beam ID FRC-100 (29days) | D | h | $\delta$ | $E_{C,0}$ | $E_{C,S}$ |
|---|---|---|---|---|---|
| | mm (in.) | mm (in.) | $kg/m^3$ ($lb/yd^3$) | GPa (msi) | GPa (msi) |
| [1] | 149.6 (5.9) | 298.6 (11.8) | 2307 (3889) | 31.49 (4.57) | 32.57 (4.72) |
| [2] | 149.5 (5.9) | 294.1 (11.6) | 2326 (3921) | 30.12 (4.37) | 31.17 (4.52) |
| | | Average | 2317 (3905) | 30.80 (4.47) | 31.87 (4.62) |
| | | CV (%) | 0.40 | 2.23 | 2.20 |

Table 3.20. Phase2 - EN 12390-3[34] for PC-0-ZZZh at 14 days of curing on cylinders (left) and cubes (right)

| Beam ID PC-0 (14days) | D | h | $F_{max}$ | $\delta$ | $f_C$ |
|---|---|---|---|---|---|
| | mm (in.) | mm (in.) | kN (kips) | $kg/m^3$ ($lb/yd^3$) | MPa (ksi) |
| [1] | 149.6 (5.9) | 294.1 (11.6) | 1033.3 (232.3) | 2360 (3979) | 58.82 (8.53) |
| [2] | 149.1 (5.9) | 294.3 (11.6) | 1037.9 (233.3) | 2372 (3998) | 59.48 (8.63) |
| | | | Average | 2366 (3988) | 59.15 (8.58) |
| | | | CV (%) | 0.24 | 0.56 |

| Beam ID PC-0 (14days) | $a_0$ | $b_0$ | h | $F_{max}$ | $\delta$ | $R_C$ |
|---|---|---|---|---|---|---|
| | mm (in.) | mm (in.) | mm (in.) | kN (kips) | $kg/m^3$ ($lb/yd^3$) | MPa (ksi) |
| [1] | 149.7 (5.9) | 149.6 (5.9) | 150.6 (5.9) | 1408.7 (316.7) | 2320 (3910) | 62.91 (9.12) |
| [2] | 151.2 (6.0) | 150.8 (5.9) | 151.2 (6.0) | 1415.4 (318.2) | 2299 (3875) | 62.11 (9.01) |
| | | | | Average | 2309 (3893) | 62.51 (9.07) |
| | | | | CV (%) | 0.44 | 0.64 |

Table 3.21. Phase2 - EN 12390-3[34] for PC-0-ZZZh at 36 days of curing on cylinders (left) and cubes (right)

| Beam ID PC-0 (36days) | D | h | $F_{max}$ | $\delta$ | $f_C$ |
|---|---|---|---|---|---|
| | mm (in.) | mm (in.) | kN (kips) | $kg/m^3$ ($lb/yd^3$) | MPa (ksi) |
| [1] | 148.9 (5.9) | 294.6 (11.6) | 1031.9 (232.0) | 2375 (4003) | 59.29 (8.60) |
| [2] | 149.8 (5.9) | 295.1 (11.6) | 1130.9 (254.2) | 2384 (4018) | 64.20 (9.31) |
| | | | Average | 2379 (4011) | 61.74 (8.96) |
| | | | CV (%) | 0.18 | 3.98 |

| Beam ID PC-0 (36days) | $a_0$ | $b_0$ | h | $F_{max}$ | $\delta$ | $R_C$ |
|---|---|---|---|---|---|---|
| | mm (in.) | mm (in.) | mm (in.) | kN (kips) | $kg/m^3$ ($lb/yd^3$) | MPa (ksi) |
| [1] | 149.5 (5.9) | 148.4 (5.8) | 149.6 (5.9) | 1562.1 (351.2) | 2357 (3973) | 70.41 (10.21) |
| [2] | 150.1 (5.9) | 149.9 (5.9) | 150.1 (5.9) | 1589.0 (357.2) | 2348 (3958) | 70.62 (10.24) |
| [3] | 150.0 (5.9) | 149.2 (5.9) | 149.9 (5.9) | 1626.0 (365.5) | 2353 (3966) | 72.65 (10.54) |
| [4] | 149.9 (5.9) | 149.7 (5.9) | 150.0 (5.9) | 1635.8 (367.7) | 2350 (3961) | 72.90 (10.57) |
| [5] | 149.9 (5.9) | 149.7 (5.9) | 149.8 (5.9) | 1655.8 (372.2) | 2360 (3978) | 73.79 (10.70) |
| [6] | 149.7 (5.9) | 149.4 (5.9) | 149.7 (5.9) | 1588.1 (357.0) | 2369 (3992) | 71.01 (10.30) |
| | | | | Average | 2356 (3972) | 71.90 (10.43) |
| | | | | CV (%) | 0.29 | 1.78 |

Table 3.22. Phase2 - EN 12390-3[34] for FRC-60-ZZZh at 14 days of curing on cylinders (left) and cubes (right)

| Beam ID FRC-60 (14days) | D | h | $F_{max}$ | $\delta$ | $f_C$ |
|---|---|---|---|---|---|
| | mm (in.) | mm (in.) | kN (kips) | $kg/m^3$ ($lb/yd^3$) | MPa (ksi) |
| [1] | 149.6 (5.9) | 290.6 (11.4) | 1018.8 (229.0) | 2398 (4042) | 57.99 (8.41) |
| [2] | 149.6 (5.9) | 291.9 (11.5) | 1006.1 (226.2) | 2376 (4005) | 57.27 (8.31) |
| | | | Average | 2387 (4024) | 57.63 (8.36) |
| | | | CV (%) | 0.46 | 0.63 |

| Beam ID FRC-60 (14days) | $a_0$ | $b_0$ | h | $F_{max}$ | $\delta$ | $R_C$ |
|---|---|---|---|---|---|---|
| | mm (in.) | mm (in.) | mm (in.) | kN (kips) | $kg/m^3$ ($lb/yd^3$) | MPa (ksi) |
| [1] | 149.8 (5.9) | 150.0 (5.9) | 149.8 (5.9) | 1417.2 (318.6) | 2357 (3973) | 63.07 (9.15) |
| [2] | 149.6 (5.9) | 148.3 (5.8) | 149.7 (5.9) | 1339.0 (301.0) | 2376 (4004) | 60.35 (8.75) |
| | | | | Average | 2366 (3989) | 61.71 (8.95) |
| | | | | CV (%) | 0.39 | 2.20 |

Table 3.23. Phase2 - EN 12390-3[34] for FRC-60-ZZZh at 33 days of curing on cylinders (left) and cubes (right)

| Beam ID FRC-60 (33days) | D | h | $F_{max}$ | $\delta$ | $f_C$ |
|---|---|---|---|---|---|
| | mm (in.) | mm (in.) | kN (kips) | $kg/m^3$ ($lb/yd^3$) | MPa (ksi) |
| [1] | 149.4 (5.9) | 292.1 (11.5) | 1086.0 (244.1) | 2385 (4019) | 61.98 (8.99) |
| [2] | 149.9 (5.9) | 293.8 (11.6) | 1201.7 (270.2) | 2395 (4037) | 68.13 (9.88) |
| [3] | 149.3 (5.9) | 294.7 (11.6) | 1221.3 (274.6) | 2418 (4076) | 69.80 (10.12) |
| [4] | 149.4 (5.9) | 291.6 (11.5) | 1155.4 (259.7) | 2386 (4022) | 65.94 (9.56) |
| | | | Average | 2396 (4038) | 66.46 (9.64) |
| | | | CV (%) | 0.56 | 4.40 |

| Beam ID FRC-60 (33days) | $a_0$ | $b_0$ | h | $F_{max}$ | $\delta$ | $R_C$ |
|---|---|---|---|---|---|---|
| | mm (in.) | mm (in.) | mm (in.) | kN (kips) | $kg/m^3$ ($lb/yd^3$) | MPa (ksi) |
| [1] | 150.0 (5.9) | 150.5 (5.9) | 150.0 (5.9) | 1634.7 (367.5) | 2365 (3986) | 72.41 (10.50) |
| [2] | 150.2 (5.9) | 149.5 (5.9) | 150.2 (5.9) | 1698.1 (381.8) | 2367 (3989) | 75.62 (10.97) |
| [3] | 150.2 (5.9) | 150.2 (5.9) | 149.6 (5.9) | 1705.0 (383.3) | 2381 (4013) | 75.57 (10.96) |
| [4] | 149.6 (5.9) | 148.6 (5.9) | 149.7 (5.9) | 1610.1 (362.0) | 2366 (3988) | 72.43 (10.50) |
| [5] | 150.1 (5.9) | 150.2 (5.9) | 150.1 (5.9) | 1648.3 (370.6) | 2380 (4012) | 73.11 (10.60) |
| [6] | 150.1 (5.9) | 149.6 (5.9) | 150.2 (5.9) | 1613.2 (362.7) | 2358 (3975) | 71.84 (10.42) |
| | | | | Average | 2369 (3994) | 73.50 (10.66) |
| | | | | CV (%) | 0.35 | 2.08 |

Table 3.24. Phase2 - EN 12390-3[34] for FRC-100-ZZZh at 14 days of curing on cylinders (left) and cubes (right)

| Beam ID FRC-100 (14days) | D | h | $F_{max}$ | $\delta$ | $f_C$ |
|---|---|---|---|---|---|
| | mm (in.) | mm (in.) | kN (kips) | $kg/m^3$ ($lb/yd^3$) | MPa (ksi) |
| [1] | 149.1 (5.9) | 296.1 (11.7) | 1283.8 (288.6) | 2355 (3969) | 73.54 (10.67) |
| [2] | 149.5 (5.9) | 296.4 (11.7) | 1290.3 (290.1) | 2348 (3958) | 73.55 (10.67) |
| | | | Average | 2351 (3964) | 73.54 (10.67) |
| | | | CV (%) | 0.13 | 0.01 |

| Beam ID FRC-100 (14days) | $a_0$ | $b_0$ | h | $F_{max}$ | $\delta$ | $R_C$ |
|---|---|---|---|---|---|---|
| | mm (in.) | mm (in.) | mm (in.) | kN (kips) | $kg/m^3$ ($lb/yd^3$) | MPa (ksi) |
| [1] | 150.7 (5.9) | 149.7 (5.9) | 150.2 (5.9) | 1799.0 (404.4) | 2320 (3911) | 79.75 (11.57) |
| [2] | 150.4 (5.9) | 150.1 (5.9) | 150.4 (5.9) | 1795.4 (403.6) | 2301 (3879) | 79.53 (11.53) |
| | | | | Average | 2311 (3895) | 79.64 (11.55) |
| | | | | CV (%) | 0.42 | 0.14 |

Table 3.25. Phase2 - EN 12390-3[34] for FRC-100-ZZZh at 29 days of curing on cylinders (left) and cubes (right)

| Beam ID FRC-100 (29days) | D | h | $F_{max}$ | $\delta$ | $f_C$ |
|---|---|---|---|---|---|
| | mm (in.) | mm (in.) | kN (kips) | $kg/m^3$ ($lb/yd^3$) | MPa (ksi) |
| [1] | 149.5 (5.9) | 294.6 (11.6) | 1476.0 (331.8) | 2356 (3972) | 84.13 (12.20) |
| [2] | 149.6 (5.9) | 288.5 (11.4) | 1549.7 (348.4) | 2375 (4003) | 88.21 (12.79) |
| [3] | 149.1 (5.9) | 294.9 (11.6) | 1527.6 (343.4) | 2376 (4004) | 87.54 (12.70) |
| [4] | 149.5 (5.9) | 294.1 (11.6) | 1523.4 (342.5) | 2326 (3921) | 86.83 (12.59) |
| [5] | 149.6 (5.9) | 298.6 (11.8) | 1489.1 (334.8) | 2368 (3992) | 84.76 (12.29) |
| | | | Average | 2360 (3978) | 86.29 (12.52) |
| | | | CV (%) | 0.78 | 1.83 |

| Beam ID FRC-100 (29days) | $a_0$ | $b_0$ | h | $F_{max}$ | $\delta$ | $R_C$ |
|---|---|---|---|---|---|---|
| | mm (in.) | mm (in.) | mm (in.) | kN (kips) | $kg/m^3$ ($lb/yd^3$) | MPa (ksi) |
| [1] | 150.3 (5.9) | 149.5 (5.9) | 150.6 (5.9) | 2085.4 (468.8) | 2337 (3939) | 92.81 (13.46) |
| [2] | 150.6 (5.9) | 149.6 (5.9) | 150.3 (5.9) | 2180.6 (490.2) | 2292 (3863) | 96.79 (14.04) |
| [3] | 149.9 (5.9) | 150.6 (5.9) | 149.8 (5.9) | 2047.2 (460.2) | 2292 (3864) | 90.68 (13.15) |
| [4] | 150.3 (5.9) | 152.6 (6.0) | 150.2 (5.9) | 2094.4 (470.8) | 2280 (3844) | 91.31 (13.24) |
| [5] | 150.1 (5.9) | 151.2 (6.0) | 150.1 (5.9) | 2037.8 (458.1) | 2290 (3859) | 89.79 (13.02) |
| [6] | 150.3 (5.9) | 150.2 (5.9) | 150.2 (5.9) | 2143.0 (481.8) | 2322 (3913) | 94.93 (13.77) |
| | | | | Average | 2302 (3880) | 92.72 (13.45) |
| | | | | CV (%) | 0.87 | 2.65 |

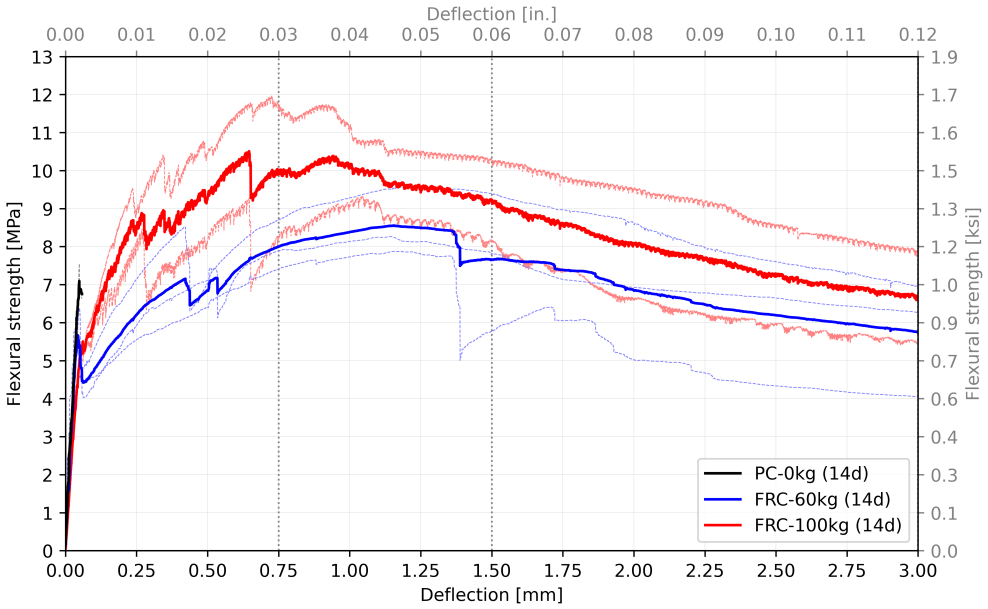



Figure 3.16. Phase2 - ASTM C1609[42] all tests at 14 days of curing

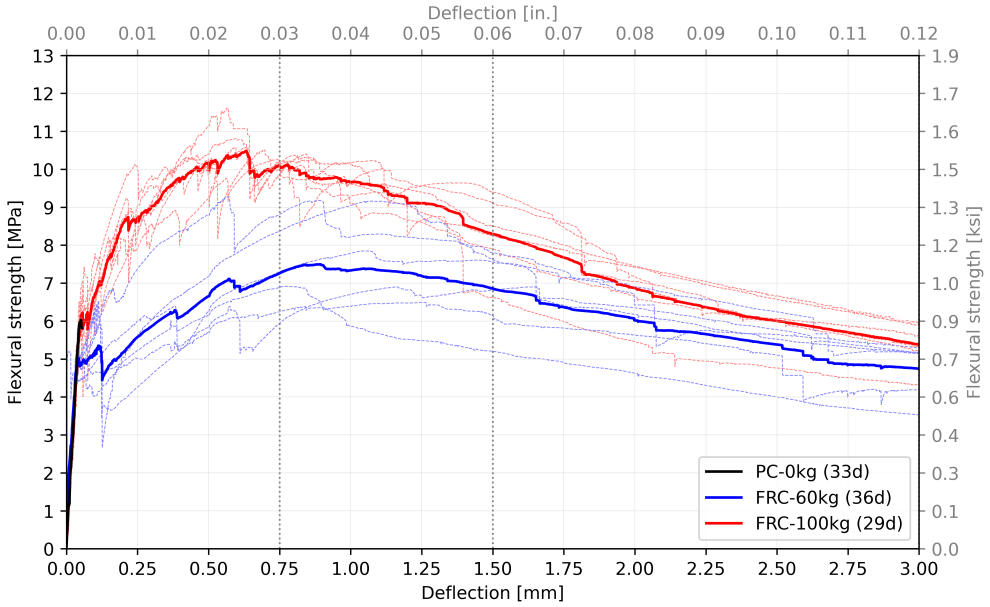



Figure 3.17. Phase2 - ASTM C1609[42] all tests at 36, 33 and 29 days of curing

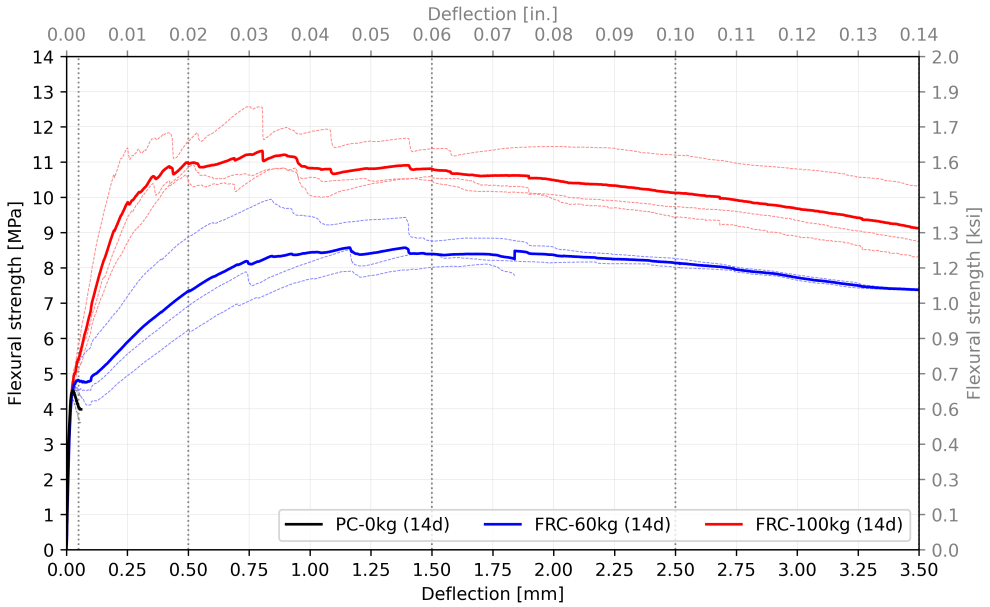



Figure 3.18. Phase2 - EN 14651[41] all tests at 14 days of curing

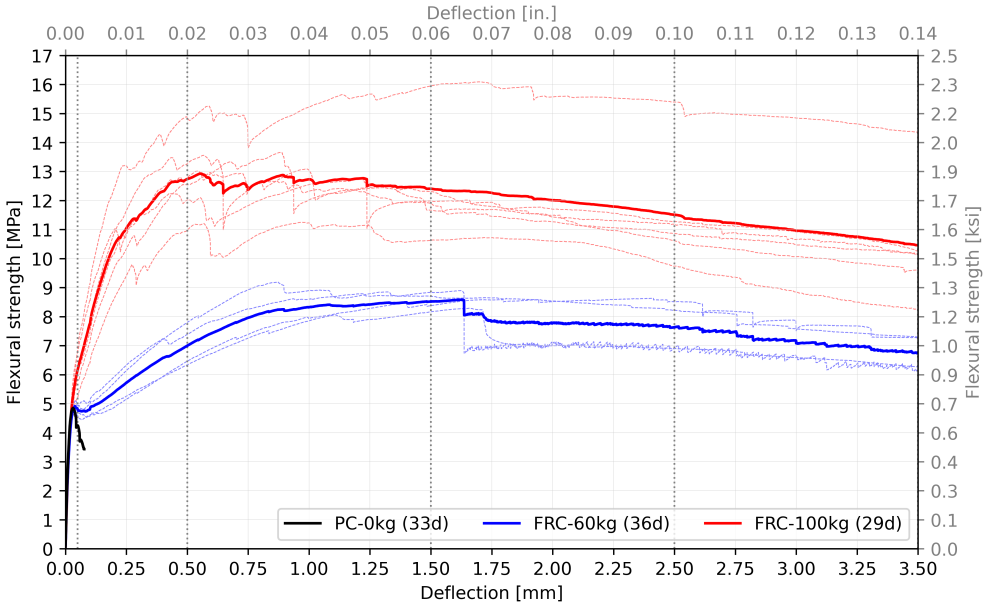



Figure 3.19. Phase2 - EN 14651[41] all tests at 36, 33 and 29 days of curing

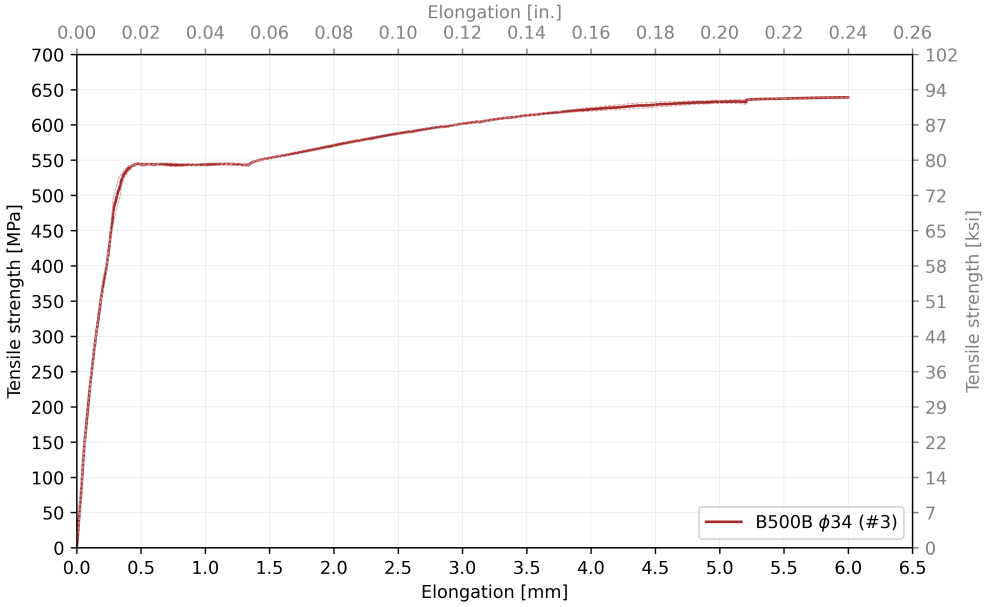



Figure 3.20. Phase2 - EN 10027[72] all tests

# Phase 3 – Size-Effect Investigation

Table 3.26. Phase3 - ASTM C1609[42] for FRC-60-ZZZh (left) and FRC-80-ZZZh (right)

| Beam ID FRC-60 | $f_{1^{st}peak}$ | $f^D_{600}$ | $f^D_{300}$ | $f^D_{150}$ | $f_P$ |
|---|---|---|---|---|---|
| | MPa (ksi) | MPa (ksi) | MPa (ksi) | MPa (ksi) | MPa (ksi) |
| [1] | 4.59 (0.67) | 7.50 (1.09) | 7.02 (1.02) | 5.80 (0.84) | 7.79 (1.13) |
| [2] | 4.89 (0.71) | 7.52 (1.09) | 7.82 (1.13) | 6.14 (0.89) | 8.09 (1.17) |
| [3] | 4.45 (0.65) | 7.26 (1.05) | 8.87 (1.29) | 6.76 (0.98) | 9.09 (1.32) |
| [4] | 4.49 (0.65) | 6.92 (1.00) | 6.57 (0.95) | 5.26 (0.76) | 7.37 (1.07) |
| [5] | 5.10 (0.74) | 8.66 (1.26) | 7.81 (1.13) | 6.31 (0.91) | 8.96 (1.30) |
| [6] | 4.79 (0.69) | 8.88 (1.29) | 10.31 (1.50) | 7.24 (1.05) | 10.58 (1.53) |
| [7] | 4.83 (0.70) | 6.77 (0.98) | 8.47 (1.23) | 7.05 (1.02) | 8.89 (1.29) |
| [8] | 4.46 (0.65) | 6.99 (1.01) | 8.06 (1.17) | 6.86 (1.00) | 8.34 (1.21) |
| Average | 4.70 (0.68) | 7.56 (1.10) | 8.12 (1.18) | 6.43 (0.93) | 8.64 (1.25) |
| CV (%) | 4.74 | 9.81 | 13.27 | 9.85 | 10.71 |

| Beam ID FRC-80 | $f_{1^{st}peak}$ | $f^D_{600}$ | $f^D_{300}$ | $f^D_{150}$ | $f_P$ |
|---|---|---|---|---|---|
| | MPa (ksi) | MPa (ksi) | MPa (ksi) | MPa (ksi) | MPa (ksi) |
| [1] | 4.73 (0.69) | 9.06 (1.31) | 9.18 (1.33) | 6.40 (0.93) | 10.21 (1.48) |
| [2] | 4.54 (0.66) | 9.43 (1.37) | 11.29 (1.64) | 8.03 (1.16) | 11.32 (1.64) |
| [3] | 4.98 (0.72) | 8.94 (1.30) | 8.56 (1.24) | 5.88 (0.85) | 9.35 (1.36) |
| [5] | 6.26 (0.91) | 9.74 (1.41) | 9.19 (1.33) | 6.49 (0.94) | 10.48 (1.52) |
| [5] | 5.00 (0.72) | 8.32 (1.21) | 7.63 (1.11) | 5.51 (0.80) | 9.01 (1.31) |
| [6] | 5.25 (0.76) | 10.33 (1.50) | 10.30 (1.49) | 7.69 (1.12) | 10.87 (1.58) |
| [7] | 5.66 (0.82) | 11.00 (1.59) | 10.59 (1.54) | 8.03 (1.16) | 12.42 (1.80) |
| [8] | 5.19 (0.75) | 7.83 (1.14) | 6.86 (0.99) | 4.40 (0.64) | 7.87 (1.14) |
| Average | 5.20 (0.75) | 9.33 (1.35) | 9.20 (1.33) | 6.55 (0.95) | 10.19 (1.48) |
| CV (%) | 9.82 | 10.34 | 15.29 | 18.60 | 13.10 |

Table 3.27. Phase3 - ASTM C1609[42] for FRC-60-900h (left) and FRC-80-900h (right)

| Beam ID FRC-60 | $f_{1^{st}peak}$ | $f^D_{600}$ | $f^D_{300}$ | $f^D_{150}$ | $f_P$ |
|---|---|---|---|---|---|
| | MPa (ksi) | MPa (ksi) | MPa (ksi) | MPa (ksi) | MPa (ksi) |
| [1] | 5.37 (0.78) | 7.42 (1.08) | 8.92 (1.29) | 6.89 (1.00) | 8.95 (1.30) |
| [2] | 5.20 (0.75) | 9.62 (1.39) | 11.28 (1.64) | 8.65 (1.26) | 11.42 (1.66) |
| [3] | 5.63 (0.82) | 8.74 (1.27) | 9.31 (1.35) | 6.80 (0.99) | 9.56 (1.39) |
| Average | 5.40 (0.78) | 8.59 (1.25) | 9.84 (1.43) | 7.45 (1.08) | 9.98 (1.45) |
| CV (%) | 3.23 | 10.54 | 10.52 | 11.47 | 10.51 |

| Beam ID FRC-80 | $f_{1^{st}peak}$ | $f^D_{600}$ | $f^D_{300}$ | $f^D_{150}$ | $f_P$ |
|---|---|---|---|---|---|
| | MPa (ksi) | MPa (ksi) | MPa (ksi) | MPa (ksi) | MPa (ksi) |
| [1] | 4.89 (0.71) | 7.51 (1.09) | 6.60 (0.96) | 5.32 (0.77) | 8.95 (1.30) |
| [2] | 5.21 (0.76) | 8.91 (1.29) | 8.78 (1.27) | 6.11 (0.89) | 11.42 (1.66) |
| [3] | 4.72 (0.68) | 8.15 (1.18) | 7.64 (1.11) | 5.29 (0.77) | 9.56 (1.39) |
| Average | 4.94 (0.72) | 8.19 (1.19) | 7.67 (1.11) | 5.57 (0.81) | 9.98 (1.45) |
| CV (%) | 4.16 | 7.00 | 11.59 | 6.81 | 10.51 |

Table 3.28. Phase3 - EN 14651[41] for FRC-60-ZZZh (left) and FRC-80-ZZZh (right)

| Beam ID FRC-60 | $f_L$ | $f_{R1k}$ | $f_{R2k}$ | $f_{R3k}$ | $f_{R4k}$ |
|---|---|---|---|---|---|
| | MPa (ksi) | MPa (ksi) | MPa (ksi) | MPa (ksi) | MPa (ksi) |
| [1] | 3.19 (0.46) | 3.93 (0.6) | 6.18 (0.9) | 6.95 (1.0) | 5.66 (0.8) |
| [2] | 5.17 (0.75) | 9.62 (1.4) | 8.82 (1.3) | 8.63 (1.3) | 8.08 (1.2) |
| [3] | 4.72 (0.68) | 7.08 (1.0) | 9.51 (1.4) | 10.16 (1.5) | 8.85 (1.3) |
| [4] | 4.81 (0.70) | 7.19 (1.0) | 7.85 (1.1) | 7.13 (1.0) | 6.43 (0.9) |
| [5] | 4.84 (0.70) | 6.11 (0.9) | 8.79 (1.3) | 9.55 (1.4) | 9.51 (1.4) |
| [6] | 4.93 (0.72) | 7.60 (1.1) | 8.70 (1.3) | 8.50 (1.2) | 7.91 (1.1) |
| [7] | 4.45 (0.65) | 6.02 (0.9) | 8.48 (1.2) | 8.57 (1.2) | 8.65 (1.3) |
| [8] | 5.65 (0.82) | 7.63 (1.1) | 10.11 (1.5) | 7.30 (1.1) | 6.74 (1.0) |
| Average | 4.72 (0.68) | 6.90 (1.0) | 8.55 (1.2) | 8.35 (1.2) | 7.73 (1.1) |
| CV (%) | 14.2 | 22.2 | 12.8 | 13.0 | 16.1 |

| Beam ID FRC-80 | $f_L$ | $f_{R1k}$ | $f_{R2k}$ | $f_{R3k}$ | $f_{R4k}$ |
|---|---|---|---|---|---|
| | MPa (ksi) | MPa (ksi) | MPa (ksi) | MPa (ksi) | MPa (ksi) |
| [1] | 5.30 (0.77) | 10.10 (1.5) | 11.16 (1.6) | 10.76 (1.6) | 10.27 (1.5) |
| [2] | 6.10 (0.89) | 11.61 (1.7) | 13.58 (2.0) | 13.30 (1.9) | 12.82 (1.9) |
| [3] | 4.31 (0.63) | 7.99 (1.2) | 9.94 (1.4) | 9.41 (1.4) | 8.80 (1.3) |
| [4] | 5.72 (0.83) | 11.74 (1.7) | 13.11 (1.9) | 13.09 (1.9) | 12.65 (1.8) |
| [5] | 5.19 (0.75) | 12.00 (1.7) | 13.31 (1.9) | 13.54 (2.0) | 12.98 (1.9) |
| [6] | 5.15 (0.75) | 10.79 (1.6) | 12.87 (1.9) | 12.94 (1.9) | 12.31 (1.8) |
| [7] | 5.30 (0.77) | 9.90 (1.4) | 11.16 (1.6) | 10.77 (1.6) | 10.29 (1.5) |
| Average | 5.30 (0.77) | 10.59 (1.5) | 12.16 (1.8) | 11.97 (1.7) | 11.45 (1.7) |
| CV (%) | 9.7 | 12.3 | 10.6 | 12.6 | 13.3 |

Table 3.29. Phase3 - EN 14651[41] for FRC-60-900h (left) and FRC-80-900h (right)

| Beam ID FRC-60 | $f_L$ | $f_{R1k}$ | $f_{R2k}$ | $f_{R3k}$ | $f_{R4k}$ |
|---|---|---|---|---|---|
| | MPa (ksi) | MPa (ksi) | MPa (ksi) | MPa (ksi) | MPa (ksi) |
| [1] | 4.45 (0.6) | 9.03 (1.3) | 10.18 (1.5) | 10.55 (1.5) | 8.60 (1.2) |
| [2] | 4.98 (0.7) | 10.14 (1.5) | 9.95 (1.4) | 10.19 (1.5) | 9.65 (1.4) |
| [3] | 4.27 (0.6) | 4.30 (0.6) | 6.07 (0.9) | 5.85 (0.8) | 5.06 (0.7) |
| [4] | 5.20 (0.8) | 11.58 (1.7) | 11.85 (1.7) | 11.43 (1.7) | 10.38 (1.5) |
| Average | 4.73 (0.7) | 8.76 (1.3) | 9.51 (1.4) | 9.50 (1.4) | 8.42 (1.2) |
| CV (%) | 8.05 | 31.17 | 22.30 | 22.72 | 24.25 |

| Beam ID FRC-80 | $f_L$ | $f_{R1k}$ | $f_{R2k}$ | $f_{R3k}$ | $f_{R4k}$ |
|---|---|---|---|---|---|
| | MPa (ksi) | MPa (ksi) | MPa (ksi) | MPa (ksi) | MPa (ksi) |
| [1] | 3.84 (0.6) | 10.04 (1.5) | 12.02 (1.7) | 10.47 (1.5) | 10.00 (1.5) |
| [2] | 4.31 (0.6) | 9.66 (1.4) | 9.46 (1.4) | 9.40 (1.4) | 8.81 (1.3) |
| [3] | 4.91 (0.7) | 10.10 (1.5) | 11.15 (1.6) | 10.52 (1.5) | 9.46 (1.4) |
| [4] | 4.18 (0.6) | 7.45 (1.1) | 8.04 (1.2) | 7.60 (1.1) | 6.88 (1.0) |
| [5] | 5.89 (0.9) | 12.82 (1.9) | 15.14 (2.2) | 14.89 (2.2) | 14.21 (2.1) |
| Average | 4.63 (0.7) | 10.02 (1.5) | 11.16 (1.6) | 10.58 (1.5) | 9.87 (1.4) |
| CV (%) | 15.55 | 17.03 | 21.66 | 22.73 | 24.41 |

Table 3.30. Phase3 - EN 12390-13[36] for PC-0-ZZZh

| Beam ID PC-0 | D | h | Weight | $\delta$ | $E_{C,0}$ |
|---|---|---|---|---|---|
| | mm (in.) | mm (in.) | kg (lb) | $kg/m^3$ ($lb/yd^3$) | GPa (msi) |
| [1] | 150.0 (5.9) | 300.0 (11.8) | 12.3 (27.1) | 2320 (3910) | 27.71 (4.02) |
| [2] | 150.0 (5.9) | 300.0 (11.8) | 12.3 (27.1) | 2320 (3910) | 28.17 (4.09) |
| | | | Average | 2320 (3910) | 27.94 (4.05) |
| | | | CV (%) | NA | 0.01 |

Table 3.31. Phase3 - EN 12390-13[36] for FRC-60-ZZZh (left) and FRC-100-ZZZh (right)

| Beam ID FRC-60 | D | h | Weight | $\delta$ | $E_{C,0}$ |
|---|---|---|---|---|---|
| | mm (in.) | mm (in.) | kg (lb) | $kg/m^3$ ($lb/yd^3$) | GPa (msi) |
| [1] | 150.0 (5.9) | 300.0 (11.8) | 12.5 (27.5) | 2349 (3959) | 28.71 (4.16) |
| [2] | 150.0 (5.9) | 300.0 (11.8) | 12.5 (27.5) | 2349 (3959) | 25.99 (3.77) |
| | | | Average | 2349 (3959) | 27.35 (3.97) |
| | | | CV (%) | NA | 0.05 |

| Beam ID FRC-80 | D | h | Weight | $\delta$ | $E_{C,0}$ |
|---|---|---|---|---|---|
| | mm (in.) | mm (in.) | kg (lb) | $kg/m^3$ ($lb/yd^3$) | GPa (msi) |
| [1] | 150.0 (5.9) | 300.0 (11.8) | 12.3 (27.2) | 2327 (3922) | 31.49 (4.57) |
| [2] | 150.0 (5.9) | 300.0 (11.8) | 12.3 (27.2) | 2327 (3922) | 30.12 (4.37) |
| | | | Average | 2327 (3922) | 30.80 (4.47) |
| | | | CV (%) | NA | 0.02 |

Table 3.32. Phase3 - EN 12390-3[34] for PC-0-ZZZh on cylinders (left) and cubes (right)

| Beam ID PC-0 | D | h | $F_{max}$ | $\delta$ | $f_C$ |
|---|---|---|---|---|---|
| | mm (in.) | mm (in.) | kN (kips) | $kg/m^3$ ($lb/yd^3$) | MPa (ksi) |
| [1] | 150* (5.9) | 300* (11.8) | 1000.3 (224.9) | 2320* (3910) | 56.60 (8.21) |
| [2] | 150* (5.9) | 300* (11.8) | 1007.2 (226.4) | 2320* (3910) | 57.00 (8.27) |
| | | | Average | 2320* (3910) | 56.80 (8.24) |
| | | | CV (%) | NA | 0.35 |

| Beam ID PC-0 | $a_0$ | $b_0$ | h | $F_{max}$ | $\delta$ | $R_C$ |
|---|---|---|---|---|---|---|
| | mm (in.) | mm (in.) | mm (in.) | kN (kips) | $kg/m^3$ ($lb/yd^3$) | MPa (ksi) |
| [1] | 150* (5.9) | 150* (5.9) | 150* (5.9) | 1167.6 (262.5) | 2320* (3910) | 51.89 (7.53) |
| [2] | 150* (5.9) | 150* (5.9) | 150* (5.9) | 1110.2 (249.6) | 2320* (3910) | 49.34 (7.16) |
| | | | | Average | 2320* (3910) | 50.62 (7.34) |
| | | | | CV (%) | NA | 2.52 |

Table 3.33. Phase3 - EN 12390-3[34] for FRC-60-ZZZh on cylinders (left) and cubes (right)

| Beam ID FRC-60 | D | h | $F_{max}$ | $\delta$ | $f_C$ |
|---|---|---|---|---|---|
| | mm (in.) | mm (in.) | kN (kips) | $kg/m^3$ ($lb/yd^3$) | MPa (ksi) |
| [1] | 150* (5.9) | 300* (11.8) | 929.2 (208.9) | 2349* (3959) | 52.58 (7.63) |
| [2] | 150* (5.9) | 300* (11.8) | 913.6 (205.4) | 2349* (3959) | 51.70 (7.50) |
| | | | Average | 2349* (3959) | 52.14 (7.56) |
| | | | CV (%) | NA | 0.85 |

| Beam ID FRC-60 | $a_0$ | $b_0$ | h | $F_{max}$ | $\delta$ | $R_C$ |
|---|---|---|---|---|---|---|
| | mm (in.) | mm (in.) | mm (in.) | kN (kips) | $kg/m^3$ ($lb/yd^3$) | MPa (ksi) |
| [1] | 150* (5.9) | 150* (5.9) | 150* (5.9) | 1101.4 (247.6) | 2349* (3959) | 48.95 (7.10) |
| [2] | 150* (5.9) | 150* (5.9) | 150* (5.9) | 1094.8 (246.1) | 2349* (3959) | 48.66 (7.06) |
| | | | | Average | 2349* (3959) | 48.80 (7.08) |
| | | | | CV (%) | NA | 0.30 |

Table 3.34. Phase3 - EN 12390-3[34] for FRC-100-ZZZh on cylinders (left) and cubes (right)

| Beam ID FRC-100 | D | h | $F_{max}$ | $\delta$ | $f_C$ |
|---|---|---|---|---|---|
| | mm (in.) | mm (in.) | kN (kips) | $kg/m^3$ ($lb/yd^3$) | MPa (ksi) |
| [1] | 150* (5.9) | 300* (11.8) | 1310.6 (294.6) | 2327* (3922) | 74.16 (10.76) |
| [2] | 150* (5.9) | 300* (11.8) | 1272.4 (286.1) | 2327* (3922) | 72.01 (10.44) |
| | | | Average | 2327* (3922) | 73.08 (10.60) |
| | | | CV (%) | NA | 1.48 |

| Beam ID FRC-100 | $a_0$ | $b_0$ | h | $F_{max}$ | $\delta$ | $R_C$ |
|---|---|---|---|---|---|---|
| | mm (in.) | mm (in.) | mm (in.) | kN (kips) | $kg/m^3$ ($lb/yd^3$) | MPa (ksi) |
| [1] | 150* (5.9) | 150* (5.9) | 150* (5.9) | 1512.0 (339.9) | 2327* (3922) | 67.20 (9.75) |
| [2] | 150* (5.9) | 150* (5.9) | 150* (5.9) | 1640.0 (368.7) | 2327* (3922) | 72.89 (10.57) |
| | | | | Average | 2327* (3922) | 70.04 (10.16) |
| | | | | CV (%) | NA | 4.06 |

Table 3.35. Phase3 - NMX B506[75] for rebars respectively #3 (9.5 mm, 0.4 in.), #4 (12.7 mm, 0.5 in.), #6 (19.1 mm, 0.8 in.), #8 (25.4 mm, 1.0 in.), and #10 (31.8 mm, 1.3 in.)

| Rebar Gr42 #3 | $f_y$ | $f_t$ |
|---|---|---|
| | MPa ksi | MPa ksi |
| [1] | 450.1 (65.3) | 751.5 (109.0) |
| [2] | 433.6 (62.9) | 724.1 (105.0) |
| [3] | 429.5 (62.3) | 722.4 (104.8) |
| Average | 437.7 (63.5) | 732.7 (106.3) |
| CV (%) | 2.0 | 1.8 |

| Rebar Gr42 #4 | $f_y$ | $f_t$ |
|---|---|---|
| | MPa ksi | MPa ksi |
| [1] | 427.5 (62.0) | 750.3 (108.8) |
| [2] | 431.5 (62.6) | 751.1 (108.9) |
| Average | 429.5 (62.3) | 750.7 (108.9) |
| CV (%) | 0.5 | 0.1 |

| Rebar Gr42 #6 | $f_y$ | $f_t$ |
|---|---|---|
| | MPa ksi | MPa ksi |
| [1] | 478.9 (69.5) | 740.1 (107.3) |
| [2] | 454.6 (65.9) | 715.6 (103.8) |
| Average | 466.7 (67.7) | 727.8 (105.6) |
| CV (%) | 2.6 | 1.7 |

| Rebar Gr42 #8 | $f_y$ | $f_t$ |
|---|---|---|
| | MPa ksi | MPa ksi |
| [1] | 482.4 (70.0) | 730.0 (105.9) |
| [2] | 468.1 (67.9) | 694.9 (100.8) |
| [3] | 471.7 (68.4) | 714.3 (103.6) |
| Average | 474.1 (68.8) | 713.1 (103.4) |
| CV (%) | 1.3 | 2.0 |

| Rebar Gr42 #10 | $f_y$ | $f_t$ |
|---|---|---|
| | MPa ksi | MPa ksi |
| [1] | 479.2 (69.5) | 750.5 (108.9) |
| [2] | 465.6 (67.5) | 732.3 (106.2) |
| Average | 472.4 (68.5) | 741.4 (107.5) |
| CV (%) | 1.4 | 1.2 |

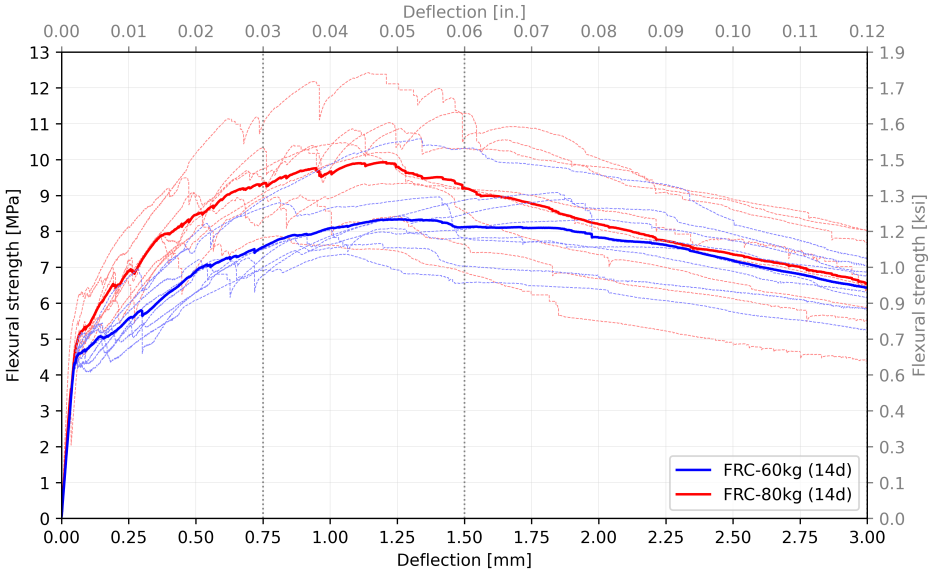



Figure 3.21. Phase3 - ASTM C1609[42] all tests at 14 days of curing

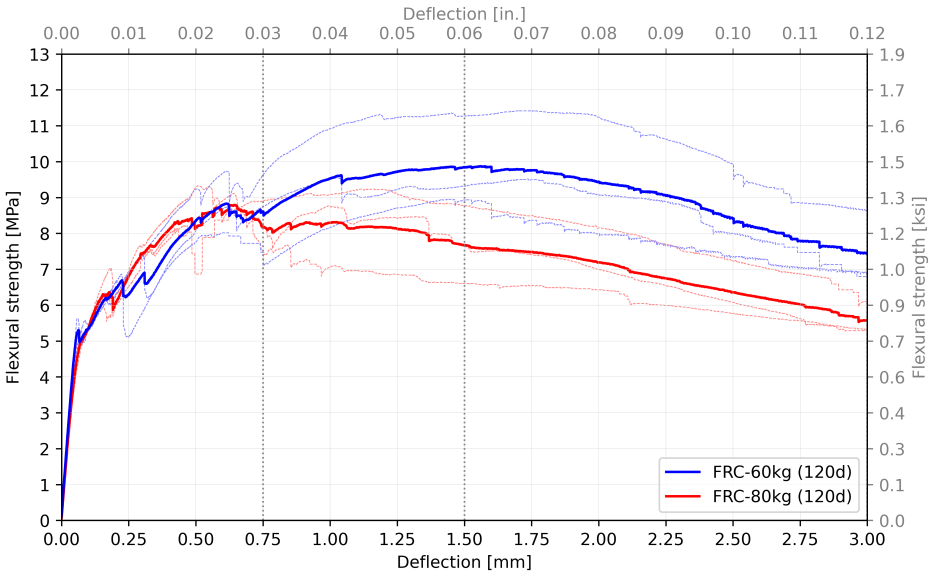



Figure 3.22. Phase3 - ASTM C1609[42] all tests at 120 days of curing

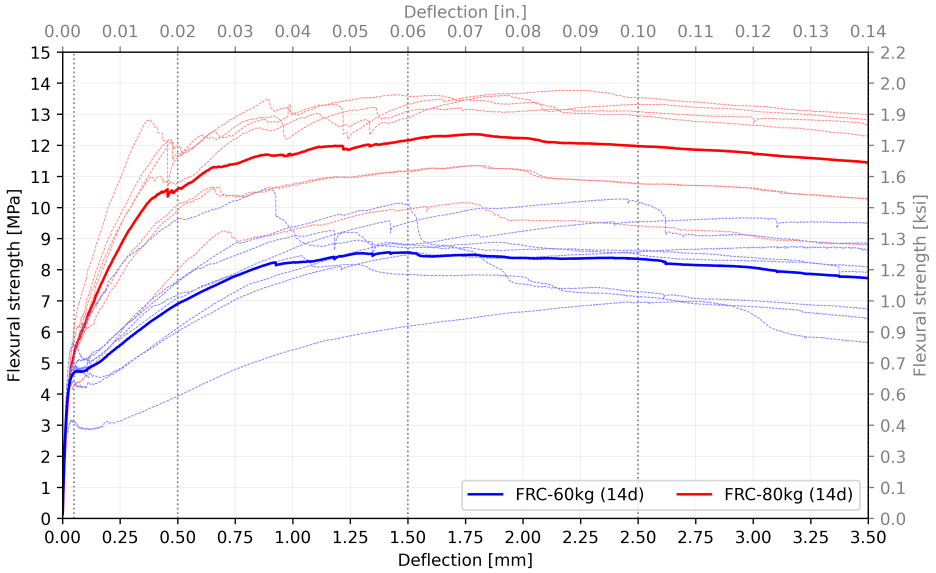



Figure 3.23. Phase3 - EN 14651[41] all tests at 14 days of curing

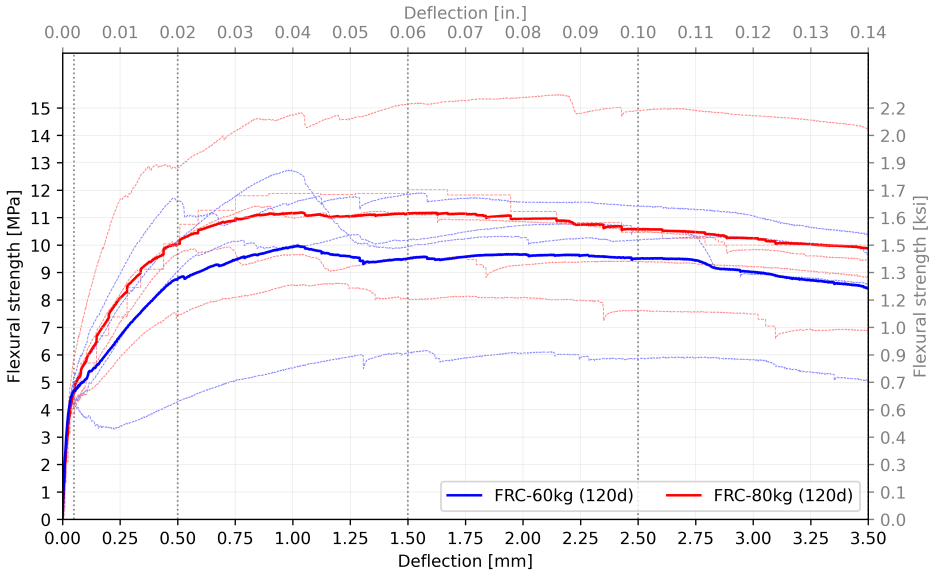



Figure 3.24. Phase3 - EN 14651[41] all tests at 120 days of curing